STRATIGRAPHY, SEDIMENTOLOGY, AND DIAGENETIC HISTORY OF THE SILURO-DEVONIAN HELDERBERG GROUP, CENTRAL APPALACHIANS

by

Steven L. Dorobek

Dissertation submitted to the Faculty of the

Virginia Polytechnic Institute and State University

in partial fulfillment of the requirements for the degree of

DOCTOR OF PHILOSOPHY

in

Geological Sciences

APPROVED:

Dr. J.F. Read

Dr. R.K. Bambach

Dr. J.R. Craig

Dr. K.A. Eriksson

Dr. J.D. Rimstidt

July, 1984
Blacksburg, Virginia

ACKNOWLEDGMENTS

I would like to extend special thanks to Dr. J. Fred Read who proposed the study and provided invaluable guidance and advice on all aspects of this study. Thanks also are extended to other past and present committee members, Drs. R.K. Bambach, J.R. Craig, K.A. Eriksson, D.R. Gray for constructive criticism and advice. Special thanks to committee members Dr. J.D. Rimstidt, for numerous lengthy discussions on low temperature aqueous geochemistry, and the late Dr. C.G. Tillman, for lending his expertise and advice on Helderberg faunas and stratigraphy.

Dr. of the Department of Geological Sciences, University of Michigan, provided the use of his stable isotope laboratory in December, 1983 for sampling of carbonate cements and ran the analyses. Thanks go out to him and other faculty, staff, and students at the University of Michigan for providing a friendly working atmosphere. Dr. of Mobil Research and Development Corporation, Dallas, Texas, spent several days in the field with me and provided insight into the complexities of siliciclastic shelf deposits. Dr. of the Anaerobe Laboratory, Virginia Tech, kindly provided the use of an epifluorescence microscope for detection of hydrocarbon inclusions.

at Virginia Tech provided invaluable assistance during electron microprobe analyses. and provided excellent and friendly technical assistance, especially for image analysis. Dr. and of the Spatial Data Analysis Lab, Virginia Tech, introduced me to image analysis and gave insight and expertise in developing the image analysis technique used in this study. and advised on photographic and developing techniques. and assisted in typing and preparation of the manuscript. , , , and drafted most of the illustrations. , , , , , , and provided field or laboratory assistance at various stages of the research.

Fianacial assistance was provided by Grant EAR 83-05878 from National Science Foundation to and by Texaco, U.S.A., who provided funds for developing image analysis techniques and supported me during the last two years of the project. Additional support came from Amoco, Atlantic Richfield, Chevron, and Mobil Oil Companies and from student grants-in-aid from Sigma Xi and the American Association of Petroleum Geologists. Early financial support came from a graduate teaching assistantship from the Department of Geological Sciences, VPI & SU.

Thanks also are due to all other faculty and staff of the Department of Geological Sciences, Virginia Tech. who helped with numerous problems during the course of this study Special thanks to friends and co-workers in the Carbonate Research Appalachian/Arctic Projects Lab,

, , and for making things interesting(?!). Finally, to my wife, , and my son,

, who provided endless emotional support during the study and who keep reminding that there really is more to life than just rocks.

LIST OF TABLES

LIST OF FIGURES

TABLE OF CONTENTS

Appendix

page

CHAPTER 1. STRATIGRAPHY AND SEDIMENTOLOGY OF THE HELDERBERG GROUP

Introduction

The Helderberg Group is a mixed siliciclastic-carbonate sedimentary sequence that formed in the Central Appalachian Basin (Virginia-West Virginia-Maryland) during Late Silurian (Cayugan)-Early Devonian (Ulsterian) time. Exposed Helderberg rocks of the Central Appalachian Valley and Ridge formed on a gently sloping carbonate ramp (after Ahr, 1973) that developed on the eastern side of the Central Appalachian foreland basin. Subsurface Helderberg equivalents formed to the west on a broad stable cratonic platform. Minor siliciclastics, derived from low relief remnants of tectonic highlands that developed during Ordovician (Taconic) orogenesis, were deposited along the basin margin during regressive events but did not stop carbonate production.

Butts (1940) mapped Helderberg rocks throughout Virginia and various workers mapped Helderberg rocks in individual counties in West Virginia and western Maryland. Swartz (1929) and Woodward (1943) provided much of the early regional stratigraphic framework for the Helderberg Group in the Central Appalachians. Subsequent work by Tillman

(1963), Head (1969, 1974), Bowen (1967), and Miller et al. (1977) has clarified stratigraphic relationships. Montgomery (1967), Head (1969), Makurath (1975, 1977), Barwis and Makurath (1978), and Smosna and Warshauer (1979) have given paleoenvironmental or paleoecological interpretations for all or parts of the Helderberg Group. Most biostratigraphic correlations have been made using brachiopod and coral zonations (Swartz, 1929; Bowen, 1966, 1967; Head, 1969) but more recent work by Helfrich (1975), Cook (1981), and Sartain (1981) have used conodont zones for correlation; conodont zones have been particularly useful for correlating the condensed Helderberg section in southwestern Virginia. Biostratigraphic time lines essentially parallel lithofacies boundaries throughout the Helderberg Group in the Central Appalachians.

The Helderberg Group was deposited in a foreland basin that initially developed to the west of an accretionary prism during the Middle-Late Ordovician (Taconic Orogeny; Read, 1980). By Late Silurian-Early Devonian time, eastern tectonic highlands were no longer major sources of siliciclastics. Carbonate ramps developed on both the eastern and western (cratonic) side of the Appalachian Basin probably because of the limited clastic influx and because the basin was not being loaded along its eastern margin with advancing thrust sheets or undergoing rapid subsidence. This period of relative tectonic quiescence allowed open

marine carbonates of the Helderberg Group to develop on a gently sloping carbonate ramp bordered by a low relief, inactive accretionary prism. The accretionary prism again became a major source of siliciclastic sediment during the Middle Devonian (Acadian Orogeny) when the Helderberg Group was buried beneath thick marine shales.

This study documents the development of a carbonate ramp that extended out from an accretionary prism and into a foreland basin that was undergoing limited subsidence between two major orogenic events (Taconic and Acadian Orogenies). Lithofacies distribution and relationships on the ramp during various stages of ramp development are documented and basin evolution is discussed.

Structural and Stratigraphic Setting

The Siluro-Devonian Helderberg Group is exposed in northeast-trending folds in the Valley and Ridge Province of the Central Appalachians (Figs. 1, 2). Helderberg outcrops on the Little North Mountain, Saint Clair, and Pulaski Thrust sheets are the only outcrops within the study area to have been affected by major overthrusting. Eastern basin margin facies are not exposed in outcrop, having been eroded or buried beneath thrust sheets. To the northwest, the Helderberg Group and its stratigraphic equivalents underlie flatlying Upper Paleozoic rocks.

Figure 1. Distribution of Helderberg Group outcrop belts, Valley and Ridge Province, Central Appalachians. Major thrust faults also indicated.

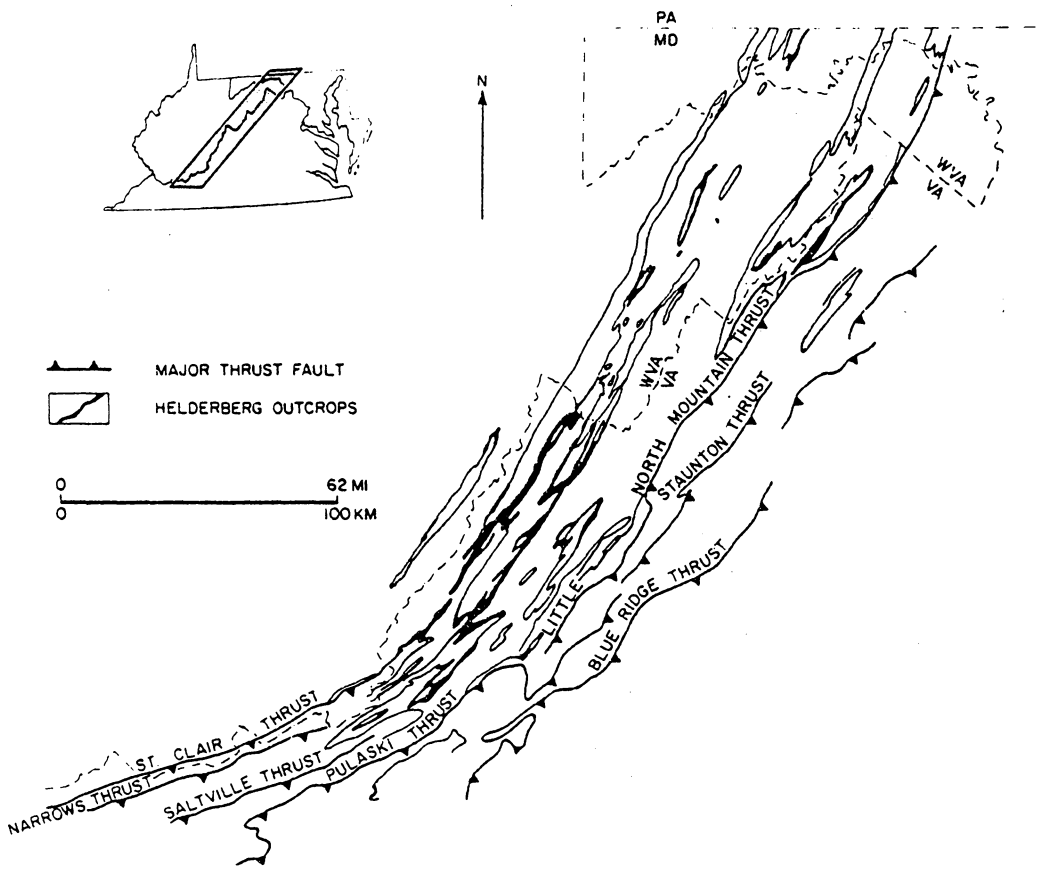
PA
MD
N
WVA
VA
WVA
VA
MAJOR THRUST FAULT
HELDERBERG OUTCROPS
0
62 MI
0
100 KM
NORTH MOUNTAIN THRUST
STAUNTON THRUST
LITTLE
BLUE RIDGE THRUST
ST CLAIR THRUST
NARROWS THRUST
SALTVILLE THRUST
PULASKI THRUST

Figure 2. Palinspastic base map; locations of stratigraphic cross sections shown in Figure 5 are indicated. This palinspastic base map is used in subsequent illustrations and is modified from Dennison (1970).

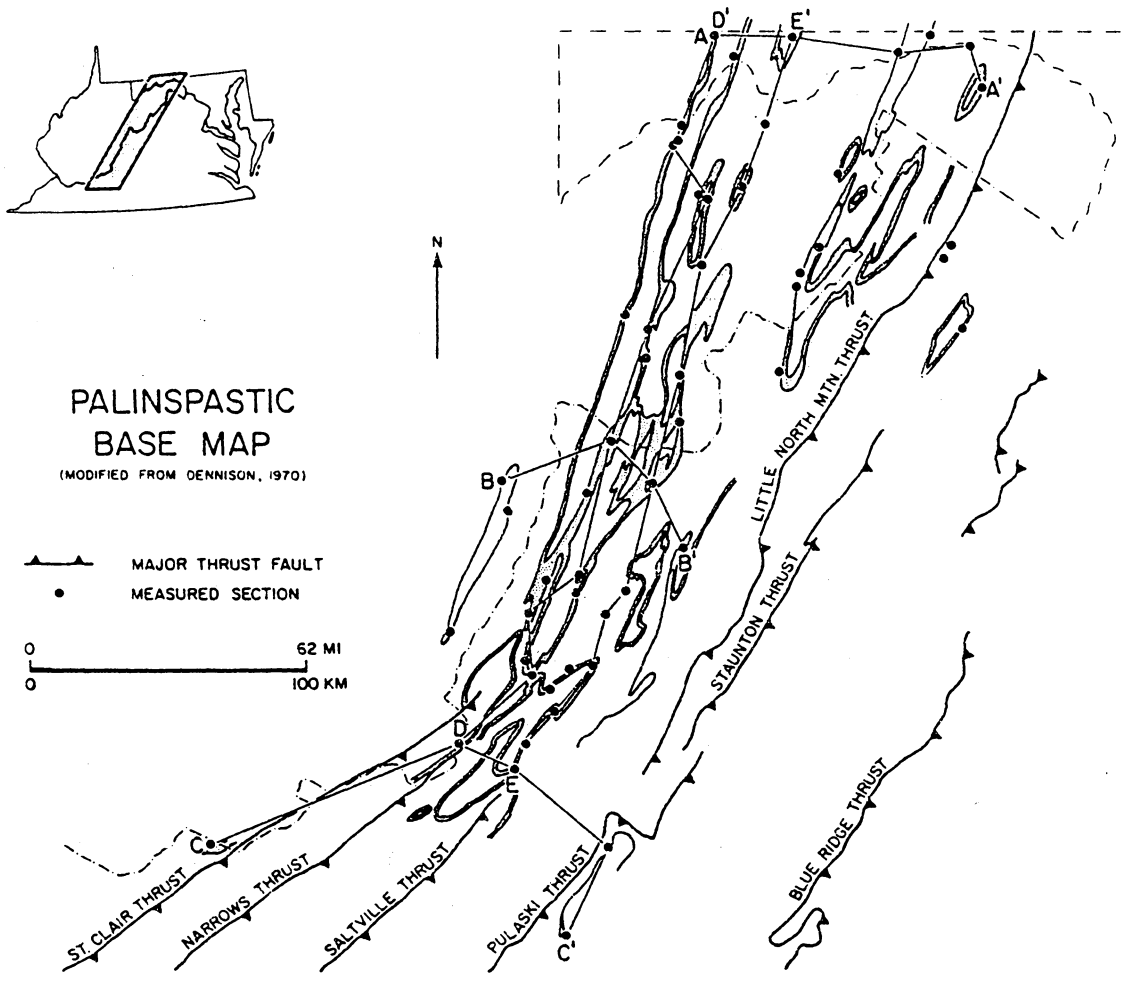
PALINSPASTIC
BASE MAP
(MODIFIED FROM DENNISON, 1970)
MAJOR THRUST FAULT
MEASURED SECTION
0
62 MI
0
100 KM
N
A
D'
E'
A'
B
B'
D
E
C
C'
LITTLE NORTH MTN. THRUST
STAUNTON THRUST
BLUE RIDGE THRUST
ST. CLAIR THRUST
NARROWS THRUST
SALTVILLE THRUST
PULASKI THRUST

Stratigraphic reconstructions indicate that Helderberg outcrop belts in the Central Appalachian Valley and Ridge trend slightly oblique to depositional strike. The basin axis trended northeast from southwestern Virginia through West Virginia to central Pennsylvania, then curved eastward to southeastern New York (Head, 1969).

Within the study area, the Helderberg Group (0-150 m thick; Figs. 3, 4) generally overlies thin-bedded limestone and calcareous shale of the Silurian Tonoloway Limestone (0-185 m thick). The Helderberg-Tonoloway contact is an erosional disconformity along the basin margin in southwestern Virginia, but is conformable in the basin in West Virginia and western Maryland. Locally in southwestern Virginia, thin Helderberg equivalents rest disconformably on Silurian sandstone (10-30 m thick; Tillman, 1963). The Helderberg Group is overlain by Middle Devonian clastics (Oriskany Sandstone, Huntersville Chert, Millboro-Needmore Shale; 80-390 m thick) that form the basal part of the Devonian-Mississippian (Acadian) clastic wedge in the Central Appalachians.

Helderberg rocks in the study area developed on a gently sloping carbonate ramp which formed the eastern margin of a foreland basin. Slopes on the ramp are estimated at 10 to 15 cm/km (calculated from thickness variation of individual onlap packages across depositional strike). These are probably minimum slopes as sediment

Figure 3. Isopach map of Helderberg Group, palinspastic base.

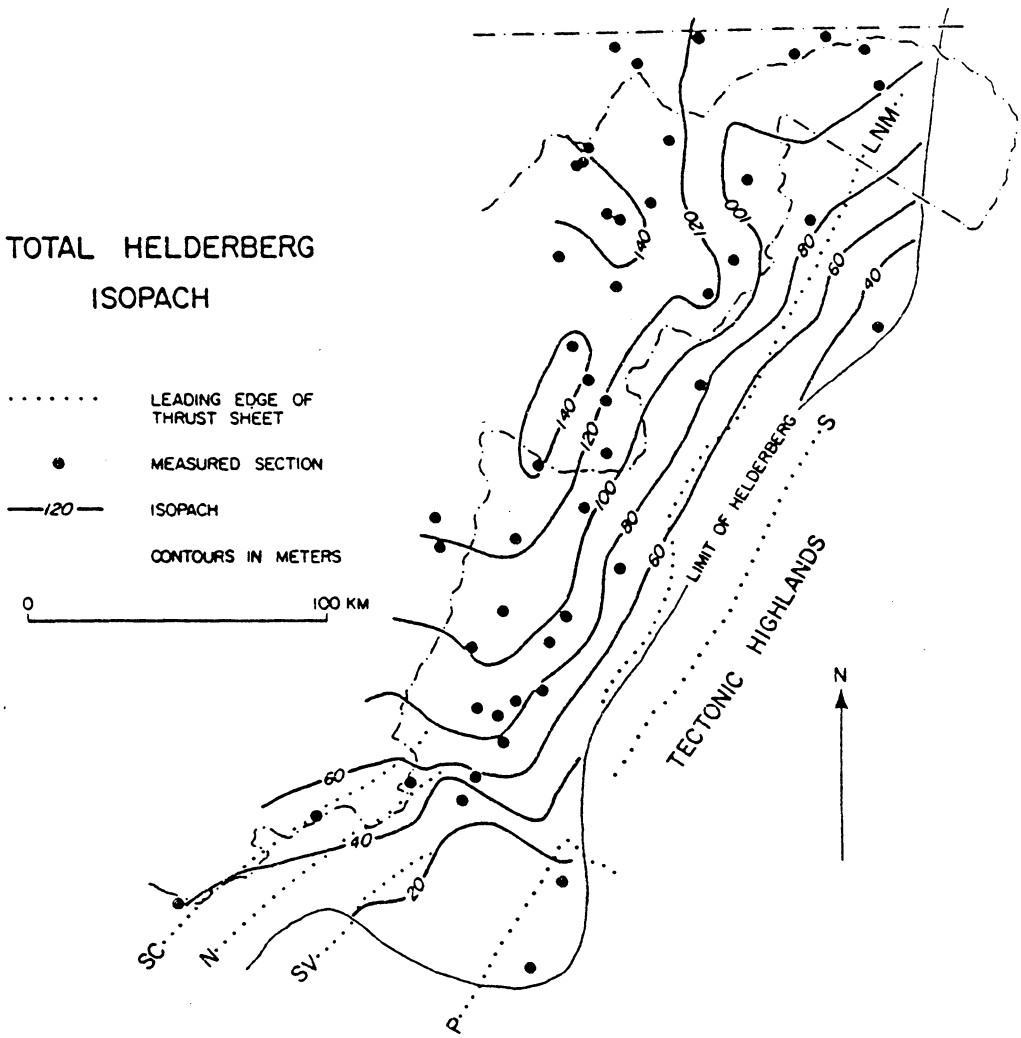
TOTAL HELDERBERG
ISOPACH
LEADING EDGE OF THRUST SHEET
MEASURED SECTION
120
ISOPACH
CONTOURS IN METERS
0
100 KM
LNM
140
120
100
80
60
40
LIMIT OF HELDERBERG
S
TECTONIC HIGHLANDS
N
60
40
20
SC
N
SV
P

compaction has not been accounted for in the calculation. Calculated slopes on the ramp were used in estimating water depths for subtidal deposits.

Regional Stratigraphy

Regional Helderberg correlations throughout the Appalachian Basin are shown in Figure 4. Stratigraphic relationships of Helderberg formations exposed within the study area are shown in cross-sections (Fig. 5).

The Helderberg Group in the Central Appalachians forms three transgressive-regressive sequences. The lower transgressive sequence consists of open marine carbonates of the lower Keyser Formation (skeletal limestone/shaly limestone/nodular-bedded limestone) that were deposited on restricted peritidal carbonates of the Upper Silurian Tonoloway Formation. This onlap sequence is overlain by the Clifton Forge Sandstone (shallow marine quartz sandstone) and laterally equivalent Big Mountain Shale (limy shale) and lower Keyser Formation (skeletal limestone).

The middle transgressive sequence consists of deep ramp limestone (upper Keyser Formation) that overlies the lower Keyser Formation. This onlap sequence is overlain by regressive skeletal sand sheets (New Creek Formation), minor shallow marine quartz sandstone (Elbow Ridge and Healing Springs Sandstone), and carbonate tidal flats (uppermost Keyser Formation).

Figure 4. Regional stratigraphic correlation chart, Helderberg Group, Central Appalachians.

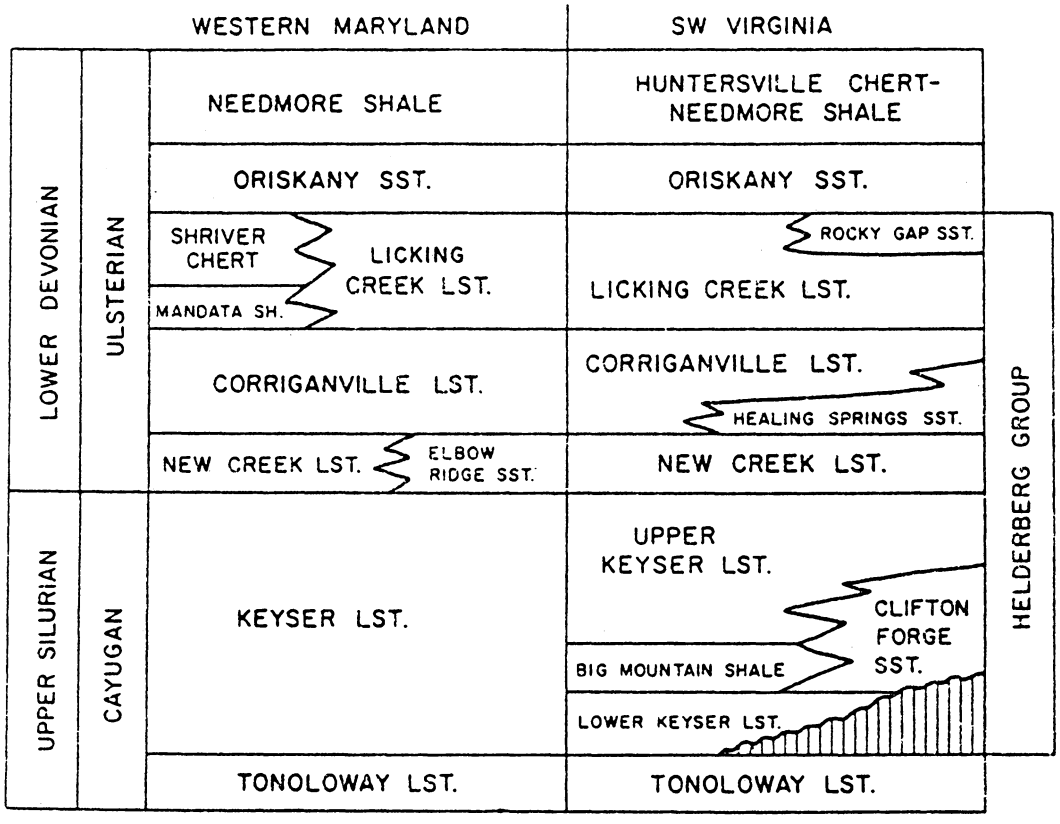
WESTERN MARYLAND
SW VIRGINIA
LOWER DEVONIAN
ULSTERIAN
NEEDMORE SHALE
HUNTERSVILLE CHERT-
NEEDMORE SHALE
ORISKANY SST.
ORISKANY SST.
SHRIVER
CHERT
LICKING
CREEK LST.
MANDATA SH.
ROCKY GAP SST.
LICKING CREEK LST.
CORRIGANVILLE LST.
CORRIGANVILLE LST.
HEALING SPRINGS SST.
NEW CREEK LST.
ELBOW
RIDGE SST.
NEW CREEK LST.
UPPER SILURIAN
CAYUGAN
KEYSER LST.
UPPER
KEYSER LST.
CLIFTON
FORGE
SST.
BIG MOUNTAIN SHALE
LOWER KEYSER LST.
HELDERBERG GROUP
TONOLOWAY LST.
TONOLOWAY LST.

Figure 5. Stratigraphic cross sections. Locations of cross-sections are shown in Figure 2. 5A,B,C are northwest to southeast cross sections; 5D,E are southwest to northeast cross sections.

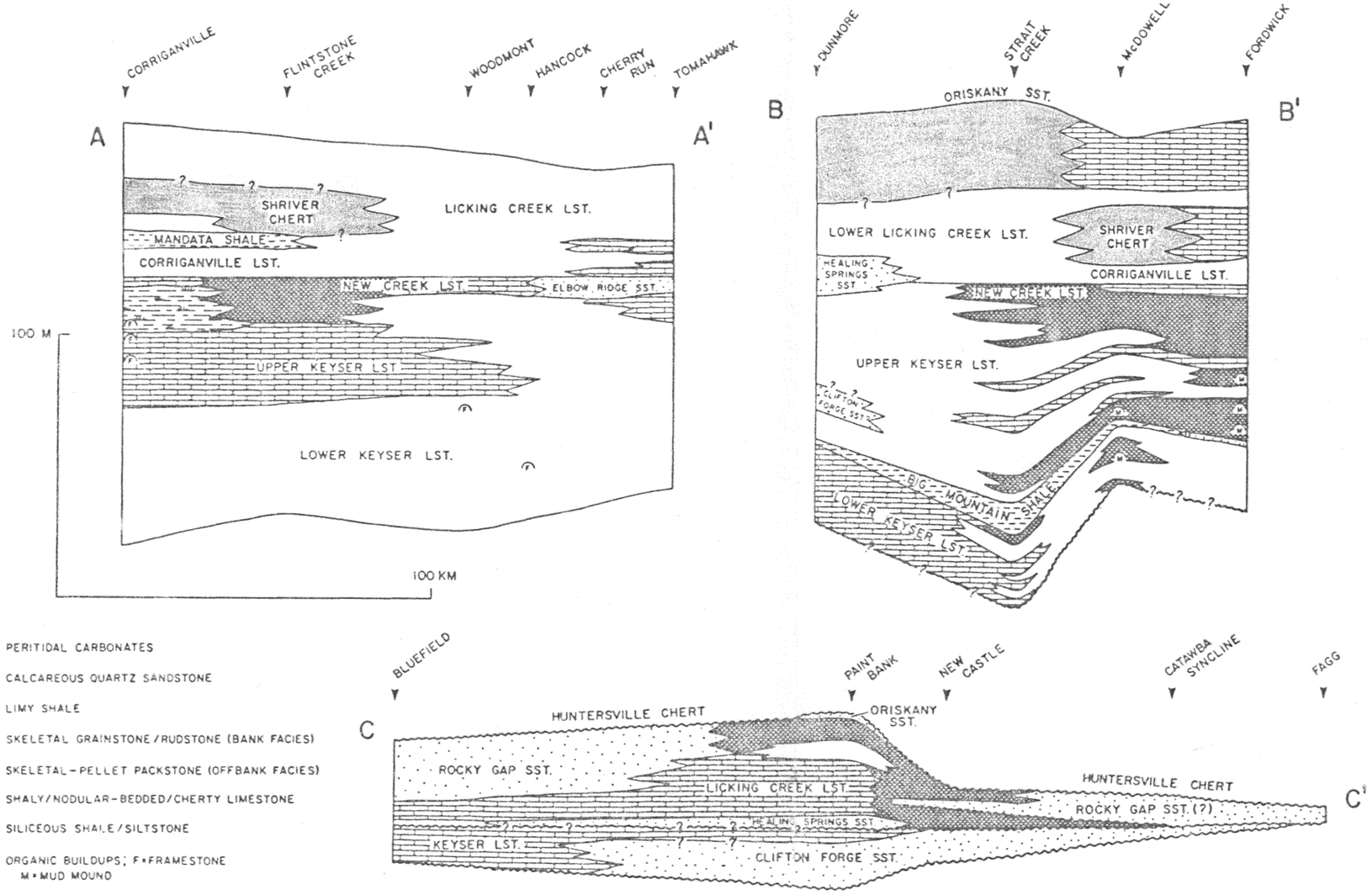
CORRIGANVILLE
FLINTSTONE CREEK
WOODMONT
HANCOCK
CHERRY RUN
TOMAHAWK
A
A'
SHRIVER CHERT
LICKING CREEK LST.
MANDATA SHALE
CORRIGANVILLE LST.
NEW CREEK LST.
ELBOW RIDGE SST.
UPPER KEYSER LST.
LOWER KEYSER LST.
100 M
100 KM
DUNMORE
STRAIT CREEK
McDOWELL
FORDWICK
B
B'
ORISKANY SST.
LOWER LICKING CREEK LST.
SHRIVER CHERT
HEALING SPRINGS SST.
CORRIGANVILLE LST.
NEW CREEK LST.
UPPER KEYSER LST.
CLIFTON FORGE SST.
BIG MOUNTAIN SHALE
LOWER KEYSER LST.
PERITIDAL CARBONATES
CALCAREOUS QUARTZ SANDSTONE
LIMY SHALE
SKELETAL GRAINSTONE/RUDSTONE (BANK FACIES)
SKELETAL-PELLET PACKSTONE (OFFBANK FACIES)
SHALY/NODULAR-BEDDED/CHERTY LIMESTONE
SILICEOUS SHALE/SILTSTONE
ORGANIC BUILDUPS; F=FRAMESTONE M=MUD MOUND
BLUEFIELD
PAINT BANK
NEW CASTLE
CATAWBA SYNCLINE
FAGG
C
C'
HUNTERSVILLE CHERT
ORISKANY SST.
ROCKY GAP SST.
LICKING CREEK LST.
HEALING SPRINGS SST.
KEYSER LST.
CLIFTON FORGE SST.
HUNTERSVILLE CHERT
ROCKY GAP SST.(?)

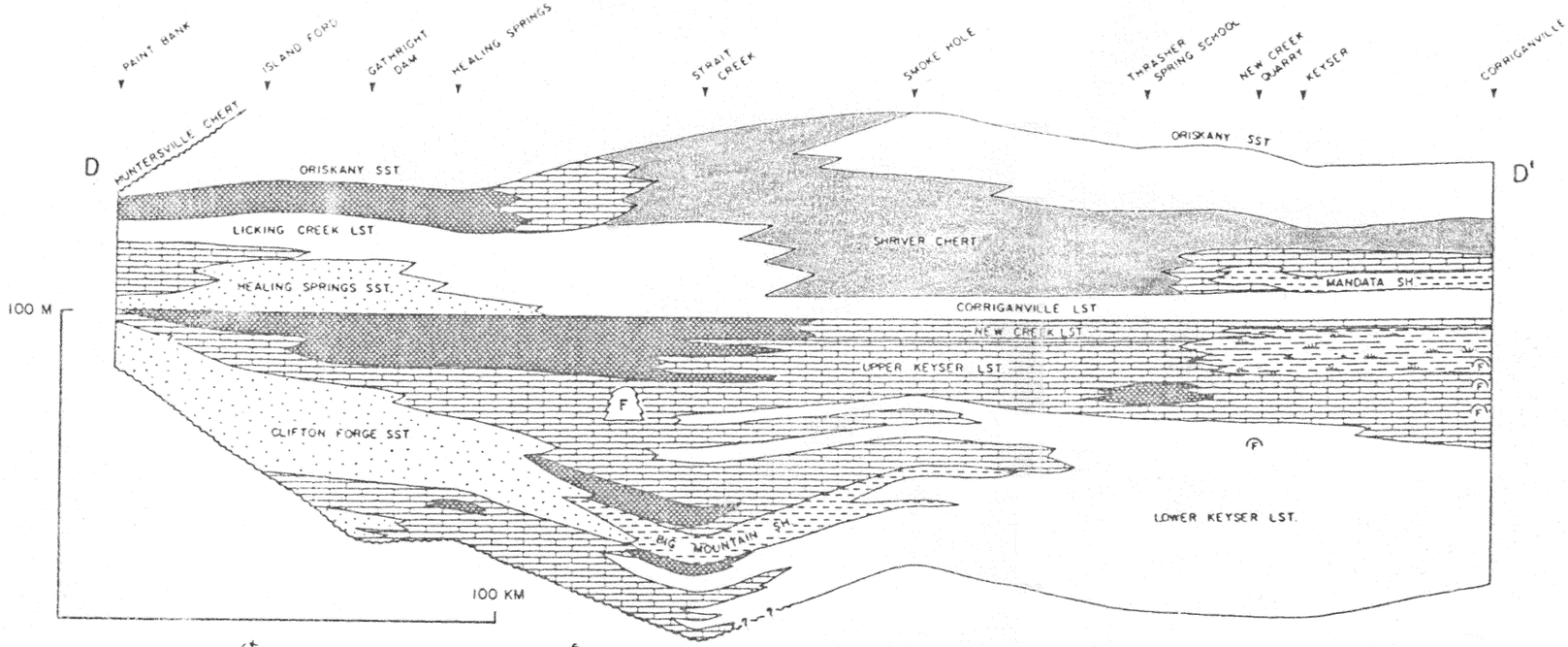
PAINT BANK
ISLAND FORD
GATHRIGHT DAM
HEALING SPRINGS
STRAIT CREEK
SMOKE HOLE
THRASHER SPRING SCHOOL
NEW CREEK QUARRY
KEYSER
CORRIGANVILLE
D
D'
HUNTERSVILLE CHERT
ORISKANY SST.
LICKING CREEK LST
HEALING SPRINGS SST.
SHRIVER CHERT
MANDATA SH
CORRIGANVILLE LST
NEW CREEK LST
UPPER KEYSER LST.
CLIFTON FORGE SST.
BIG MOUNTAIN SH.
LOWER KEYSER LST.
100 M
100 KM

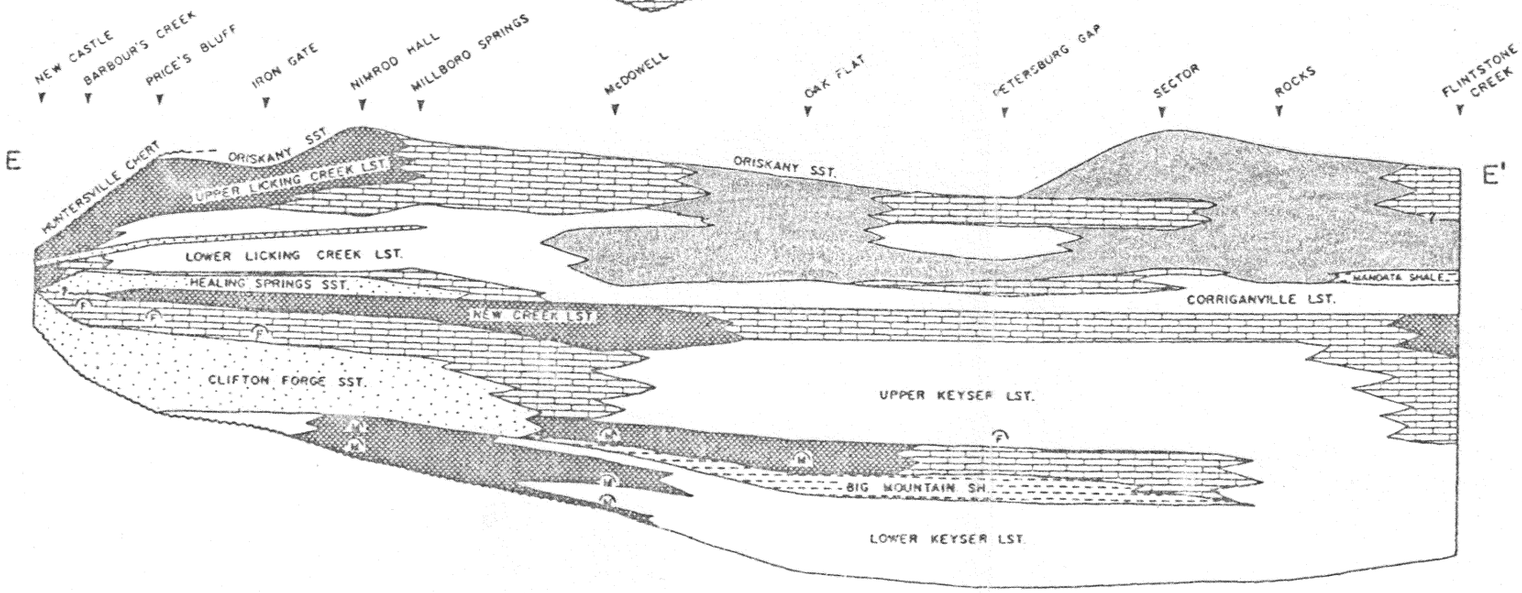
NEW CASTLE
BARBOUR'S CREEK
PRICE'S BLUFF
IRON GATE
NIMROD HALL
MILLBORO SPRINGS
McDOWELL
OAK FLAT
PETERSBURG GAP
SECTOR
ROCKS
FLINTSTONE CREEK
E
E'
HUNTERSVILLE CHERT
ORISKANY SST.
UPPER LICKING CREEK LST.
LOWER LICKING CREEK LST.
HEALING SPRINGS SST.
NEW CREEK LST.
CLIFTON FORGE SST.
MANDATA SHALE
CORRIGANVILLE LST.
UPPER KEYSER LST.
BIG MOUNTAIN SH.
LOWER KEYSER LST.

The uppermost transgressive sequence consists of deep ramp cherty limestone (Corriganville Limestone and lower Licking Creek Formation) and basin facies (Mandata Shale and Shriver Chert) that rest on the upper Keyser Formation. These units are overlain by regressive coarse-grained skeletal limestone (upper Licking Creek Formation) and near the southern basin margin, the Rocky Gap Sandstone; thin calcareous sandstone (lower Wildcat Valley Sandstone) also was deposited in southwest Virginia and Tennessee at this time (Miller et al., 1977).

Lithofacies

Peritidal Carbonate Facies

Description. Finely laminated limestone/dolomitic limestone, fenestral limestone, and skeletal-pellet limestone occur as laterally continuous units (less than 5 m thick) within the Keyser Formation (Fig. 5). These beds form thin (less than 2 m thick), upward shallowing, cyclic sequences (Fig. 6). Thick peritidal sequences are best developed in western Maryland and West Virginia and consist of interbedded cryptalgalaminite and intraclast packstone that grade basinward into and overlie cross-bedded skeletal-pellet limestone. Peritidal beds also occur in southwestern Virginia on local paleotopographic highs (shallow water bioherms and quartz sandstone lobes); lateral progradation was minimal and these beds can not be traced laterally

Figure 6. Peritidal carbonate facies.

A. Cryptalgalamanite bed overlain by intraclast-pellet packstone; note sharp erosional contact; lens cover 6 cm diameter.

B. Etched slab of cryptalgalaminite; scale in centimeters.

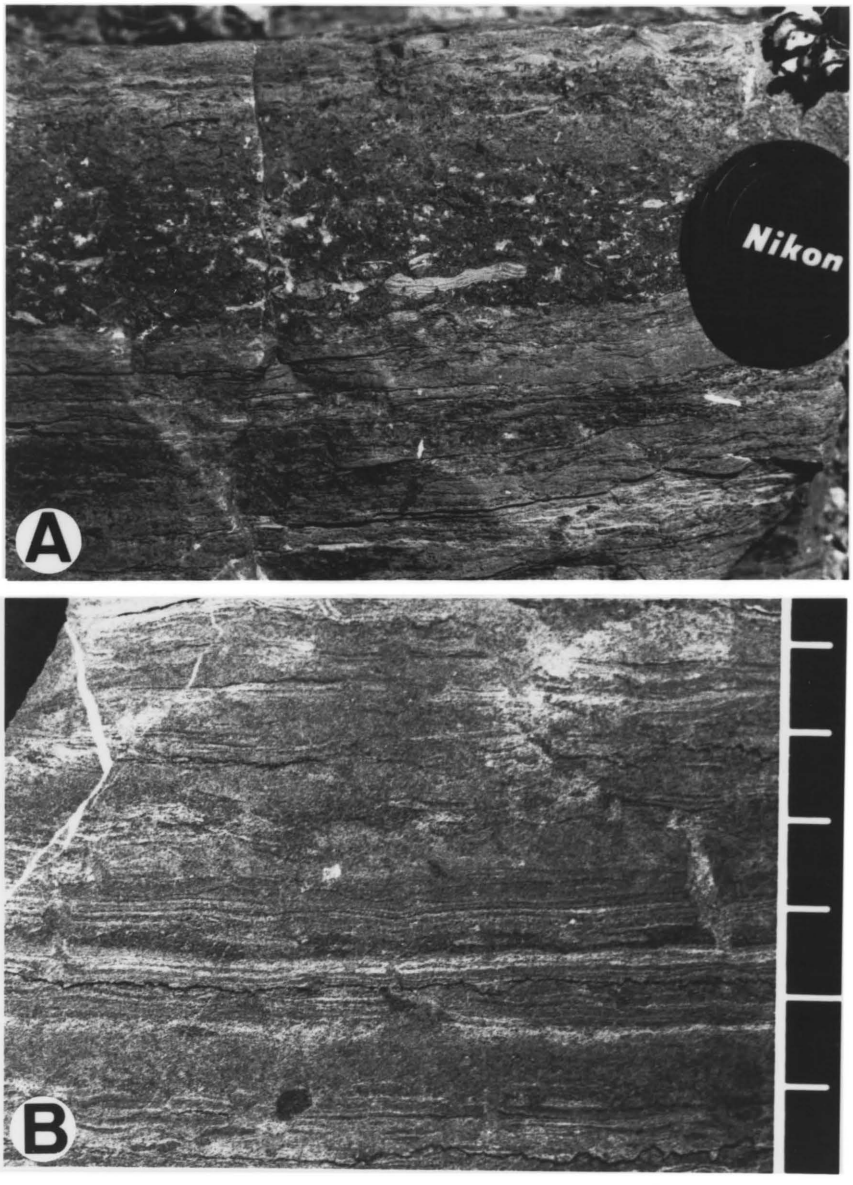
Nikon
A
B

between adjacent measured sections. Local siliciclastic tidal flat facies occur in the Clifton Forge Sandstone in southwestern Virginia (Barwis and Makurath, 1979).

Peritidal cycles consist of, from top to bottom:

Cryptalgalaminite: Lime mudstone and pellet packstone beds (10 cm to 1 m thick) with wavy, crinkly, and irregular millimeter scale lamination, locally preserved palisade structure composed of spar-filled algal filaments, shallow mudcracks, and rare deep prism cracks that occur at tops of some peritidal cycles. These may overlie fenestral lime mudstone/intraclastic layers.

Fenestral lime mudstone/intraclastic packstone: Massive lime mudstone and intraclastic packstone (20 cm to 2 m thick) are the main peritidal facies. Fenestrae include tubular, irregular, and laminar types. Intraclasts of pellet packstone/wackestone and lime mudstone form thin (less than 10 cm thick) packstone layers with sharp erosional bases. Erosional surfaces can be correlated for over 50 km in Upper Keyser peritidal carbonates of Maryland-West Virginia. Scattered subhedral to euhedral dolomite replaces lime mud in some beds. Ostracodes, microgastropods, and tentaculitids are rare.

Pellet-ostracode packstone/wackestone: Basal units of cycles consist of 40 cm to 2 m thick beds of pellet-ostracode packstone/wackestone that contain wave ripple cross-lamination, small-scale tabular and trough cross-

bedding, small scale hummocky cross-stratification, and fining-upward skeletal layers. Large leperditid ostracodes and microgastropods are scattered throughout bioturbated skeletal wackestone or occur as abraded debris in thin lags. Rare interbeds of coral-stromatoporoid framestone/floatstone also occur at bases of peritidal cycles.

Interpretation. Helderberg peritidal carbonate facies probably developed in a humid climatic setting. Desiccation features are rare, evaporite facies are absent, and cycles locally have open marine biotas.

Packstone/wackestone and local reefy beds are shallow subtidal deposits that were overlain by low energy fenestral lime mudstone and storm-deposited intraclastic sheets when sediments aggraded to tidal levels. In high intertidal areas of flats, these were overlain by cryptalgal laminite beds.

Peritidal beds in Maryland and West Virginia were deposited on regional tidal flats that prograded and thinned from west to east and indicate regional shallowing of the ramp in western Maryland during upper Keyser time. These restricted tidal flats formed behind skeletal barrier banks (New Creek Formation). Peritidal facies in Virginia developed on local paleotopographic highs during regressive periods.

Calcareous Quartz Sandstone

Description. Calcareous quartz sandstone makes up the Clifton Forge (0-45 m thick), Healing Springs (0-17 m thick), Elbow Ridge (0-7 m thick), and Rocky Gap (0-20+ m thick) Sandstones (Figs. 7, 8). They form sand lobes near the eastern shoreline and are interbedded with shallow ramp skeletal limestones (Fig. 5). In southwestern Virginia, Helderberg sandstones merge, disconformably overlie Silurian sandstone (Tillman, 1963), and ultimately pinch out to the south and east.

Calcareous quartz sandstone is cross-bedded, white to light gray, very well to moderately sorted, fine- to very coarse-grained with scattered skeletal grains and argillaceous stringers. Skeletal debris and argillaceous content increases basinward; quartz grain size decreases basinward. Quartz is well-rounded, monocrystalline, with slight undulose extinction; polycrystalline quartz and vein quartz grains are rare. Skeletal grains include crinoids, bryozoans, pelecypods, favositids, stromatoporoids, and brachiopods. Quartz and skeletal grains commomly are segregated into alternating laminae. Paleocurrents are dominantly bimodal and trend oblique to the shoreline (Fig. 9; Montgomery, 1967; Barwis and Makurath, 1978).

Sands deposited closest to the paleoshoreline ("nearshore sands") are medium to very coarse-grained and contain low-angle tabular and trough cross-beds (5-15 cm

Figure 7. Isopach map of Clifton Forge Sandstone; palinspastic base.

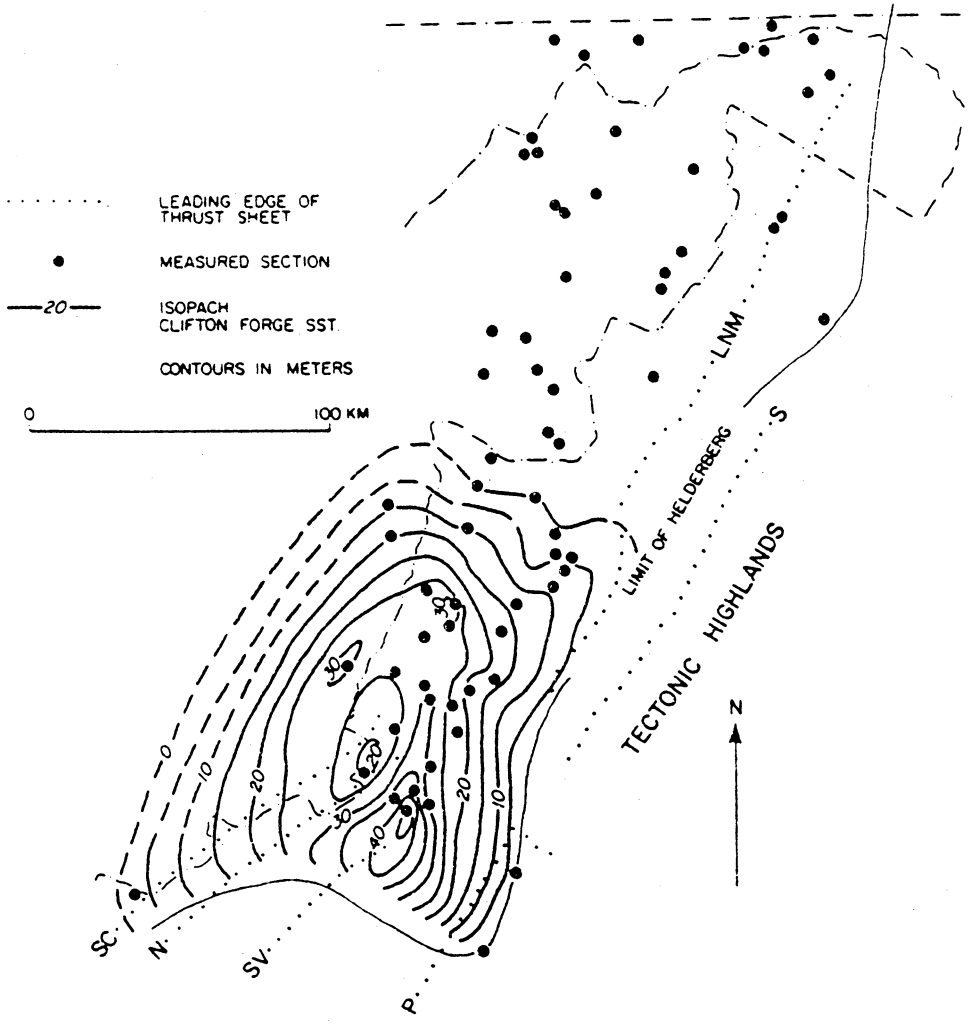
LEADING EDGE OF THRUST SHEET
MEASURED SECTION
20
ISOPACH CLIFTON FORGE SST.
CONTOURS IN METERS
0
100 KM
LNM
S
LIMIT OF HELDERBERG
TECTONIC HIGHLANDS
N
SC
N.
SV.
P.
0
10
20
30
40
50

Figure 8. Isopach maps, Healing Springs Sandstone and Elbow Ridge Sandstone; palinspastic base.

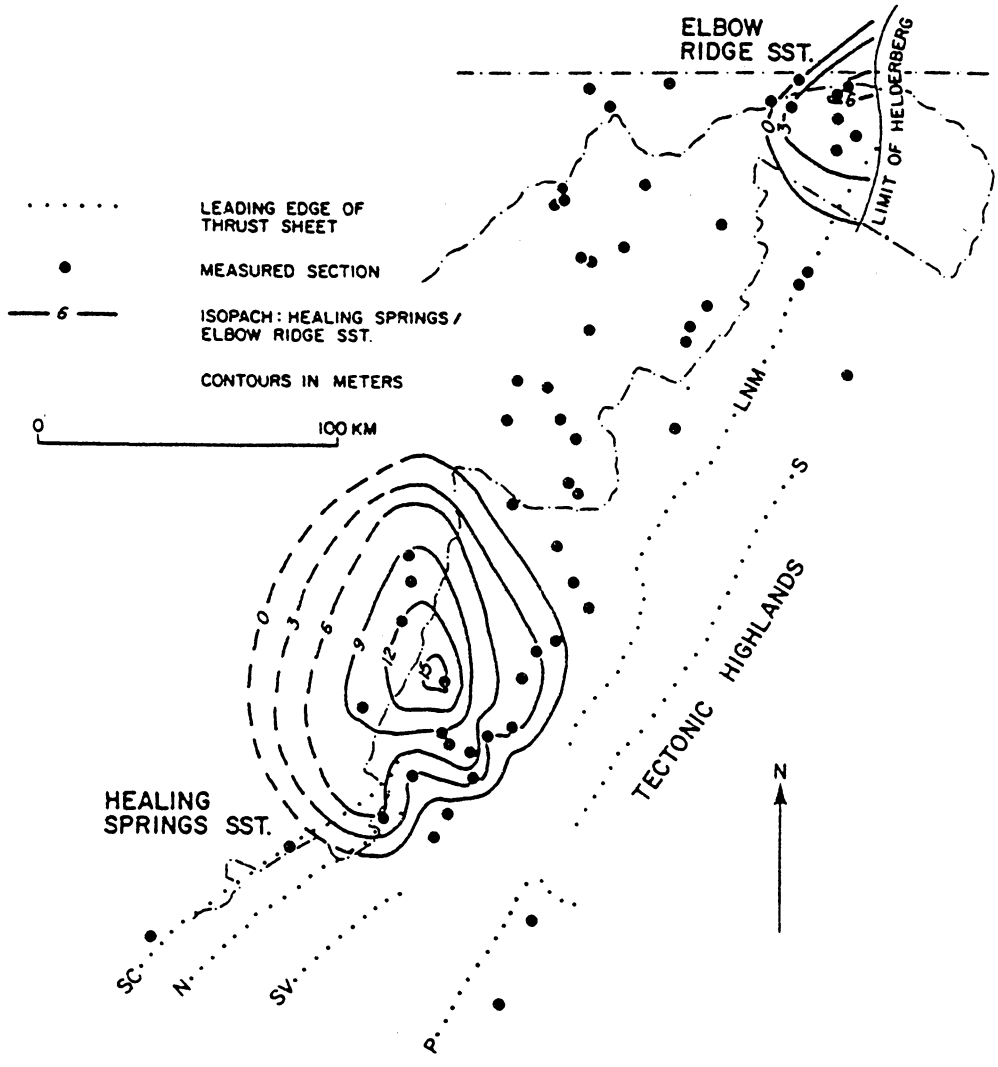
ELBOW
RIDGE SST.
LIMIT OF HELDERBERG
LEADING EDGE OF
THRUST SHEET
MEASURED SECTION
6
ISOPACH: HEALING SPRINGS /
ELBOW RIDGE SST.
CONTOURS IN METERS
0
100 KM
LNM
S
TECTONIC HIGHLANDS
N
HEALING
SPRINGS SST.
SC
N
SV
P

Figure 9. Paleocurrents, Clifton Forge Sandstone (most data from Montgomery, 1967).

CLIFTON FORGE SST.
PALEOCURRENTS

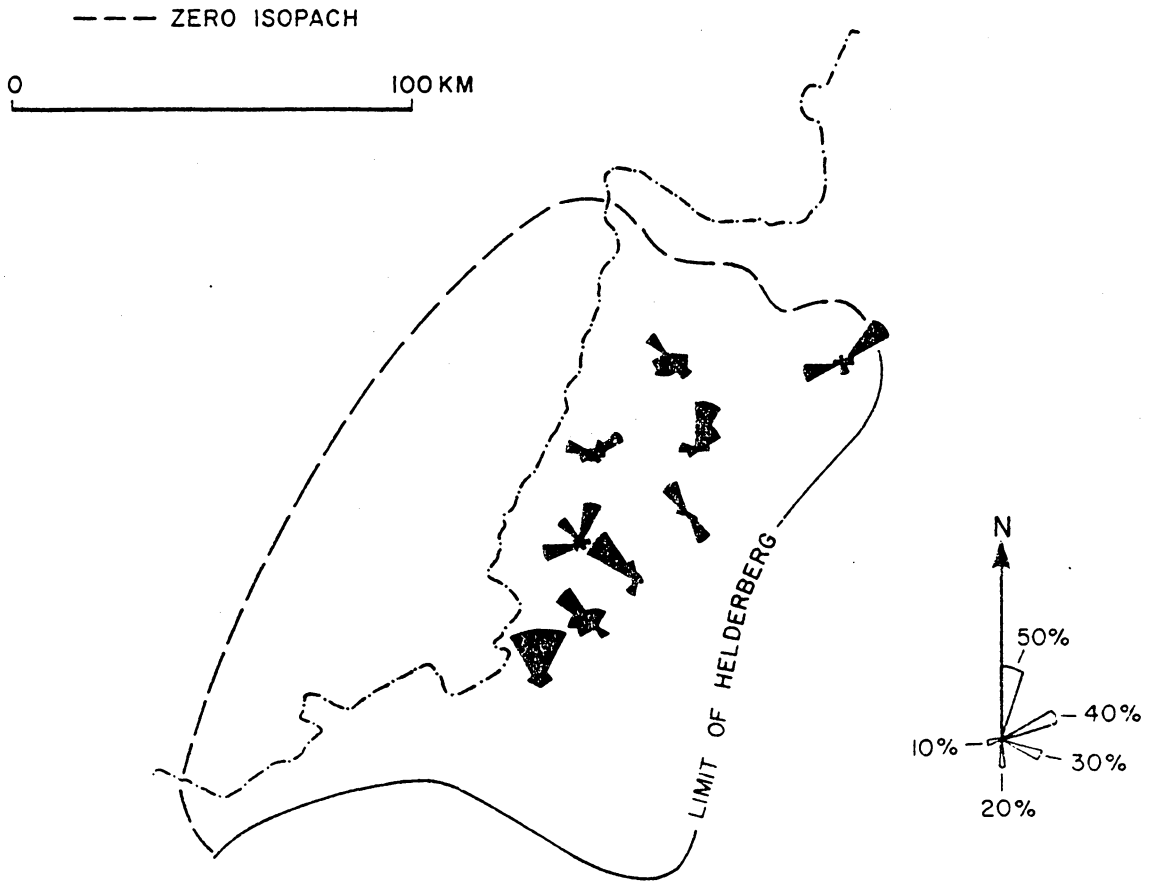

thick). They contain reactivation surfaces, tidal bundles (beds deposited during a single tidal event) with "pause planes" (Fig. 10A; Boersma, 1969; R.D. Kreisa, pers. comm., 1984), ripple cross-lamination, clay drapes and mud flasers locally, and broad scour surfaces (up to 15 cm relief) with overlying quartz pebble layers. Large scale (up to 2 m high) tabular cross-beds with foresets that dip 5-20° and opposing small scale cross-lamination that locally climbs up toeset and foreset beds also occur (Fig. 10B). Nearshore sands are nonfossiliferous to very fossiliferous with diverse biotas; vertical burrows (3-8 cm wide, 5-30 cm deep; Monocraterion ?) are rare. Thin interbeds (less than 2 m thick) of peritidal carbonate facies locally are interbedded with nearshore sands.

Sands deposited in more basinward positions are fine to medium-grained and have large scale (15-40 cm thick, up to 3 m wide) tabular and trough cross-beds that occur as wedge and lenticular sets, 1-2 m high tabular cross-beds with foresets that dip less than 5° and have interbedded small scale trough and tabular cross-beds, ramose bryozoan and Cladopora (stick corals) bafflestone pods (20-40 cm thick or wide), and broad scour troughs (2-15 cm deep, <2 m wide). These sands are very fossiliferous.

Sands deposited furthest from the paleoshoreline ("offshore sands") are fine-grained and have higher argillaceous content than other sands. They contain

Figure 10. Calcareous quartz sandstone facies.

A. Cross-bedded sandstone. Note bidirectional cross-bedding and lenticular bounding surfaces on cross-bed sets. Arrows indicate lower bounding surfaces on two "tidal bundles"; centimeter scale in lower left.

B. Large-scale tabular cross-bed foresets formed by migrating sand wave. Base at photo bottom. Note trough cross-beds at upper bounding surface. Hammer is 30 cm long.

C. Hummocky cross-stratified sandstone overlain by heavily bioturbated sandstone.

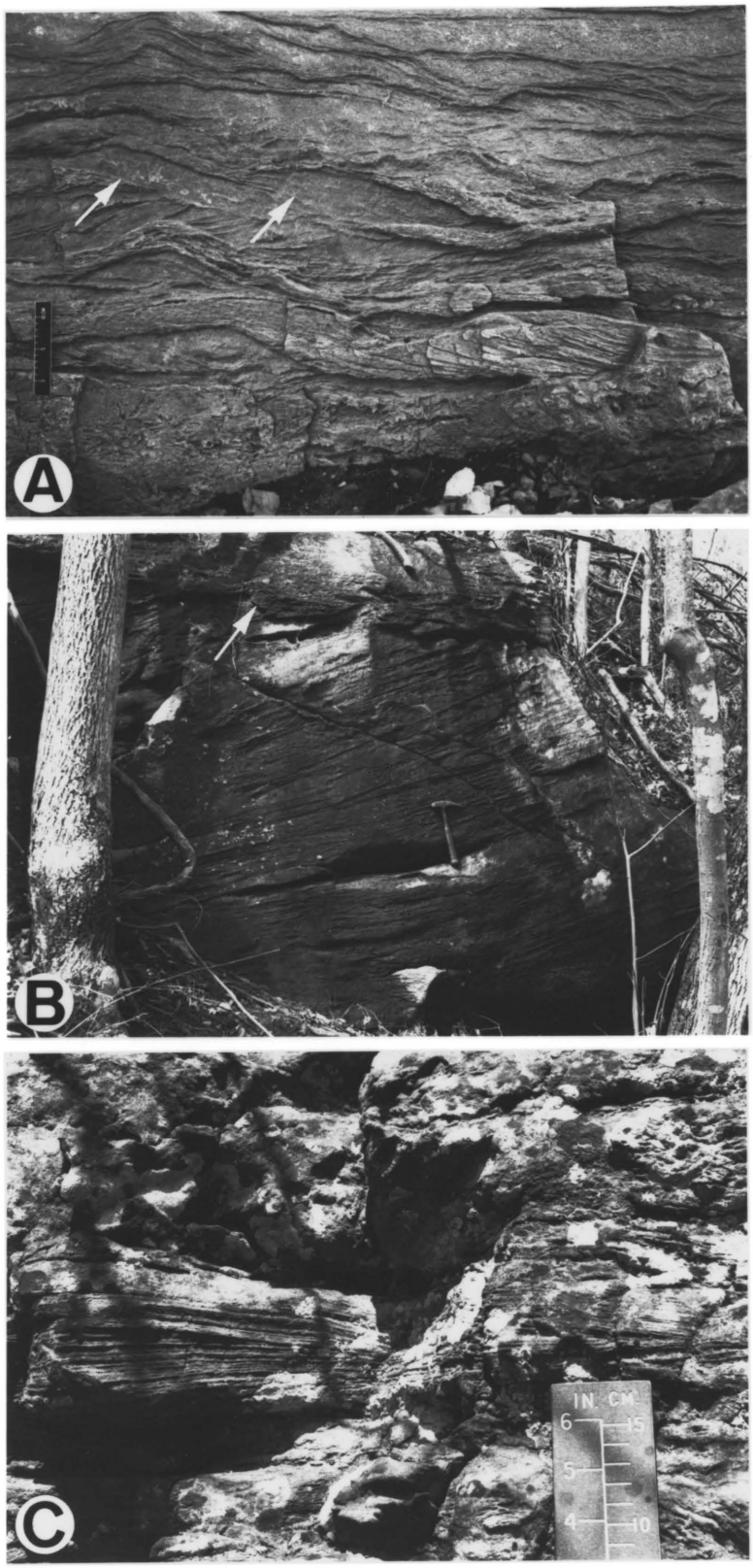
A
B
C
IN CM
6
5
4
15
10

parallel plane lamination, hummocky cross-stratification (Fig. 10C), ripple cross-lamination, and abundant burrows (some escape burrows). Offshore sands are massive and structureless where burrowing is intense. Centimeter thick glauconitic shale overlies thin (1 m thick) bioturbated, offshore sandstone beds.

Interpretation. Helderberg sands were deposited in intertidal to open shelf environments during regressions and early phases of transgressions (where sedimentation exceeded relative sea level rise). Biostratigraphic (Head, 1969; Cook, 1981; Sartain, 1981) and facies relationships (Fig. 5) indicate that lower parts of sandstones are correlative with upper parts of regressive (offlap) carbonate sequences and upper parts of sandstones are correlative with lower parts of transgressive (onlap) carbonates. During regressions, Helderberg carbonates quickly prograded basinward, followed by sandstones that prograded more slowly. During ensuing transgression, sandstone lithotopes migrated landward.

Sandstones were reworked from exposed Silurian quartz sandstone (Dennison, 1970; Tillman, 1963) and possibly from Chilhowee clastics. These clastic sources were exposed in highlands to the east. Ancestral rivers draining eastern highlands maintained nearly the same position from the Early Silurian and into the Early Devonian. Consequently, Helderberg sandstone lobes are superimposed on earlier, Silurian sandstone lobes (Dennison, 1970; Smosna and

Patchen, 1978). By Middle Devonian time, drainage systems apparently had shifted from ancestral Silurian systems (Dennison and DeWitt, 1972; Woodward, 1943).

Detailed facies analysis of Helderberg sands is beyond the scope of this study, but some generalizations can be made. Helderberg beach or fluvial-deltaic deposits are not preserved along the basin margin, possibly having been eroded or overthrust (Swartz, 1929; Dennison and Boucot, 1974).

Well-sorted, coarse, poorly fossiliferous sands with large scale, steeply dipping (angle of repose) tabular cross-beds are similar to Holocene tidal estuarine deposits in the North Sea that form from migrating sand waves (R.D. Kreisa, pers. comm., 1984). Sand waves in peritidal environments may indicate unequal ebb and flood tidal currents (Harms et al., 1975). Opposing small scale cross-lamination that climb up large scale foresets were deposited by subordinate tidal currents.

Sands that contain ripple cross-lamination, plane lamination, reactivation surfaces, clay drapes, flaser-bedding, and tidal bundles with pause planes were deposited in intertidal zones. By comparison with Holocene deposits of the North Sea, tidal bundles form on shallow sand berms in intertidal zones where tidal ranges are mesotidal to macrotidal (Boersma and Terwindt, 1981). Small scale trough and tabular cross-beds occur in fining upward sequences

locally and formed during in-fill of shallow tidal channels that swept across intertidal zones.

Shallow subtidal marine sands are fine to medium-grained with argillaceous stringers. They have diverse and abundant marine faunas (with local bafflestone patches), and storm deposits locally. Migrating sand waves (up to 2 m high) produced low-angle planar foresets; sand was transported over the sand waves by straight- and sinuous-crested megaripples as indicated by small scale trough and tabular cross-bed sets on tops and stoss sides of large scale planar foresets. Large scale trough and tabular cross-beds also were deposited by migrating megaripples.

Offshore sands were highly reworked by storms as indicated by fining upward sequences of plane lamination, hummocky cross-stratification, and ripple cross-stratification with vertical escape burrows. Massive bioturbated sands were deposited farthest offshore where burrowers destroyed all primary structures. Thin glauconitic sands formed prior to (or during) marine transgression where sedimentation rates were low and interstitial waters reducing (cf. Pryor, 1975).

Limy Shale

Description. The Big Mountain Shale (0-12 m thick) overlies shaly/nodular-bedded limestone (Lower Keyser Limestone), interfingers with the Clifton Forge Sandstone,

and is overlain by skeletal limestone (Upper Keyser Formation; Fig. 5). It is a thin-bedded, olive gray, weakly fissile, calcareous shale with lenses (less than 2 cm thick, 10 cm wide) of wave-rippled quartz or calcareous siltstone, rare whole brachiopods, ramose bryozoans, and crinoid fragments, and abundant burrows.

The Mandata Shale (0-6 m thick) overlies Corriganville Limestone (cherty limestone), interfingers with lower Licking Creek Formation (cherty limestone), and is overlain by Shriver Chert (basinal siliceous shale/siltstone) in western Maryland and northern West Virginia (Fig. 5; Head, 1974). It is a massive to fissile, dark gray to black, calcareous shale with scattered whole brachiopods, bryozoans, crinoid fragments, and networks of burrows (< 1 cm diameter) on some bedding planes. The lower part is more fossiliferous and also contains bored calcareous nodules. Unfossiliferous shale is very fissile (nonbioturbated) and darker than massive, fossiliferous shale.

Interpretation. The Big Mountain Shale formed in offshore deeper waters from the Clifton Forge Sandstone during regional regression. Suspension deposition of fines was infrequently interrupted by traction deposition of silts by wave currents.

The Mandata Shale was deposited below wave base on the deep ramp and basin during regional transgression (lower Licking Creek interval). Decreasing fossil content, darker

color, and increasing fissility towards the top of the Mandata Shale indicate waters became progressively deeper and more oxygen depleted. Sediments were probably derived from eastern highlands that bordered the basin.

Skeletal Grainstone/Rudstone (Banks)

Description. Very coarse-grained, massive to thick-bedded, pink to light gray skeletal grainstone/rudstone forms extensive sheets (3-12 m thick) near the basin margin in the Keyser, New Creek, and Licking Creek Formations (Figs. 5, 11). Bidirectional tabular and less common trough cross-bed sets (10-30 cm thick), planar lamination, gently undulatory lamination, and broad, trough-like scour surfaces are common (Fig. 12A). Sands are well-sorted to moderately sorted; sorting decreases basinward. They consist of pelmatozoan debris (locally articulated), lesser brachiopods, bryozoans, corals, and well-rounded quartz grains. Argillaceous wisps and seams and gray to black chert nodules increase basinward. Marine cement is patchily distributed. Skeletal grains commonly are silicified.

Interpretation. Skeletal grainstone/rudstone formed fringing skeletal banks along the eastern shoreline and barrier banks in western Maryland-northern West Virginia (Fig. 11). Bi-directional cross-bedding and scour troughs waves and tidal currents reworked skeletal sands. Water

Figure 11. Isolith map, skeletal grainstone/rudstone bank facies, Helderberg Group.

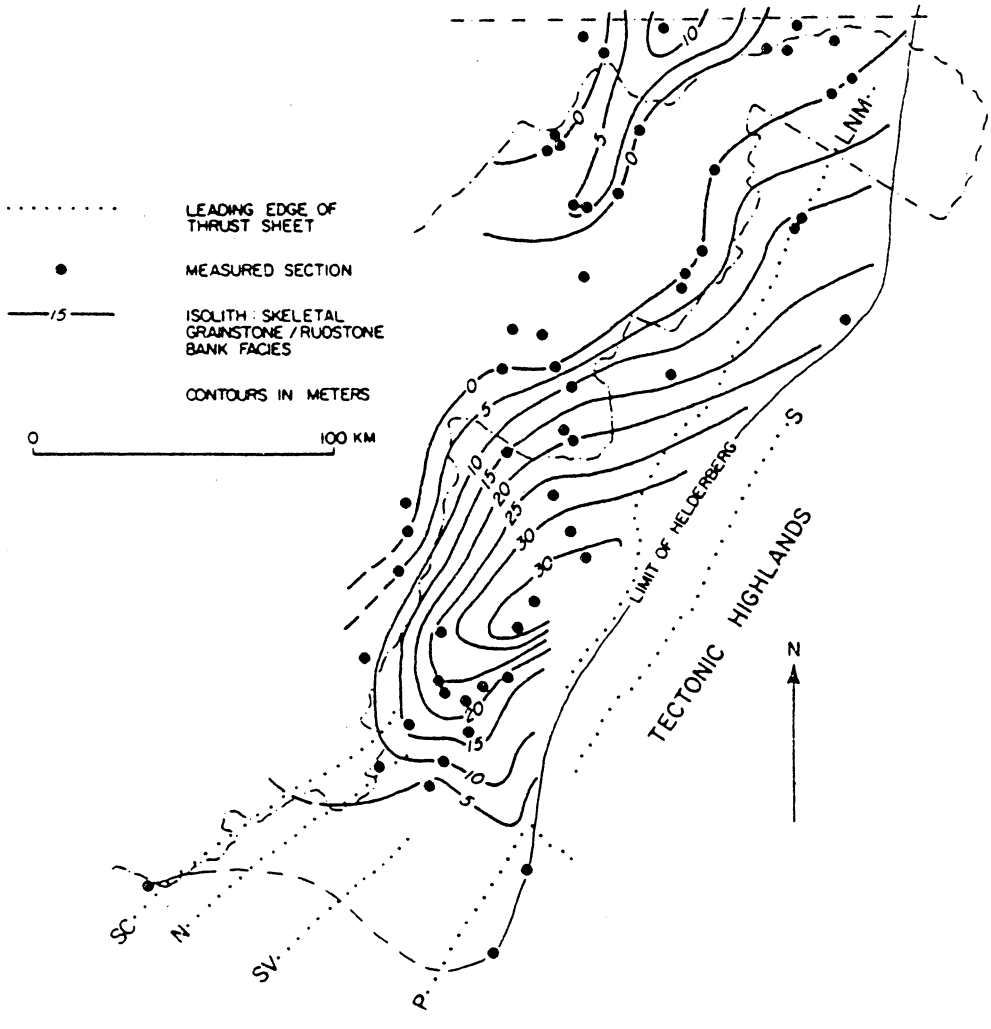
LEADING EDGE OF THRUST SHEET
MEASURED SECTION
15
ISOLITH : SKELETAL GRAINSTONE / RUDSTONE BANK FACIES
CONTOURS IN METERS
0
100 KM
LNM
LIMIT OF HELDERBERG
TECTONIC HIGHLANDS
N
S
SC
N
SV
P

Figure 12. A. Cross-bedded skeletal grainstone/rudstone, Upper Keyser Formation. Note trough cross-beds, left center. Hammer (45 cm long) for scale.

B. Mud mound (outlined in black) interbedded with quartz-rich skeletal grainstone. Arrow indicates coral colony at mound cap. Hammer (30 cm long) for scale.

C. Stromatoporoid framestone. Stromatoporoids partially silicified. Hammer (45 cm long) for scale.


A


B


C

depths were probably less than 15 m (calculated from slopes on the platform). Pelmatozoans produced much of the skeletal detritus and locally stabilized skeletal sand substrates to form thick coarse sands in high energy, open marine areas. Scarcity of burrows suggests sediments were constantly reworked and that high energy mobile sands and/or lack of organic detritus inhibited burrowers.

Buildup Facies

Description. Organic buildups in the Helderberg Group occur as mud mounds and coral-stromatoporoid framestone mounds. Buildups were observed only in the Keyser Formation (Fig. 5).

Mud mounds occur close to the basin margin in the lower Keyser Formation as isolated buildups and small irregular pods that interfinger with thick skeletal grainstone/rudstone facies (Figs. 5, 12B). Isolated buildups are 2-25 m thick, 3-50 m wide and consist of skeletal wackestone and mudstone capped by stromatoporoid boundstone. In situ fascilloid corals, encrusting stromatoporoids and bryozoans, ramose bryozoans, articulated crinoid columnals, and very rare Halysites acted as sediment binders and bafflers in these mounds. Other skeletal grains include ostracodes, small gastropods, brachiopods, and rare trilobites and coralline algae. Small, irregular pods (20 cm to 1 m thick or wide) of lime mudstone and skeletal

wackestone interfinger with massive grainstone/rudstone facies and mainly contain crinoid fragments. Stromatactoid cavities are common in isolated mud mounds; they have flat floors of lime mud or pelletal sediment and often have isopachous linings of turbid neospar cement. Mud mounds are heavily bioturbated and contain bored hardgrounds.

Coral-stromatoporoid framestone buildups occur basinward of mud mounds. They form biostromes (1-3 m thick by 30 to over 50 m wide) and bioherms (2-13 m thick by 5 to over 50 m wide) that interfinger with deeper ramp, nodular-bedded skeletal limestone (Figs. 5, 12C). Ecological zonation is well-developed only in large framestone buildups (see Smosna and Warshauer, 1979). Framestone buildups may be capped by erosional surfaces which are overlain by peritidal carbonate facies. The largest exposed framestone buildup occurs at Mustoe, Virginia (Smosna and Warshauer, 1979). Large hemispherical, nodular, and rare branching stromatoporoids are the dominant frame builders. Nodular and tabular Favosites, stick-like Cladopora (corals), and rare rugose corals and articulated pelmatozoans grew between large stromatoporoids. Ostracodes, bryozoans, brachiopods, gastropods, and trilobites are scattered in the interframe argillaceous lime mud. Frame builders are heavily bored. Marine cementation in framestone buildups is minor; fossils commonly are replaced by silica and saddle dolomite.

Interpretation. Mud mounds in the lower Helderberg Group generally developed during regressive phases (Fig. 5). The association of mud mounds with tidally reworked grainstone/rudstone facies and their occurrence nearshore indicate that they developed in high energy, shallow subtidal environments (<15 m water depth). They probably formed where thickets of stalked and encrusting organisms created local, quiet energy environments where lime mud could be baffled and trapped.

Framestone buildups formed in more basinward positions than mud mounds. Thus their faunas are more diverse and they are interbedded with nodular-bedded limestone. They were initiated during regional offlap in deeper water, more open marine subtidal conditions. Some buildups grew upward into shallow water and were ecologically zoned. Growth ceased when they shoaled to sea level, or when they were exposed during sea level drops which allowed local progradation of peritidal facies over buildups.

Skeletal-Pellet Packstone (Offbank Facies)

Description. Irregularly thin- to thick-bedded, light gray, fine- to medium-grained, locally argillaceous skeletal-pellet packstone (Keyser Limestone, Corriganville Limestone, upper Licking Creek Formation) occurs basinward of correlative skeletal grainstone/rudstone facies and stratigraphically between deep ramp carbonates (Fig. 5).

Packstone consists dominantly of poorly sorted and abraded skeletal debris (crinoids, brachiopods, ramose bryozoans, and rare trilobites), pellets, and scattered whole fossils (brachiopods, corals, and rare stromatoporoids). Many corals and stromatoporoids are overturned. Pellets are 20 to 250 micron diameter grains and include small ovoid pellets in shelter voids or lining burrows and large irregularly shaped pellets that probably are micritized skeletal grains. Oncolites (up to 2.5 cm diameter) form thin beds that can be correlated over 30 km. Most skeletal-pellet packstones are heavily bioturbated and structureless, with local, gently undulatory to planar parallel lamination and low-angle tabular cross-beds.

Interpretation. Skeletal-pellet packstones formed in shallow subtidal offbank environments that were inhabited by diverse open marine biotas, in water depths of 15-25 m. Oncolites indicate the sea floor was within the photic zone. Storm-generated currents reworked sediments, but abundant infauna reworked sediments between storm events so that storm-generated deposits (rare undulatory to planar laminated beds) are only locally preserved.

Shaly/Nodular-bedded/Cherty Limestone

Description. Nodular-bedded, shaly, or cherty limestone are the main Helderberg lithofacies in the area. Nodular-

bedded limestone is dominant in the lower Keyser Formation; shaly limestone and nodular-bedded limestone are abundant in the upper Keyser Formation; cherty limestone forms the Corriganville Limestone and lower Licking Creek Formation (Fig. 5).

Shaly limestone (0-12 m thick) consists of skeletal sand lags, pellet packstone, bryozoan bafflestone, and limy shale. Skeletal sands and laminated pellet packstone form 5-15 cm thick fining-upward couplets with sharp, erosional bases and tops that grade upward into overlying 3-10 cm thick, olive gray, calcareous shale layers. Limestone layers pinch and swell and may pinch out laterally over a few meters. Lamination in pellet packstone resembles small scale hummocky cross-stratification (Harms, et al., 1975). Vertical burrows (0.5-1.0 cm wide) locally extend downward from shale layers into laminated layers. Limy shales are weakly fissile (bioturbated?), have rare lenses (less than 1 cm thick, 5 cm wide) of wave-rippled pelletal limestone and scattered whole fossils.

Thin, stick-like ramose bryozoans form patches (5 cm thick, up to 1 m wide) of bafflestone in thicker shale layers (Fig. 13A). They consist of flat-lying, in place, monospecific bryozoans in shale matrix. Small brachiopods and tentaculitids also occur as local monospecific patches in limy shale.

Figure 13. Deep ramp facies.

A. Ramose bryozoan bafflestone. Field of view approximately 10 cm wide.

B. Nodular-bedded argillaceous skeletal wackestone and lime mudstone. Hammer (45 cm long) for scale.

C. Cherty limestone; modular-bedded chert weathers out in relief. Hammer (45 cm long) for scale.

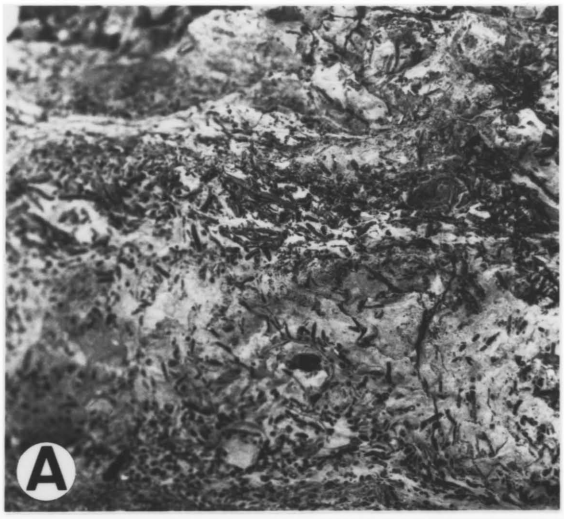
A

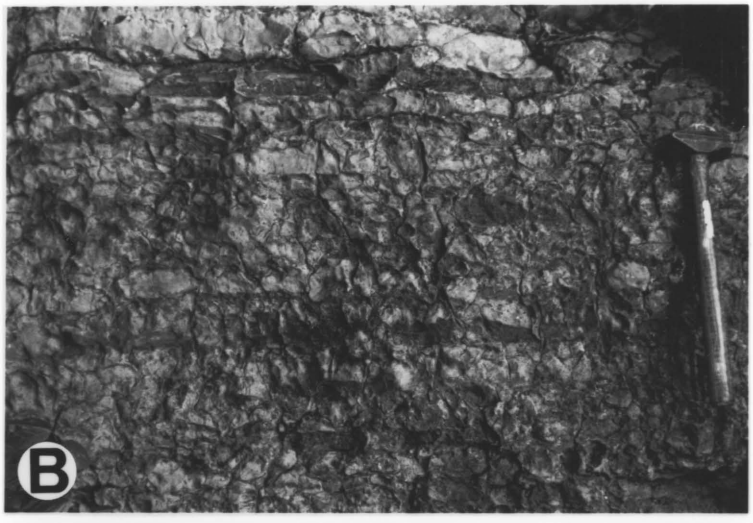
B


C

Nodular-bedded limestone (0-20 m thick units) consists of medium to dark gray skeletal-pelletal wackestone and mudstone with some skeletal packstone (Fig. 13B). Nodular beds have dark, argillaceous wisps and seams (less than 1 cm thick) and are heavily burrow-homogenized with branching networks of 0.5-1 cm wide burrows; rare horizontal lamination is preserved locally. Skeletal grains are very poorly sorted and include crinoid, brachiopod, and trilobite fragments, encrusting and ramose bryozoans, favositid corals, ostracodes, tentaculitids, rhynchonellid brachiopods, pelecypods, and stromatoporoids. Intraclasts overlie erosional surfaces cut into skeletal wackestone and mudstone. Hardgrounds are common.

Cherty limestone (2-25 m thick; Fig. 13C) is medium to dark gray, poorly sorted, skeletal wackestone and mudstone with irregularly bedded nodular chert and highly irregular, dark gray to black shaly interlayers. Chert is light gray to white in the Corriganville Limestone and gradually becomes darker gray to black upward into the lower Licking Creek Formation (possibly reflecting an increase in organic content into the Licking Creek Formation). Faunas resemble those in nodular-bedded and shaly limestone but contain numerous large, robust, articulated brachiopods, rugose corals, and sponge spicules; many fossils are silicified. This facies is burrow-homogenized with some preserved networks of 0.5 to 2 cm wide burrows; rarely there are

poorly preserved undulatory to planar parallel lamination and 2-10 cm thick skeletal lags with sharp bases.

Interpretation. Nodular-bedded limestone, shaly limestone, and cherty limestone were formed in deeper ramp settings below fair-weather wave base. This is indicated by their basinward location, lack of shallow water sedimentary structures, poor sorting, high argillaceous content, diverse open marine fauna, abundant whole fossils, extensive bioturbation, and local preservation of storm-generated structures (cf. Kreisa, 1981). Water depths were approximately 25-50 m.

Shaly limestone probably was deposited in shallower water than nodular-bedded or cherty limestone. Shaly limestone consists of storm-generated layers (interbedded limy shales and fining-upward, laminated skeletal-pellet limestone; cf. Kreisa, 1981). Burrows are concentrated in shale layers and only locally penetrate skeletal-pellet layers.

Storm deposits such as those in shaly limestone have highest preservation potential where they formed below fairweather wave base in shallow areas where bioturbation was minor. Farther offshore, sediment that was below storm wave base was burrow-homogenized by the abundant infauna to form nodular-bedded limestone.

Pelmatozoan sand and minor quartz sand in shaly limestone was derived from shallow ramp environments and

transported up to 80 km (palinspastic) offshore by storm currents. This is suggested by absence of pelmatozoans in shale layers (bryozoan/brachiopod dominated). Bryozoan bafflestone and brachiopod lenses in limy shale probably were local sea floor communities that were not reworked by storm currents.

Nodular-bedded limestone was deposited below storm wave base in deeper water. Locally preserved lamination and shell lags resulted from infrequent, extreme storms. Early cementation of limestone "nodules", compaction, and pressure-solution formed nodular bedding (Shinn et al., 1977; Wanless, 1979). Hardgrounds and darker color in nodular-bedded limestone also indicate slower deposition rates and less oxidizing, deeper water conditions.

Cherty limestone was probably deposited on the deepest part of the ramp during a major transgression in middle Helderberg time (Fig. 5). This is suggested by high argillaceous content, dark color, heavy bioturbation, diverse and robust faunas, basinal location, and stratigraphic position between underlying skeletal limestone (skeletal packstone/shaly limestone/nodular-bedded limestone) and overlying basin facies (siliceous shale/siltstone). Siliceous sponge spicules probably were the major source of silica for the chert. Rare shell lags and laminated layers formed during infrequent major storms.

Siliceous Shale/Siltstone

Description. Siliceous shale and siltstone comprises the basinal Shriver Chert (30-55 m thick; Fig. 5) in western Maryland and northern West Virginia. It overlies the Mandata Shale and is laterally equivalent to the Licking Creek Formation and lower Oriskany Sandstone (Head, 1974). The Shriver Chert becomes less cherty and more calcareous upwards.

The Shriver Chert and Mandata Shale consist of massive to thin-bedded or nodular, dark gray to black, siliceous shale and calcareous to quartzose siltstone. Siltstone occurs as thin- to medium-bedded, structureless layers interbedded with siliceous shale in the upper Shriver Chert. This facies is heavily bioturbated (mainly branching burrow networks) and contains rare, silicified, robust brachiopods, pelecypods, trilobites, and corals. Rare small scale hummocky cross-stratified siltstone layers occur in the upper Shriver Chert.

Interpretation. Siliceous shale formed in the basin during late Helderberg transgression. Lack of sedimentary structures, faunas, and dark color indicate sub-wave base, deep water conditions (slopes on the ramp indicate >50 m).

Stratigraphic relations indicate that the Shriver Chert formed during Late Helderberg regression. Rare hummocky cross-stratified siltstone in the upper Shriver Chert

indicates transport of silt into the deep basin by infrequent storms during Late Helderberg regression.

Basin Evolution

The Helderberg Group forms a series of transgressive-regressive sequences that developed in response to basinwide changes in relative sea level caused by eustatic sea level changes and/or basin subsidence (Figs. 5, 14). Sediment distribution patterns were drastically affected by slight changes in relative sea level because of low slopes on the ramp.

Stage 1: Deposition of the Helderberg Group commenced with regional transgression (Head, 1969; Smosna and Patchen, 1978) and began earlier in the Central Appalachians than in New York, New Jersey, and Pennsylvania (Head, 1969) probably because of increased subsidence in the southern part of the basin. Open marine carbonates of the lower Keyser Formation were deposited on restricted evaporites and tidal flat carbonates (Tonoloway Formation) during the transgression. The Keyser-Tonoloway contact is gradational basinward and indicates continuous sedimentation during Upper Silurian time. However, the contact is an erosional disconformity with crude paleosols where it is exposed in southwest Virginia and indicates that Tonoloway rocks were exposed subaerially along the eastern side of the basin prior to lower Keyser deposition. Thick grainstone/rudstone with

Figure 14. Paleogeographic maps showing distribution of depositional environments during stages of Helderberg Group deposition. Dots are reference localities: B, Bluefield; C, Catawba; PB, Price's Bluff; F, Franklin; P, Petersburg Gap; K, Keyser; H, Hancock. Location of framestone buildups (F) and mud mounds (M) are approximate; framestone buildups and mud mounds not to scale.

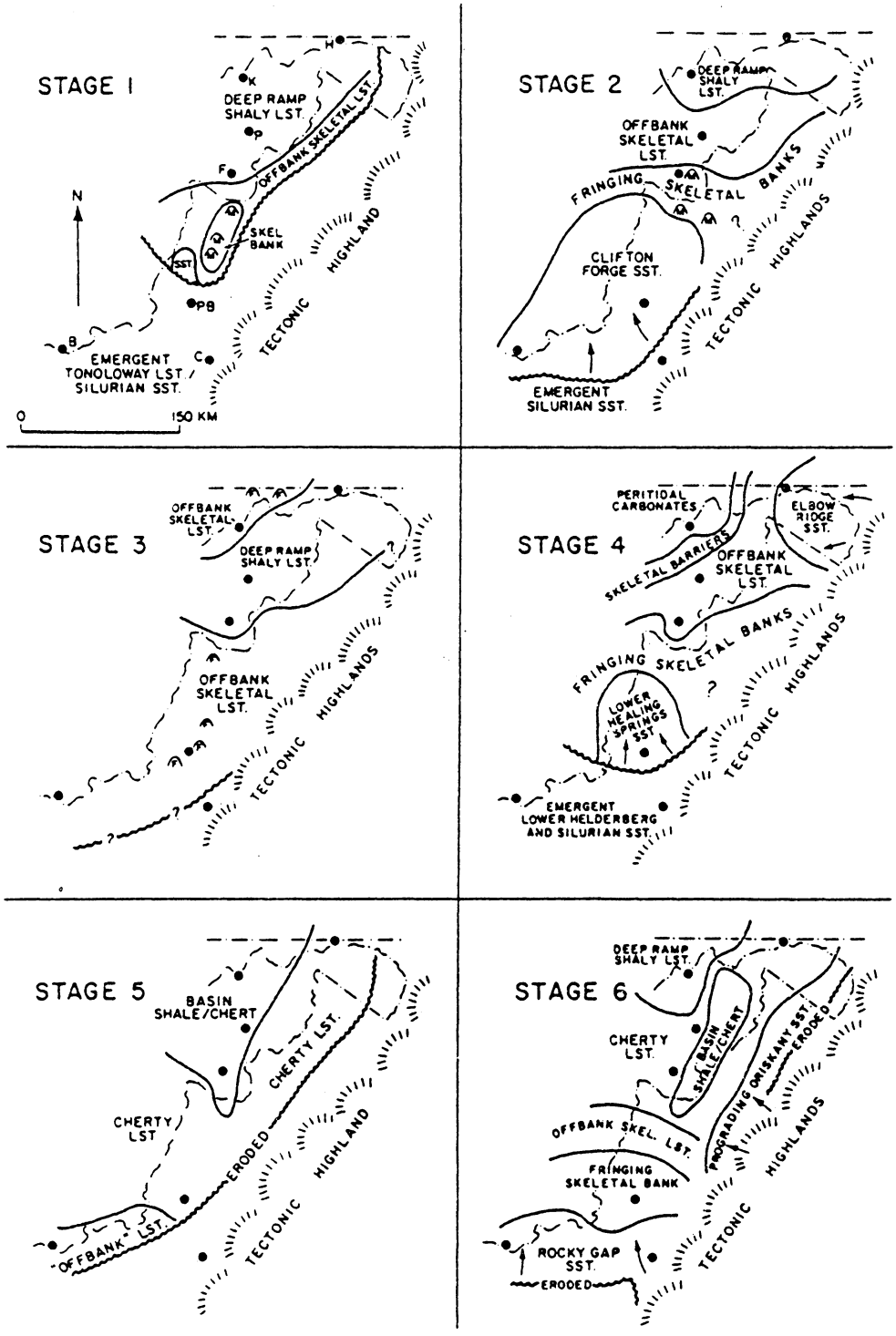
STAGE 1
DEEP RAMP SHALY LST.
OFFBANK SKELETAL LST.
SKEL BANK
SST
TECTONIC HIGHLAND
EMERGENT TONOLOWAY LST / SILURIAN SST.
0
150 KM
STAGE 2
DEEP RAMP SHALY LST.
OFFBANK SKELETAL LST.
FRINGING SKELETAL BANKS
CLIFTON FORGE SST.
TECTONIC HIGHLANDS
EMERGENT SILURIAN SST.
STAGE 3
OFFBANK SKELETAL LST.
DEEP RAMP SHALY LST.
OFFBANK SKELETAL LST.
TECTONIC HIGHLANDS
STAGE 4
PERITIDAL CARBONATES
ELBOW RIDGE SST.
SKELETAL BARRIERS
OFFBANK SKELETAL LST.
FRINGING SKELETAL BANKS
LOWER HEALING SPRINGS SST.
TECTONIC HIGHLANDS
EMERGENT LOWER HELDERBERG AND SILURIAN SST.
STAGE 5
BASIN SHALE/CHERT
CHERTY LST.
CHERTY LST
ERODED
OFFBANK LST.
TECTONIC HIGHLAND
STAGE 6
DEEP RAMP SHALY LST.
CHERTY LST.
BASIN SHALE/CHERT
PROGRADING ORISKANY SST.
ERODED
OFFBANK SKEL. LST.
FRINGING SKELETAL BANK
ROCKY GAP SST.
ERODED
TECTONIC HIGHLANDS

associated mud mounds were deposited near the basin margin and aggraded vertically to form barrier skeletal banks that interfingered basinward with bioturbated, nodular-bedded limestone. Lagoonal facies (nodular-bedded skeletal packstone) developed locally behind barrier sands along the basin margin.

Stage 2: Nearshore calcareous quartz sandstone (Clifton Forge Sandstone) and equivalent deep ramp shale (Big Mountain Shale) were deposited over the lower Keyser Formation during regression. Sedimentary structures and bimodal paleocurrents indicate tidal currents (that trended subparallel to the basin axis) reworked quartz sand that was derived from low-relief highlands along the eastern basin margin. After cessation of siliciclastic influx into the basin, skeletal grainstone/rudstone and skeletal-pellet grainstone/packstone formed sand sheets that extended nearly to the basin center.

Stage 3: Basinwide transgression caused onlap of deeper ramp skeletal limestone over Clifton Forge Sandstone/Big Mountain Shale. Minor siliciclastics were deposited in the basin during early stages of the transgression. As clastic influx decreased skeletal-pellet grainstone/packstone and reefal biostromes were deposited over the Clifton Forge Sandstone. Deep ramp and basinal shaly limestones were reworked by storms, indicating greater storm influence during this transgression than during initial basin flooding (Stage 1).

Stage 4: Shallow marine sediments prograded over deeper ramp facies during basinwide regression. New Creek skeletal grainstone/rudstone formed extensive skeletal sheets bordering the basin in Virginia. Skeletal barrier banks (New Creek Formation) in western Maryland were overlain by peritidal carbonates (uppermost Keyser Formation) These tidal flats prograded (and thinned) from west to east during regional shallowing of the ramp. Shallowing also allowed calcareous quartz sandstone to be deposited along the eastern basin margin (Elbow Ridge Sandstone-eastern West Virginia; Healing Springs Sandstone-southwest Virginia) during later stages of the regression. Most of southwest Virginia was probably emergent throughout this stage.

Stage 5: Gradual basinwide transgression caused onlap of cherty limestone (Corriganville Limestone-lower Licking Creek Limestone) and basin facies (Mandata Shale-lower Shriver Chert) over New Creek Limestone and Healing Springs Sandstone. Most of southwest Virginia probably was emergent at this time (as suggested by erosional pinchout of units).

Stage 6: Final Helderberg deposition occurred during basinwide regression. Thick skeletal grainstone/rudstone and skeletal-pellet grainstone/packstone (upper Licking Creek Limestone) offlapped over cherty limestone. Basin facies (upper Shriver Chert) became siltier, more fossiliferous, and were influenced more by storms. Lower

Oriskany, Rocky Gap, and parts of Wildcat Valley Sandstones were deposited near the basin margin (Head, 1969; Jones, 1982; Miller et al., 1977). Southwest Virginia again became emergent as indicated by missing Oriskany Sandstone. This was followed by deposition of the thick Middle Devonian-Mississippian clastic wedge in the basin after renewed tectonic uplift of highlands to the southeast during the Acadian Orogeny.

Discussion

The Helderberg Group was deposited in a basin whose overall geometry was inherited from the Cambro-Ordovician passive margin basin that persisted into the Late Paleozoic (Colton, 1970; Read, 1980). To the south, Late Silurian-Early Devonian sediments were not deposited because of limited post-Ordovician subsidence.

The Helderberg Group is a third order Vail cycle, approximately 8 to 10 m.y. duration. It is bounded by unconformities at the base and top, reflecting low sea level stand during Late Silurian (Tonoloway time), followed by transgression and initiation of Helderberg deposition, which was terminated by sea level drop at the end of the Early Devonian. This third order cycle contains three smaller scale transgressive-regressive cycles (each 2 to 3 m.y. duration), which are marked by transgressive, upward-deepening sequences, followed by regressive offlap of

shallow water facies. Regressive facies are barrier and fringing banks, along with shallow marine quartz sands derived from tectonic uplands along the eastern basin margin.

The carbonate ramp built out cratonward from eroded Taconic highlands which represent the accretionary prism from Ordovician collisional orogeny. Slopes on the ramp were 10 to 15 cm/km, which are similar to slopes on modern ramps such as the Persian Gulf and Shark Bay (Purser, 1973; Logan et al., 1974). Maximum water depths in the basin during Helderberg deposition were about 60 m. Subsidence rates of about 1 to 2 cm/1000 years are extremely low values for foreland basins, but are compatible with the tectonically quiescent period of the Silurian-Early Devonian. Rates of progradation of the shallow water banks during regressive events were about 35 to 50 m/1000 years, using palinspastic width of the banks and assuming regression occurs during the last half of the cycle (i.e., over 1 to 1.5 m.y. duration).. Actually, the regressive events may have started earlier, which would make the progradation rates even slower. Modern fringing/barrier banks may prograde at rates of 200 m to 1 km/1000 years (Davies, 1970; J.F. Read, pers. comm., 1984). The much lower rates of Helderberg bank progradation may reflect the lower rates of carbonate production on the Devonian banks, perhaps reflecting absence of photosynthetic seagrasses that

dominate modern banks and provide favorable habitats for bank-building skeletal organisms.

Tidal flat caps are rare on the regressive cycles, which is surprising in view of the large scale progradational sequences. Progradation of sequences probably resulted from long-term sea level oscillation superimposed on gradual teconic subsidence. Given 2 to 3 m.y. cycles, by the time one-half period of the sea level oscillation had elapsed (1 to 1.5 m.y.), approximately 15 to 30 m of subsidence would have occurred. For the 30 to 45 m thick cycles (of which 15 to 30 m is due to basin subsidence), the remaining 15 m would be due to filling to the sea level highstand, suggesting that the sea level oscillation amplitudes were about 15 m. During regression, sea level would drop at the rate of about 1 m/1000 years. Given the slopes of 10 cm/km for the ramp, this would mean that tidal flats would have to prograde at rates of 10 km/1000 years, which is far greater than most modern flats prograde (1 to maximum of 5 km/1000 years; Read et al., in prep.). Thus, during regressive events, tidal flats would be stranded near the basin margin early in the regressive event, and only skeletal and quartz sand facies would prograde seaward. Consequently, the 2 to 3 m.y. cycles lack tidal flat caps. This implies that updip areas may be up to 15 m higher than downdip regions, although sedimentary evidence for this is not obvious.

Final drowning of the Helderberg carbonates resulted from increased downwarping and relative sea level rise, accompanying the onset of the Acadian Orogeny. Widespread deposition of deeper water marine shales buried the Helderberg and also covered recharge areas for porous Helderberg facies that acted as conduits for meteoric fluids involved in shallow burial diagenesis (Part II).

Conclusions

1. The Late Silurian-Early Devonian Helderberg Group of the Central Appalachians was deposited during relative tectonic quiescence in a foreland basin bordered by low-relief tectonic highlands along its eastern margin. It developed as a thin, mixed siliciclastic-carbonate ramp sequence that extended out from an inactive(?) accretionary prism. Exposed Helderberg rocks were deposited on the eastern side of the basin on a gently sloping carbonate ramp that had estimated slopes of 10 to 15 cm/km and estimated subsidence rates of 1 to 2 cm/1000 years. Similar carbonate ramp sequences may develop in other foreland basins during periods of tectonic quiescence between major orogenic events.

2. The Helderberg Group is a third order Vail cycle that lasted about 8 to 10 m.y. Three smaller-scale, transgressive-regressive sequences of 2 to 3 m.y. duration also are recognized. Lithofacies patterns resulted from

eustatic sea level changes, differential basin subsidence, and varying sedimentation rates.

Transgressive ramp-to-basin sequences consist of: 1) skeletal-pellet grainstone/packstone; 2) scattered coral-stromatoporoid framestone biostromes/bioherms; 3) deep ramp cherty limestone; and 4) basinal limy shale and siliceous shale. Regressive ramp-to-basin sequences consist of: 1) basin margin quartz sandstones and local peritidal carbonates; 2) shallow ramp, high-energy skeletal grainstone/rudstone fringing banks (with associated mud mound facies) that grade basinward into skeletal-pellet grainstone/packstone; 3) deep ramp limy shale and shaly/nodular-bedded limestone; and 4) basinal siliceous shale and siltstone (upper Shriver Chert).

3. Helderberg fringing banks prograded seawards at rates of 35 to 50 m/1000 years, which are much lower than modern bank progradation rates, possibly indicating absence of photosynthetic seagrasses during the Devonian. Tidal flat caps are rare on the regressive cycles probably because rates of relative sea level drop were too high and progradation rates for tidal flats were too low for tidal flats to prograde basinward.

4. Quartz sandstone was probably reworked from underlying Silurian sandstone and introduced to the basin by rivers that nearly coincided with ancestral Silurian drainage systems. Siliciclastic influx was never great

enough to completely shut-off carbonate production on the ramp.

5. Shallow ramp sediments were reworked by strong tidal currents, fairweather wave-generated currents, and storms. Deeper ramp sediments were reworked by storms or were heavily bioturbated. Basin sediments have rare storm-generated deposits and are either dark, unfossiliferous, and fissile (poorly oxygenated waters) or lighter, fossiliferous, and bioturbated (oxygenated waters).

6. Skeletal grainstone/rudstone formed highly prograded sand sheets along the southeastern basin margin that resemble fringing skeletal banks from other carbonate ramps. Skeletal grainstone/rudstone generally fringes the eastern basin margin as opposed to forming barrier skeletal banks (cf. Helderberg Group, New York; Laporte, 1967) probably because of steeper slopes on the eastern side of the foreland basin.

7. Final drowning of the Helderberg carbonates occurred during the Middle Devonian, accompanying the onset of the Acadian Orogeny. Deeper water Middle Devonian marine shales buried the Helderberg Group and updip subaerial outcrops.

CHAPTER 2. DIAGENETIC HISTORY OF THE HELDERBERG GROUP

Introduction

Many diagenetic studies of ancient carbonate rock sequences have emphasized the role of either near surface or deep burial processes on diagenetic alteration and cementation, when most ancient carbonate sediments probably are affected during all stages of burial. Many studies also are local in extent, which limits understanding of timing and pathways of fluid migration.

This study documents regional diagenetic trends in the Siluro-Devonian Helderberg Group, Central Appalachians. By using a combined petrographic and geochemical approach, within a well-defined stratigraphic framework and geologic history, the timing, temperatures, and chemistries of diagenetic fluids that affected the Helderberg Group can be estimated.

Cathodoluminescent petrography provided the framework for subsequent analytical techniques. Calcite cements in the Helderberg Group have three basic types of cathodoluminescent zonation (Fig. 15) which have regional distribution patterns.

Figure 15. Paired plane light and cathodoluminescent photomicrographs of skeletal grainstone showing types of cathodoluminescent cement zonation in Helderberg Group limestones, Central Appalachians.

A,B. Updip skeletal grainstone with well-developed nonluminescent (N) - bright (B) - void-filling dull (D) cement sequence. Unlabeled arrow in lower left indicates irregular contact between nonluminescent and bright cement suggesting local dissolution(?) of nonluminescent cement prior to precipitation of bright cement.

C,D. Intermediate skeletal grainstone with early "subzoned" dull syntaxial rim cement on pelmatozoan grains (opposing arrows labeled SD) followed by void-filling dull cement (D) with pyrite crystals (P).

E,F. Downdip skeletal grainstone with nonzoned dull cement (D). Note inclusion-rich syntaxial rim cement (IR) and pelmatozoan grains have same luminescence as clear calcite cement. Fractured brachiopod (FB) was broken by compaction prior to precipitation of dull cement.

Note cleavage traces, deformation twins through all cement zones and local sutured contacts between grains and cement in all photomicrographs.

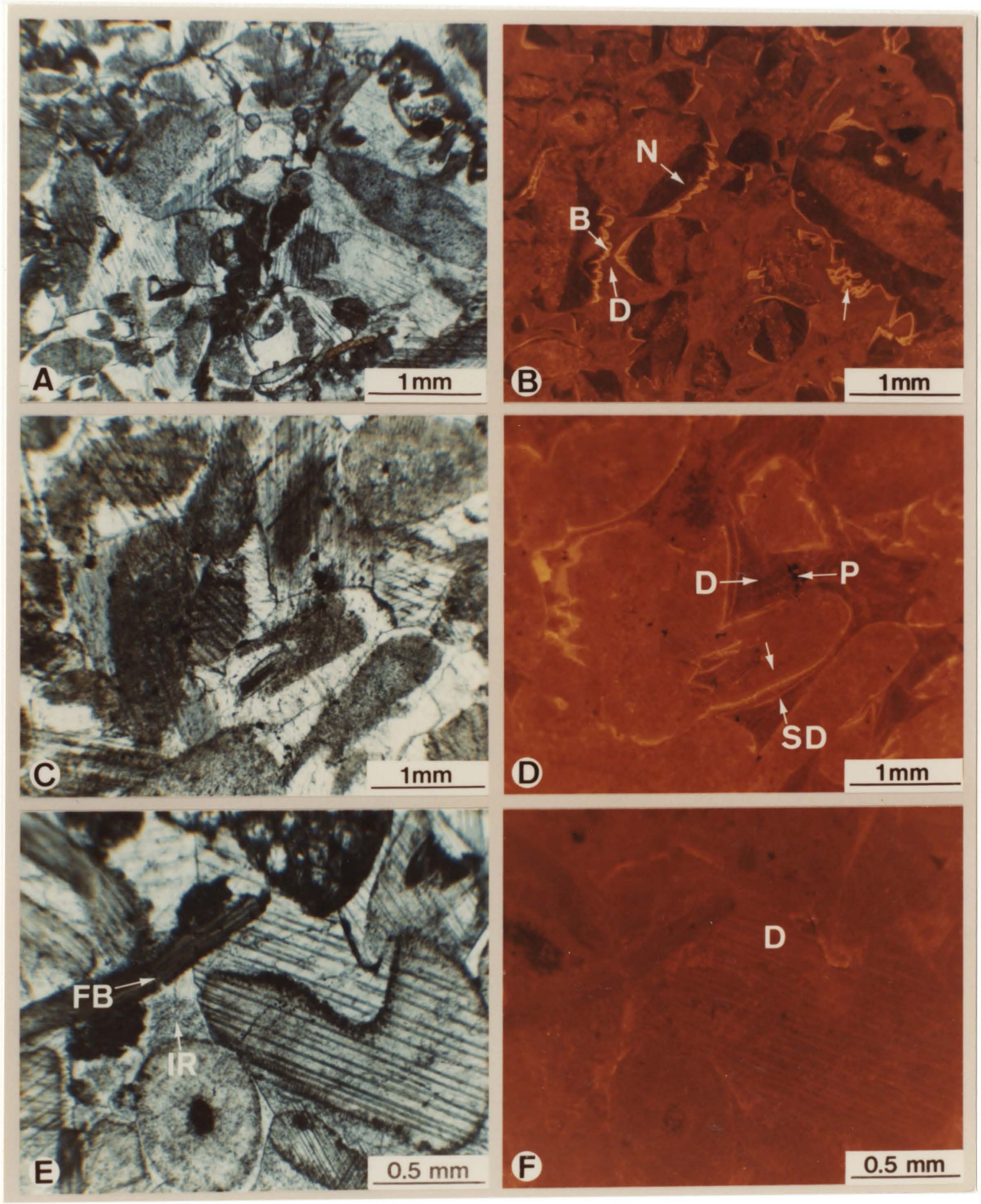
A
1mm
B
N
B
D
1mm
C
1mm
D
D
P
SD
1mm
E
FB
IR
0.5 mm
F
D
0.5 mm

Cementation of the Helderberg Group initially began on the sea floor during Helderberg deposition. After slight burial by overlying sediments (<300 m), meteoric groundwater systems developed and altered carbonate skeletal grains and caused much cementation of the Helderberg Group. Paleohydrology and geochemistry of early meteoric fluids are discussed with emphasis on regional diagenetic effects and duration of shallow subsurface diagenesis. Deeper burial fluids also affected the Helderberg Group when the sediments were removed from near surface diagenetic processes by deposition of overlying sediments. Burial cements occluded most remaining porosity, although hydrocarbons migrated during cementation. Evidence for late stage migration of high-temperature, high-pressure fluids through completely cemented Helderberg rocks is presented, and timing and sources for these fluids are discussed.

Finally, application of computer-assisted image analysis in estimating volumetric abundance of various stages of cementation (defined by cathodoluminescence) is presented. This allows the amount of cementation that occurred in specific diagenetic environments to be rapidly quantified.

Methods

Thirty measured sections of the Helderberg Group in Virginia-West Virginia-Maryland were sampled at 1-10 m intervals for cements. Samples were taken from all lithologies, with emphasis on lithologies with sparry cements.

Conventional and cathodoluminescent petrography was done on over 700 uncovered, unstained, and polished thin sections (about 100 thin sections were later stained with potassium ferricyanide solution and examined). Cathodoluminescent petrography was done with a Nuclide Corporation ELM-2A Luminoscope attached to a Leitz Ortholux II POL-MX microscope. Operating conditions for cathodoluminescent petrography and photography were 16 kV gun potential, 0.6 milliamps beam current, and about 1 cm focused beam at 120 millitorrs vacuum. Black and white cathodoluminescent photographs were taken with Kodak Panatomic-X film (ASA 32), exposed for 60 to 90 seconds (depending upon luminescent intensity). Color slides for image analysis were taken with Kodak Ektachrome film (ASA 200) with exposure time of 60 to 90 seconds. Color cathodoluminescent photomicrographs were taken with Kodak Kodacolor II color print film (ASA 100) with exposure time of 90 to 120 seconds.

Trace element analyses of cement zones were done on 35 unstained, highly polished, and ultrasonically cleaned thin

sections using a nine spectrometer ARL SEMQ electron microprobe housed at VPI & SU, Blacksburg, Virginia. Automated traverses were made across cathodoluminescent zoned calcite cements; step size was 10-50 um. Microprobe operating conditions were 15 KeV accelerating voltage, 10 nA beam current, approximately 10 micron beam diameter, and 50 second counting times. Data reduction was by the Bence-Albee method. Individual analyses were correlated with analytical spots on microprobe traverses. After correlation with cement zones, data were entered into the SAS program according to cathodoluminescent characteristics (Appendix A). Statistical manipulation and graphics were then performed by SAS. Limits of detection in microprobe analyses were determined using the procedure outlined in Goldstein (1976). Detection limits for manganese, iron, and magnesium in calcite cements and skeletal grains are 290 ppm, 310 ppm, and 410 ppm, respectively. Values below microprobe detection limits are reported as "zero" in the text, but actual analytical determinations are given in Appendix A.

Fluid inclusion samples were selected and prepared using procedures outlined in Hollister et al. (1981). Rock chips were mounted to glass slides with DUCO cement. Samples were cut with water-cooled saws and were never heated above room temperature during preparation.

Two-phase fluid inclusions were analyzed using a U.S.G.S.-type gas-flow heating/freezing stage (described in Woods et al., 1981, and built at VPI & SU) mounted to a Leitz Orthoplan microscope with a Leitz UT 50 objective. Temperature measurements were made with an Omega Scass 020-G 6-inch thermocouple connected to a Leeds and Northrup Numatron digital temperature display. For determination of homogenization temperatures, compressed air was blown through a Sylvania-Exeter heating coil and into the fluid inclusion stage. The heating coil was connected to a Fisher Powerstat transformer with rheostat. Freezing temperatures were determined by connecting a cylinder of N_2 gas to a liquid N_2 flask and then forcing the cooled N_2 gas into the inclusion stage via the tube and nozzle arrangement used during the heating process (with the heating element turned off). The thermocouple was calibrated periodically to insure accuracy of temperature determinations. The thermocouple was consistently about 1°C too high; temperatures were corrected accordingly. For a more detailed description of fluid inclusion procedures at VPI & SU, see Caless (1981).

Hydrocarbon inclusions were examined with a Leitz Orthoplan epifluorescence microscope with a 200 W mercury arc lamp source and 63X objective. Exposure times for Kodak Ektachrome slides were 1 to 5 seconds, depending on fluorescence intensity; color prints were made from Ektachrome slides.

Microsamples from individual carbonate components were obtained for stable isotopic analyses using a microscope-mounted drill assembly coupled to an X-Y translation stage. Sampling to as fine as 100 um was accomplished using drill bits faceted to a 20 micron point. Samples were taken from potassium ferricyanide-stained rock chips and thin sections. Staining allowed differentiation of early cements with low Fe levels (unstained) from later, Fe-enriched (stained blue) cements. Stained thin sections made from the same rock chips sampled for isotopes were cross-checked under cathodoluminescence to make certain cathodoluminescent zones coincided with stained/unstained cement phases sampled for isotopic analyses. Samples (0.2 to 0.5 mg-sized) were roasted at 380°C for one hour under vacuum to remove volatile organic contaminants. Samples were subsequently reacted with anhydrous phosphoric acid at 50°C in a reaction/extraction line coupled directly to the inlet of a VG Micromass 602D ratio gas mass spectrometer. Isotopic enrichments were converted to the PDB based on calibration relative to NBS 20. Correction for ^{17}O was made in accordance with procedures of Craig (1957). Precision was measured by daily measurement of NBS 20 as unknown sample powder and precision was maintained at better than $1\sigma = \pm 0.1\%$ for both carbon and oxygen.

Instrumentation and methods for quantitative image analysis of zoned calcite cements are discussed separately in Chapter 3.

Burial History

A burial history plot for northern West Virginia is shown in Figure 16 and allows estimation of the thermal regime at any time for the sedimentary section. Timing of generation and destruction of hydrocarbons from various source beds also may be estimated using the diagram. A geothermal gradient of 30°C/km was assumed throughout the burial and uplift history of the Helderberg Group; surface temperature of 20°C was also assumed throughout burial and uplift.

The Appalachian Basin was subsiding at a rate of about 100 m/10 m.y. (about 1 cm/1000 years) during Helderberg deposition. Shallow burial freshwater cementation of Helderberg sediments occurred at burial depths less than 300 m when recharge areas for Helderberg paleoaquifers were subaerially exposed in tectonic uplands along the eastern basin margin. The Helderberg Group then underwent a phase of very rapid burial during deposition of the thick Middle Devonian clastic wedge (Acadian Orogeny). Upland-sourced recharge areas were buried by these thick Middle Devonian marine facies, and shallow burial cementation from oxidizing freshwaters ceased. At maximum burial depths (4 km), the Helderberg Group was at an ambient burial temperature of approximately 150°C (Fig. 16).

Figure 16. Burial history plot for Helderberg Group using compacted stratigraphic thickness data for Pendleton County, West Virginia (from West Virginia State Geologic Map, 1968; dates from 1983 Decade of North American Geology Time Scale). Helderberg Group shaded gray. 20°C surface temperature and 30°C/km average geothermal gradient assumed throughout burial history. See Waples (1980) for details on construction of burial history plots and use of Lopatin's Method for calculating time-temperature index values (TTI). Plot ends at Late Pennsylvanian time and does not show uplift history to present time.

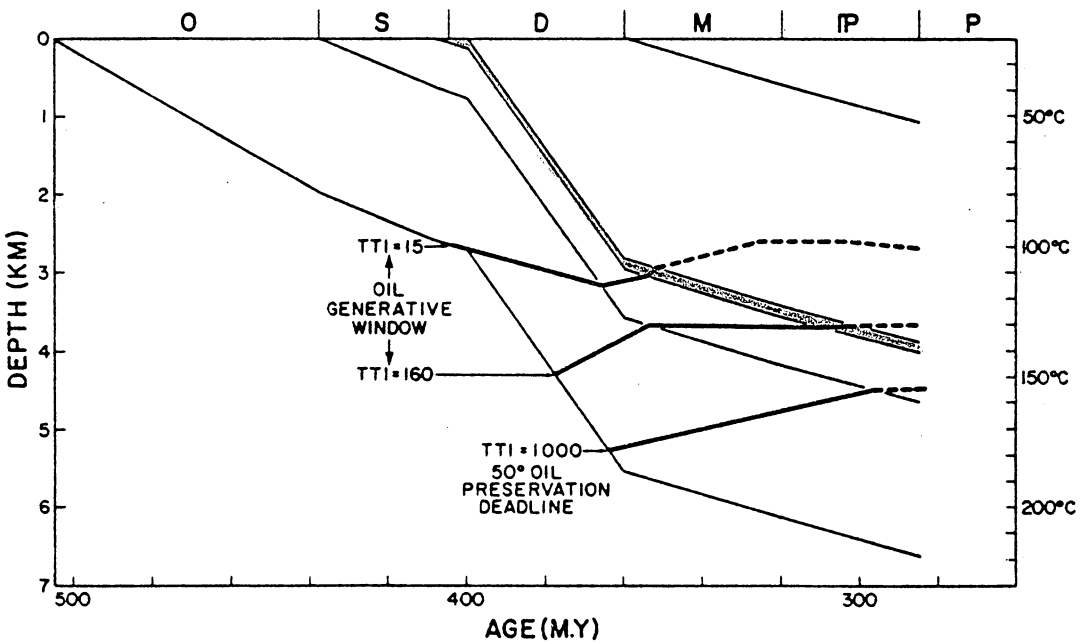
O
S
D
M
IP
P
0
1
2
3
4
5
6
7
DEPTH (KM)
50°C
100°C
150°C
200°C
TTI = 15
OIL
GENERATIVE
WINDOW
TTI = 160
TTI = 1000
50° OIL
PRESERVATION
DEADLINE
500
400
300
AGE (M.Y)

Marine Cement

Synsedimentary marine cement is common in mud mounds and is irregularly distributed in skeletal grainstone and packstone. In deep ramp beds, only microcrystalline calcite cement was precipitated from marine pore fluids. These cements predate clear equant calcite, quartz, and dolomite cement.

Cements with Bladed or Relict Rhombohedral Fabrics

Isopachous cements line stromatactis cavities in mud mounds where they comprise 5 to 20% of cement. They are interlayered with lime mud or pelletal sediment (Fig. 17A) and contain inclusions (hydrocarbons, pyrite, and iron oxides) that locally define relict scalenohedral, rhombohedrally terminated crystals. Luminescence is blotchy, dull orange.

Cements on polycrystalline skeletal substrates in skeletal grainstone/packstone are isopachous, bladed, scalenohedral druse (10-30 um wide, 30-65 um long), with straight cleavage planes and uniform extinction (Fig. 17B). They typically are inclusion-free, lack microdolomite, and are nonluminescent to dull orange.

These early cements are interpreted as marine cements because they are interlayered with marine internal sediment and predate equant calcite cement of shallow to deep burial origin. Bladed cement and isopachous cements with relict

Figure 17. Marine cement fabrics.

A. Isopachous marine cement lining stromatactis cavity in mud mound. Note lime mud with spar-filled ostracode resting on inclusion-rich cement crystals with crude rhombohedral terminations (arrow).

B. Bladed scalenohedral druse on polycrystalline skeletal substrates with remaining void space filled with clear equant spar.

C. Inclusion-rich syntaxial rim cement on pelmatozoan grain.

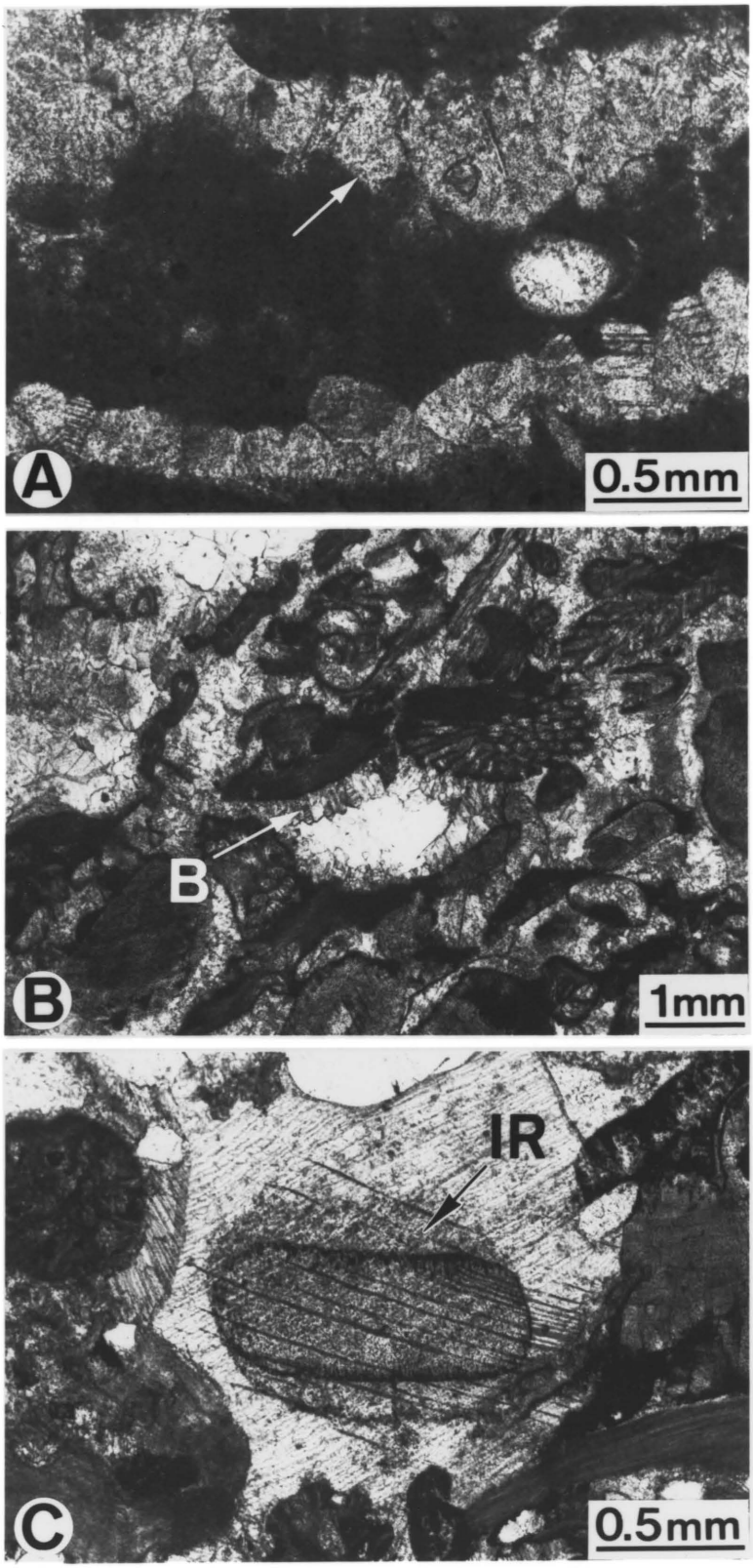
A
0.5mm
B
B
1mm
IR
C
0.5mm

rhombohedral terminations, probably were calcite originally. However, lack of microdolomite in these cements (and its abundance in pelmatozoans and syntaxial rim cements) suggests that they originally were low magnesium-calcite or high magnesium-calcite that lost magnesium during alteration. Bladed scalenohedral druse cement is similar morphologically to modern marine magnesium calcite cements (James et al., 1976; James and Ginsburg, 1979). The necessity for hydraulic pumping of marine pore fluids by waves may explain restriction of coarse-grained marine cement to shallow ramp deposits. Marine pore fluids in wave-agitated, coarse-grained sediments would have been continuously exchanged, allowing marine cements to precipitate (James and Choquette, 1983). Marine pore fluids in deep ramp deposits were not continuously exchanged because they were deposited below fairweather wave base. Thus, deep ramp deposits are more highly compacted and stylolitized than shallow ramp grainstone and packstone probably because of the lack of marine cementation and higher argillaceous content in deep ramp skeletal packstone (cf. Moore and Druckman, 1981). The more permeable fabric of these cements, compared with syntaxial rim cement may have allowed them to lose magnesium easily during shallow burial meteoric diagenesis.

Inclusion-rich Syntaxial Rim Cement

Inclusion-rich syntaxial rim cement occurs on pelmatozoan grains in shallow ramp skeletal limestone. It locally is overlain by mud and contains inclusions of pyrite, microdolomite, hydrocarbons(?), and iron oxides that locally define indistinct rhombohedral terminations (Fig. 17C). Luminescence is blotchy nonluminescent to very dull red-orange. Blotchiness is due to 1-3 um inclusions (mostly microdolomite) which luminesce bright orange or yellow. These cements contain 0-1070 ppm Mn (av. 70 ppm), 0-3260 ppm Fe (av. 610 ppm), and 130-10360 ppm Mg (av. 2180 ppm; Appendix A).

These cements probably were marine high magnesium-calcite (cf. Lohmann and Meyers, 1977) because they have abundant microdolomite inclusions and inclusion-rich zones define crude rhombohdral terminations. Inclusion-rich syntaxial rim cement generally has the same cathodoluminescence as earliest clear burial cement (Fig. 15), except for blotchy inclusions. If inclusion-rich syntaxial rim cement was formerly high-magnesium calcite, then it stabilized to low-magnesium calcite and microdolomite and inherited similar Mn and Fe levels as clear equant calcite cement that precipitated from earliest burial pore fluids. Unstable high-magnesium calcite pelmatozoan grains underwent similar trace element and stable isotopic re-equilibration and fabric neomorphism during shallow burial diagenesis.

Microcrystalline Hardground Cement

Microcrystalline cement occurs in hardgrounds in mud mounds and in deep ramp sediments. It has dull red-orange luminescence. Bladed scalenohedral druse cement and inclusion-rich syntaxial rim cement are generally absent from deep ramp deposits. Microcrystalline hardground cements in deep ramp facies probably resulted from seafloor dissolution and reprecipitation of carbonate near the sediment-water interface (cf. Schlager and James, 1978; Grover, 1981) and probably did not require extensive circulation of marine pore fluids.

Early Meteoric Skeletal Diagenesis

Pelmatozoan grains in the Helderberg Group occur as three end-member diagenetic fabrics: 1) grains with well-preserved, original stereom; 2) "neomorphosed" inclusion-rich grains; and 3) leached grains.

Pelmatozoan grains in which original stereom fabric is defined by coats of brown iron oxides(?) are rare (Fig. 18C). They occur in updip portions of skeletal grainstone and sandstone units.

Leached pelmatozoan grains also occur in updip portions of sandstone and grainstone units. Some leached intraskeletal voids locally are floored by crystal silts and are filled by later nonluminescent and bright equant calcite cement (Fig. 18A, B).

Figure 18. Skeletal diagenesis fabrics.

A,B. Paired plane light (A) and cathodoluminescence (B) photomicrographs of leached crinoid ossicle. Note geopetal silt flooring void and complex nonluminescent-bright-dull cement filling void.

C. Pelmatozoan fragment with preserved stereom fabric (P) and neomorphosed pelmatozoan (N) with thin rim of preserved fabric. Dark color due to iron oxide(?) coat on grains.

D. Gastropods neomorphosed to blocky calcite mosaics.

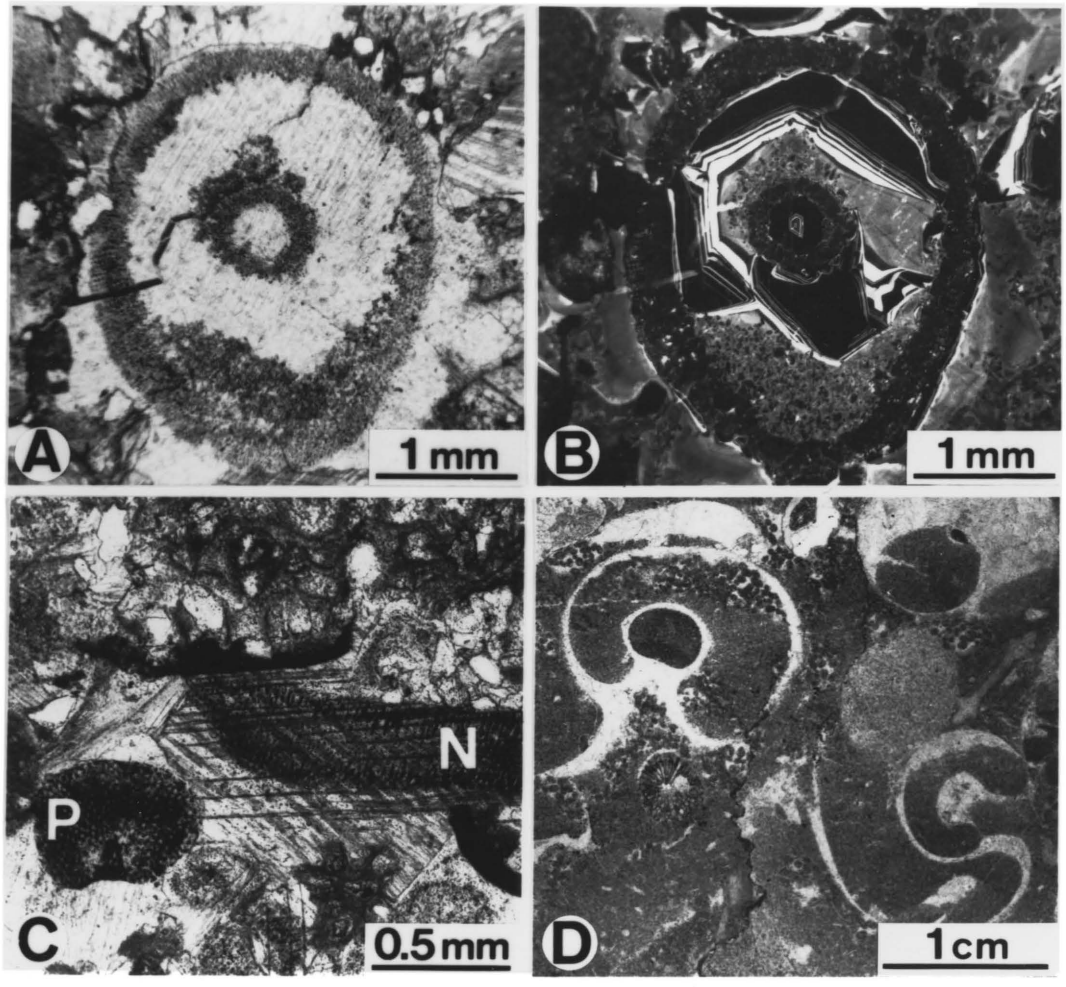
A
1 mm
B
1 mm
N
P
C
0.5 mm
D
1 cm

Neomorphosed pelmatozoan grains do not have any primary stereom preserved (Fig. 18C). They contain abundant submicron to 15 um inclusions of microdolomite, pyrite, hydrocarbons, and one- and two-phase fluid inclusions. Microdolomites are oriented crystallographically along cleavage traces and indicate that Helderberg pelmatozoans probably secreted magnesian calcite (Lohmann and Meyers, 1977). Neomorphosed pelmatozoans (and inclusion-rich syntaxial rim cements that coat them) generally have the same luminescence (although blotchy because of inclusions) as the first generation of clear equant calcite cement (Fig. 15). Neomorphosed pelmatozoan average 110 ppm Mn, 1420 ppm Fe, and 2110 ppm Mg (Table 1). Iron and magnesium "spikes" in microprobe traverses across pelmatozoan grains indicate pyrite and microdolomite inclusions, respectively, and these data were not included in Table 1. Stable isotopic analyses of pelmatozoan grains average -0.3% $\delta^{18}O$ and +0.2% $\delta^{13}C$ difference from earliest syntaxial rim cement (Table 1).

Aragonitic molluscan grains (pelecypods and gastropods) are neomorphosed to equant calcite mosaics (Fig. 18D). Leached former aragonite grains were not observed.

Discussion

Early diagenesis of magnesian calcite and aragonite skeletal grains provides evidence for chemical evolution of pore fluids. Incongruent dissolution of magnesian calcite

Table 1. Summary of geochemical data for components and pelmatozoan grains.

N = number of analyses; T_e = eutectic temperature; $T_{m\text{-}ice}$ = melting temperature of ice; $T_{HL\text{-}V}$ = homogenization temperature of liquid and vapor phases; $T_{HP\text{-}C}$ = 400 bar hydrostatic pressure-corrected trapping temperature. Stable isotopes reported relative to PDB standard.

			NONLUM.	BRIGHT	DULL	PELMATAZOANS
PERCENT TOTAL CEMENT		N	66	84	122	
		RANGE	0 - 60%	0 - 5%	23 - 100%	
		MEAN	28%	13.8%	76.2%	
TRACE ELEMENTS	MN	N	69	42	743	215
		RANGE	0 - 403	31 - 3408	0 - 1053	0 - 798
		MEAN	20	1164	293	106
	FE	RANGE	0 - 700	0- 1143	0 - 42,500	0 - 21,146
		MEAN	150	376	1261	1417
	MG	RANGE	0 - 2111	0 - 3492	0 - 10,699	0 - 9288
		MEAN	1146	803	1801	2106

		LATE DULL CEMENT	QUARTZ CEMENT
PRIMARY TWO-PHASE FLUID INCLUSIONS	N	20	3
	T_E	-45.2 to -24.0	-25.5 to -23.9
	$T_{m\text{-}ice}$	-28.8 to -1.7	-5.0 to -1.4
	$T_{h_{L\text{-}v}}$	46.2 to 160.3	139.6 to 175.0
	$T_{h\text{-}c}$	128.1 to 201.3	181.6 to 220.0
	wt. % NaCl	2.9 to >23	2.4 to 7.9

			NONLUM. W/ THIN LUM. LAMINAE	"SUBZONED" DULL	EARLY DULL	PELMATAZOAN GRAINS	DIFFERENCE BETWEEN PELMATAZOANS AND EARLIEST CEMENT	LATE DULL	FRACTURE-FILLING CALCITE
STABLE ISOTOPES	$\delta^{18}O$	N	15	7	5	22	23	65	32
		RANGE	-7.6 to -4.7	-6.8 to -4.7	-7.0 to -4.7	-8.7 to -4.4	-4.0 to +2.0	-12.0 to -4.7	-10.3 to -5.2
		MEAN	-5.8	-6.0	-5.4	-6.0	-0.3	-8.7	-7.4
		σ	0.8	0.7	0.9	1.2	1.2	1.8	1.0
	$\delta^{13}O$	N	15	7	5	22	23	65	32
		RANGE	-2.9 to +4.2	+0.6 to +4.6	+2.6 to +4.7	+0.4 to +4.7	-2.5 to +3.3	-1.0 to +5.8	-0.5 to +4.8
		MEAN	+2.6	+2.4	+3.5	+3.1	+0.2	+2.8	+2.5
		σ	1.7	1.7	1.0	1.3	1.1	1.8	1.3

and aragonite dissolution are often cited as causing groundwater chemistries in modern carbonate aquifers (Plummer et al., 1976; Land, 1970).

All modern echinoderms secrete magnesian calcite (Wilkinson, 1979; Mackenzie et al., 1983) and presumably so did ancient echinoderms (Lohmann and Meyers, 1977; Blake et al., 1982). Pelmatozoan grains in the Helderberg Group probably also were magnesian calcite prior to diagenetic stabilization.

Neomorphism of molluscan and pelmatozoan grains is pervasive, although stereom preservation or leaching of magnesian calcite occurs only in select grains. This suggests that groundwaters were near saturation with respect to aragonite and most high magnesium calcite, causing neomorphism to proceed by thin film inversion to low magnesium calcite.

Stability constants obtained by Walter and Morse (1984) show that 12 mole % magnesian calcite is equivalent in stability to aragonite, and 18 mole % magnesian calcite is twice as soluble as aragonite. Variability in magnesium content in modern echinoderm skeletons occurs on the taxonomic level, between individuals of the same species, and even within single skeletal parts (Chave, 1952; Mackenzie et al., 1983). Leached pelmatozoan grains in the Helderberg may have been more magnesium-rich than the majority of pelmatozoan grains and thus were more soluble.

However, trapped organic matter, differences in microstructure, or total grain surface area exposed to diagenetic fluids also may have influenced solubility of specific grains (Walter, 1983; Mackenzie et al., 1983).

Dissolution of pelmatozoan grains probably occurred early in updip portions of aquifers containing oxidizing pore fluids. Early updip meteoric groundwaters may have been slightly undersaturated with respect to aragonite and magnesian calcite with <12 mole % $MgCO_3$ (causing skeletal neomorphism by thin-film solution-precipitation); leached pelmatozoan grains may have contained more magnesium than most unleached pelmatozoans, suggesting that early fluids were very undersaturated with respect to magnesian calcite with >12 mole % $MgCO_3$. Lack of leached pelmatozoans downdip indicates that downdip pore fluids became more saturated with respect to high magnesium calcite through progressive rock-water reaction.

Similarity in luminescence between neomorphosed pelmatozoan grains (and overlying inclusion-rich syntaxial rim cement) and first generation equant cement suggests that neomorphosed magnesian calcites inherited their trace elements (Mn and Fe) during alteration by meteoric groundwaters. Similar stable isotopic compositions of pelmatozoan grains and early meteoric cement also suggest that pelmatozoan grains re-equilibrated with meteoric groundwaters.

Pelmatozoans with preserved original stereom were "armored" by iron oxides(?) that precipitated from oxidizing meteoric groundwaters in updip portions of aquifers prior to extensive neomorphism/leaching.

Shallow to Deep Burial Clear Equant Calcite Cements

Clear equant calcite cement postdates marine cement and occludes most of the porosity. Cathodoluminescent petrography, staining (Dickson, 1965), and trace element analysis (Fig. 19) show that equant calcite is compositionally zoned. The cements include nonluminescent, bright, and dull cement. Nonluminescent cement, where present, is the earliest generation of cement, followed by bright, and then dull cement. Elsewhere, bright cement may be the first cement and may be interlayered with later dull cement. Clear cements also may lack zoning and are homogeneously dull.

Nonluminescent Cement

Description. Nonluminescent cement, where it occurs, is the first generation of clear calcite cement. It occurs as inter- and intragranular scalenohedral druse (3-35 um thick) on polycrystalline skeletal substrates and monocrystalline pelmatozoan grains, or as syntaxial rhombohedral overgrowths (up to 1.5 mm wide) on pelmatozoan grains. It is thickest

Figure 19. Electron microprobe traverses across zoned cements. Traverses start from grain (left) and end at crystal termination in center of void. Note nonluminescent cement has low Mn and Fe, bright cement has high Mn and low Fe, dull cement has low to high Mn and Fe > Mn. Also note Mg levels increase in later dull cement.

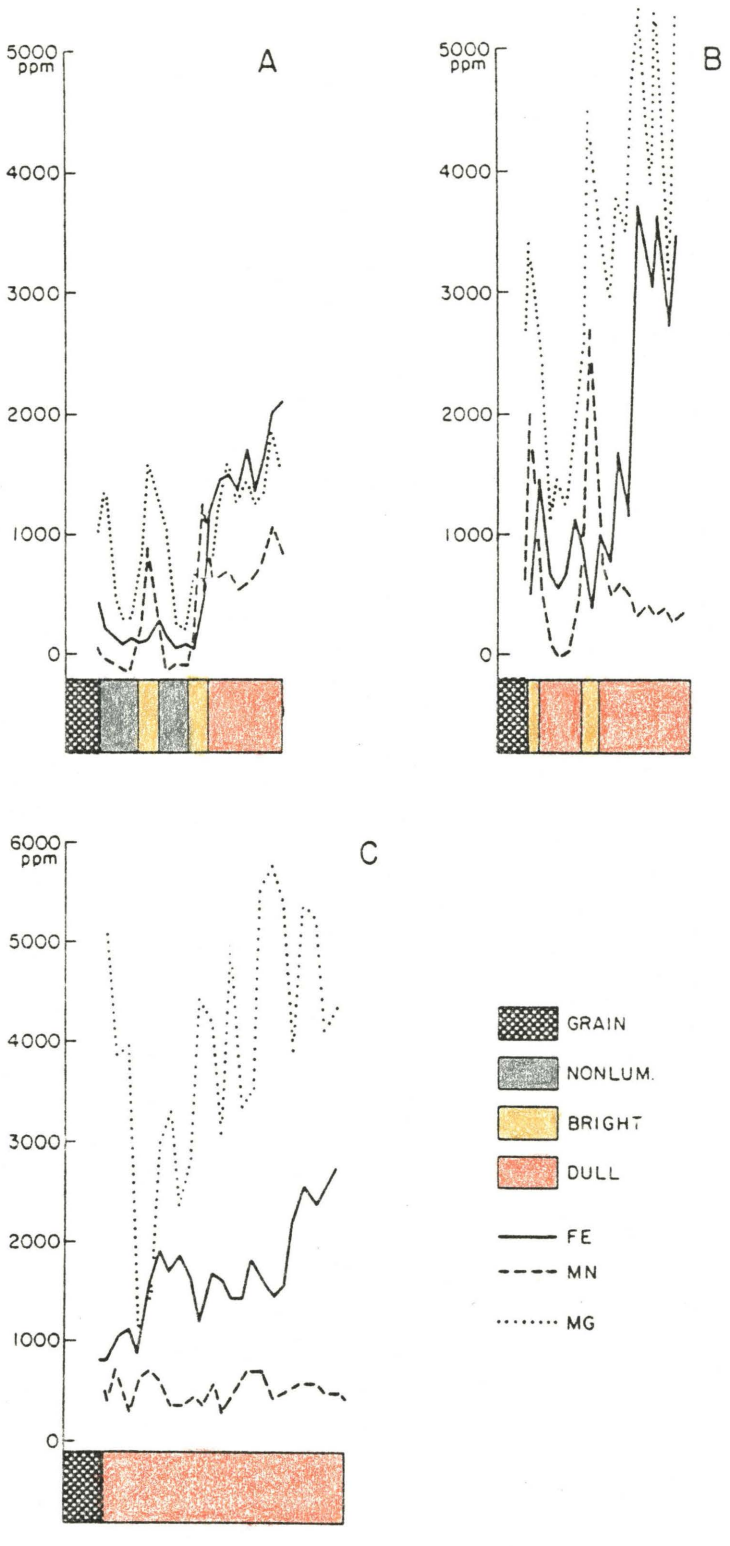
A
B
C
5000 ppm
4000
3000
2000
1000
0
6000 ppm
GRAIN
NONLUM.
BRIGHT
DULL
FE
MN
MG

on surfaces normal to c-axes of calcite pelmatozoan grains (cf. Evamy and Shearman, 1965; 1969). Polycrystalline skeletal substrates adjacent to pelmatozoan grains with thick nonluminescent cement have thin or absent nonluminescent druse cement (cf. Grover and Read, 1983). Under cathodoluminescence, nonluminescent cement is black to slightly luminescent red-brown and may contain thin (submicron to 40 um thick) interlayers of bright or dull cement. Most luminescent interlayers have sharp planar contacts with nonluminescent cement but some contacts are highly irregular (Figs. 16B, 20A).

Nonluminescent calcite cement in quartz sandstone only occurs on scattered skeletal grains and never on quartz grains (Fig. 20C, D). Some nonluminescent cement crystals are broken (Fig. 20B) or show minor dissolution prior to deposition of later calcite. Nonluminescent cement locally overlies iron oxide coats on skeletal grains (Fig. 20C, D). It postdates leaching of pelmatozoan fragments (Fig. 18A, B) and some is replaced by microcrystalline quartz and chalcedony (Fig. 20E, F). Nonluminescent cement has cleavage traces, deformation twins, and locally is crosscut by tectonic fractures, stylolites, and secondary fluid inclusion trains.

Trace Elements. Nonluminescent cement contains 0-400 ppm Mn (av. 20 ppm), 0-700 ppm Fe (av. 150 ppm), and 0-2100 ppm Mg (av. 1150 ppm; Table 1). Mn levels in slightly

Figure 20. Nonluminescent cement fabrics.

A. Common nonluminescent-bright-dull cement sequence. Note pelmatozoan grains are nonluminescent (except for bright inclusions), as is earliest cement generation. Bright cement outlines well-developed crystal terminations and highly irregular contact (dissolution?) with nonluminescent cement.

B. Broken brachiopod fragment with nonluminescent-bright cement on underside. Arrow indicates fragment of nonluminescent-bright cement that broke off brachiopod during mechanical compaction.

C,D. Paired plane light (C) and cathodoluminescent (D) photomicrographs of quartz-rich skeletal grainstone. Note iron oxide(?) coats on pelmatozoan grains followed by nonluminescent calcite cement. Quartz grains with overgrowths (quartz is nonluminescent in D) have no nonluminescent calcite cement on them, but are surrounded by dull calcite cement.

E,F. Paired crossed nicols (E) and cathodoluminescent photomicrographs (F) of microcrystalline silica (S) replacing pelmatozoan fragment (P) and early zoned calcite cement. Arrows indicate cross-cutting relationships with thin luminescent laminae in nonluminescent calcite cement.

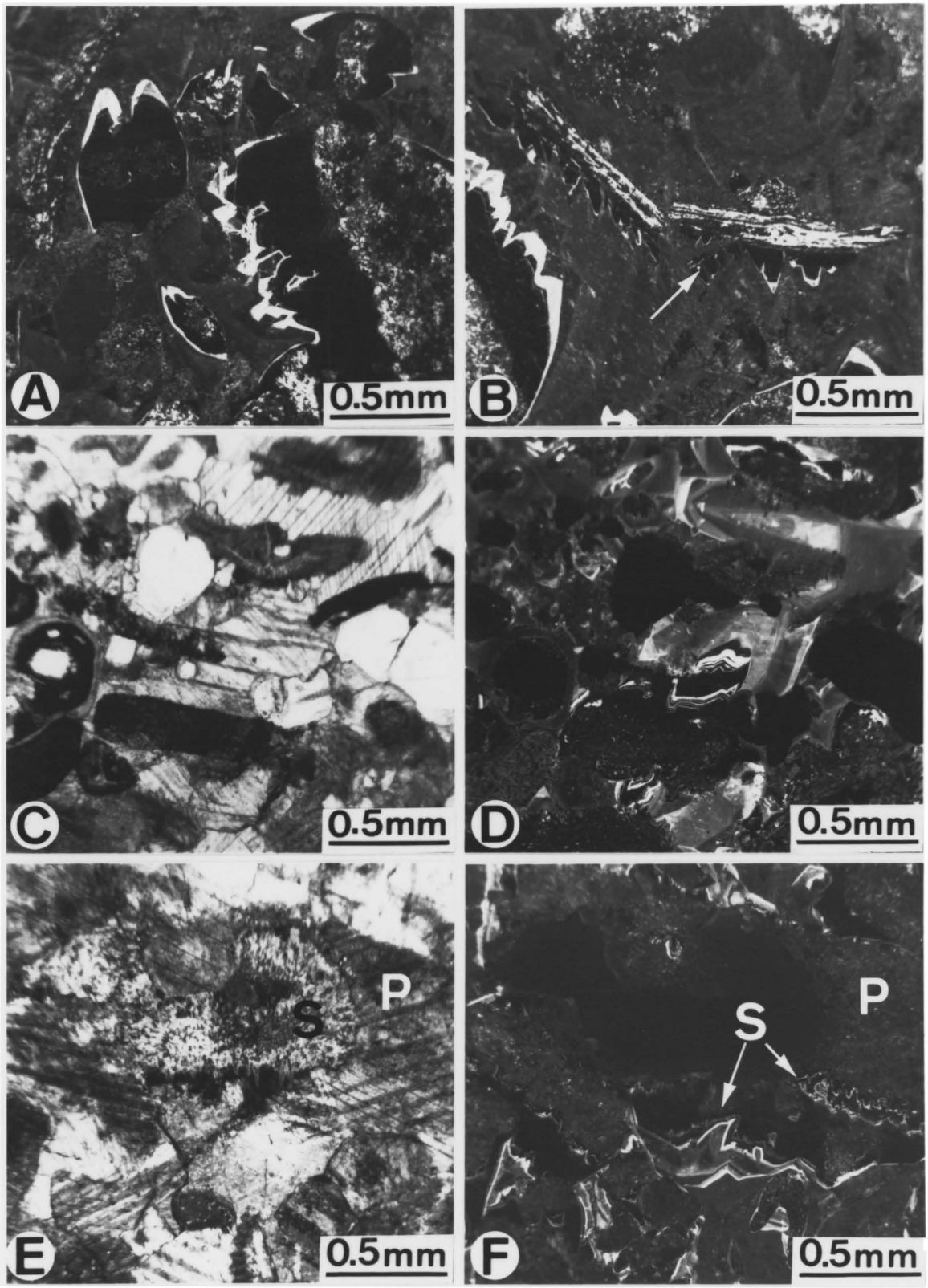
A
0.5mm
B
0.5mm
C
0.5mm
D
0.5mm
S
P
E
0.5mm
S
P
F
0.5mm

luminescent red-brown cement are higher than in completely nonluminescent cement (av. 370 ppm Mn; av. 160 ppm Fe; Table 1). Levels of Sr, Na, K, Pb, Zn, Ni, and Cl were below microprobe detection limits.

Regional Distribution. Nonluminescent cement makes up 0 to 60% of equant calcite cement, decreasing in abundance basinward (Table 1 and Figs. 21, 22). Nonluminescent cement in the New Creek Limestone is more abundant in coarse-grained skeletal limestone that is proximal to the basin margin and decreases basinward (Fig. 23). Early iron oxide crusts also only occur in coarse-grained sandstone and skeletal limestone in eastern sections.

Timing and Origin of Nonluminescent Cement. Nonluminescent cement was the earliest equant cement and predates silicification, mechanical and chemical compaction, and tectonism (Fig. 24). It postdates leaching of pelmatozoan grains and precipitation of iron oxide crusts. Precipitation of nonluminescent cement probably occurred at less than 300 m burial depth (burial depths discussed later).

Low iron and manganese levels in nonluminescent cement (Table 1; Figs. 19, 25) and iron oxide crusts predating nonluminescent cement suggest that nonluminescent cement precipitated from oxidizing pore fluids. Iron and manganese would not have been in reduced (2+) valence states and

Figure 21. Stratigraphic variation in amount of nonluminescent cement. Nonluminescent cement decreases basinward. Abundance of cement determined by image analysis (see Chapter 3).

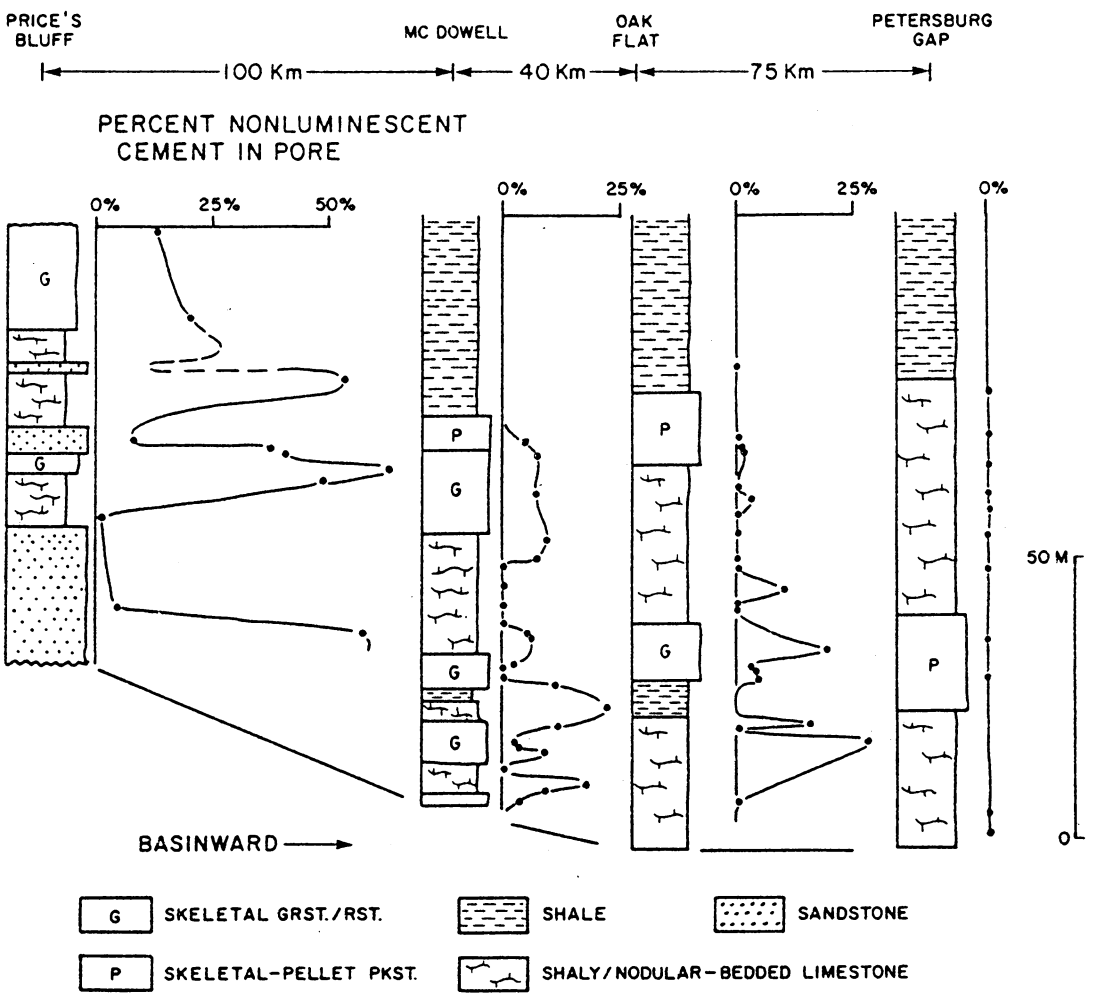
PRICE'S BLUFF
MC DOWELL
OAK FLAT
PETERSBURG GAP
100 Km
40 Km
75 Km
PERCENT NONLUMINESCENT CEMENT IN PORE
0%
25%
50%
BASINWARD
50 M
0
G
P
SKELETAL GRST./RST.
SKELETAL-PELLET PKST.
SHALE
SHALY/NODULAR-BEDDED LIMESTONE
SANDSTONE

Figure 22. Regional distribution of cathodoluminescent cement zones superimposed on stratigraphic cross-sections. Tick marks are sample locations. Boundaries queried where sample coverage is poor. Note coincidence of nonluminescent cements with distribution of updip sandstone and skeletal limestone. Leached pelmatozoan grains (L) and iron oxide coats on grains (Fe) also coincide with distribution of nonluminescent cement.

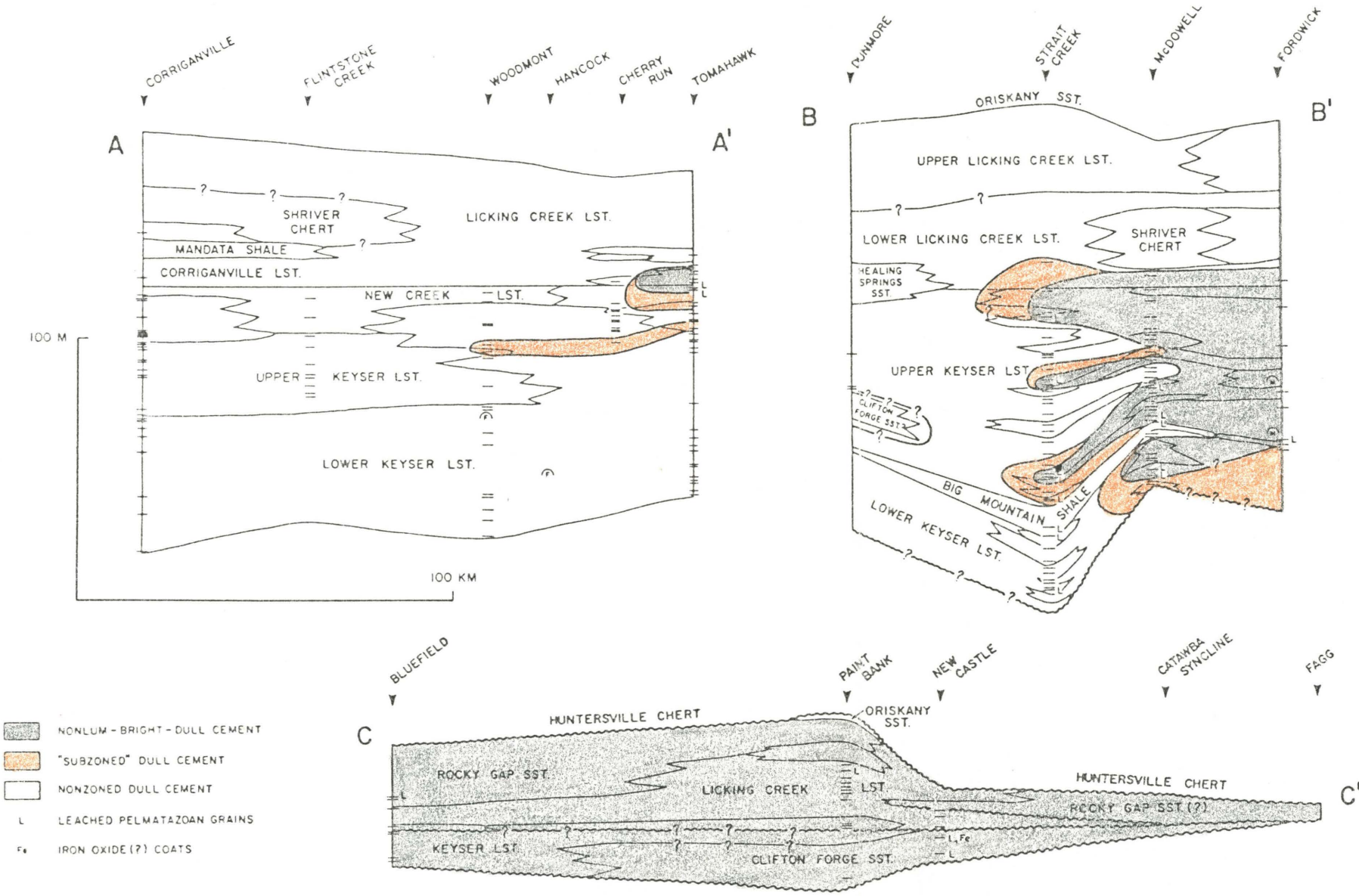
CORRIGANVILLE
FLINTSTONE CREEK
WOODMONT
HANCOCK
CHERRY RUN
TOMAHAWK
A
A'
SHRIVER CHERT
LICKING CREEK LST.
MANDATA SHALE
CORRIGANVILLE LST.
NEW CREEK LST.
UPPER KEYSER LST.
LOWER KEYSER LST.
100 M
100 KM
DUNMORE
STRAIT CREEK
McDOWELL
FORDWICK
B
B'
ORISKANY SST.
UPPER LICKING CREEK LST.
LOWER LICKING CREEK LST.
SHRIVER CHERT
HEALING SPRINGS SST.
UPPER KEYSER LST.
CLIFTON FORGE SST.
BIG MOUNTAIN SHALE
LOWER KEYSER LST.
BLUEFIELD
PAINT BANK
NEW CASTLE
CATAWBA SYNCLINE
FAGG
C
C'
HUNTERSVILLE CHERT
ORISKANY SST.
ROCKY GAP SST.
LICKING CREEK LST.
KEYSER LST.
CLIFTON FORGE SST.
HUNTERSVILLE CHERT
ROCKY GAP SST.(?)
NONLUM - BRIGHT - DULL CEMENT
"SUBZONED" DULL CEMENT
NONZONED DULL CEMENT
L LEACHED PELMATAZOAN GRAINS
Fe IRON OXIDE (?) COATS

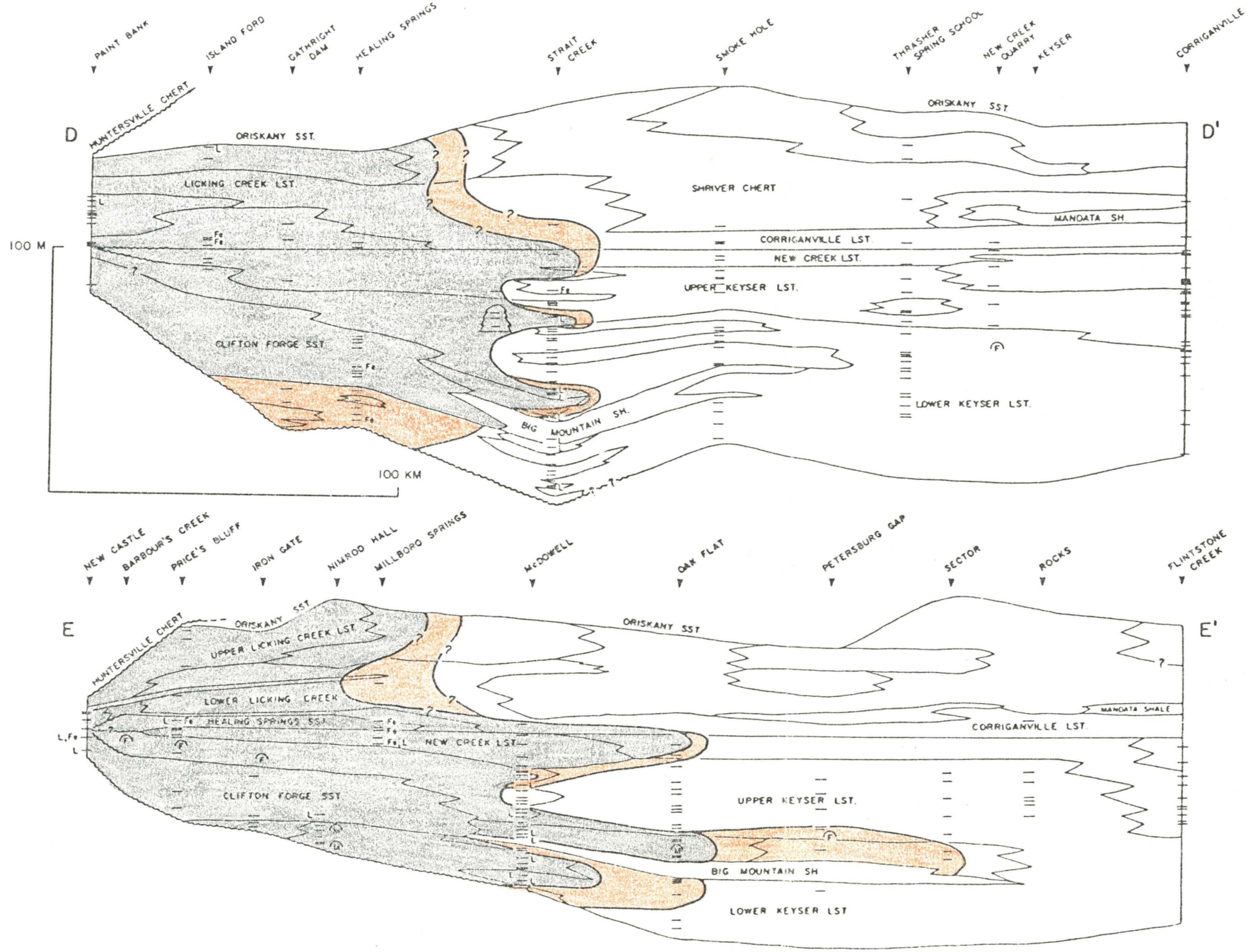
PAINT BANK
ISLAND FORD
GATHRIGHT DAM
HEALING SPRINGS
STRAIT CREEK
SMOKE HOLE
THRASHER SPRING SCHOOL
NEW CREEK QUARRY
KEYSER
CORRIGANVILLE
D
D'
HUNTERSVILLE CHERT
ORISKANY SST.
LICKING CREEK LST.
CLIFTON FORGE SST.
SHRIVER CHERT
MANDATA SH.
CORRIGANVILLE LST.
NEW CREEK LST.
UPPER KEYSER LST.
LOWER KEYSER LST.
BIG MOUNTAIN SH.
100 M
100 KM
NEW CASTLE
BARBOUR'S CREEK
PRICE'S BLUFF
IRON GATE
NIMROD HALL
MILLBORO SPRINGS
McDOWELL
OAK FLAT
PETERSBURG GAP
SECTOR
ROCKS
FLINTSTONE CREEK
E
E'
HUNTERSVILLE CHERT
ORISKANY SST.
UPPER LICKING CREEK LST.
LOWER LICKING CREEK
HEALING SPRINGS SST.
NEW CREEK LST.
CLIFTON FORGE SST.
ORISKANY SST.
MANDATA SHALE
CORRIGANVILLE LST.
UPPER KEYSER LST.
BIG MOUNTAIN SH.
LOWER KEYSER LST.

Figure 23. Contour map of abundance of nonluminescent and bright cement in the New Creek Limestone and laterally equivalent beds. Amount of nonluminescent and bright cement decreases basinward.

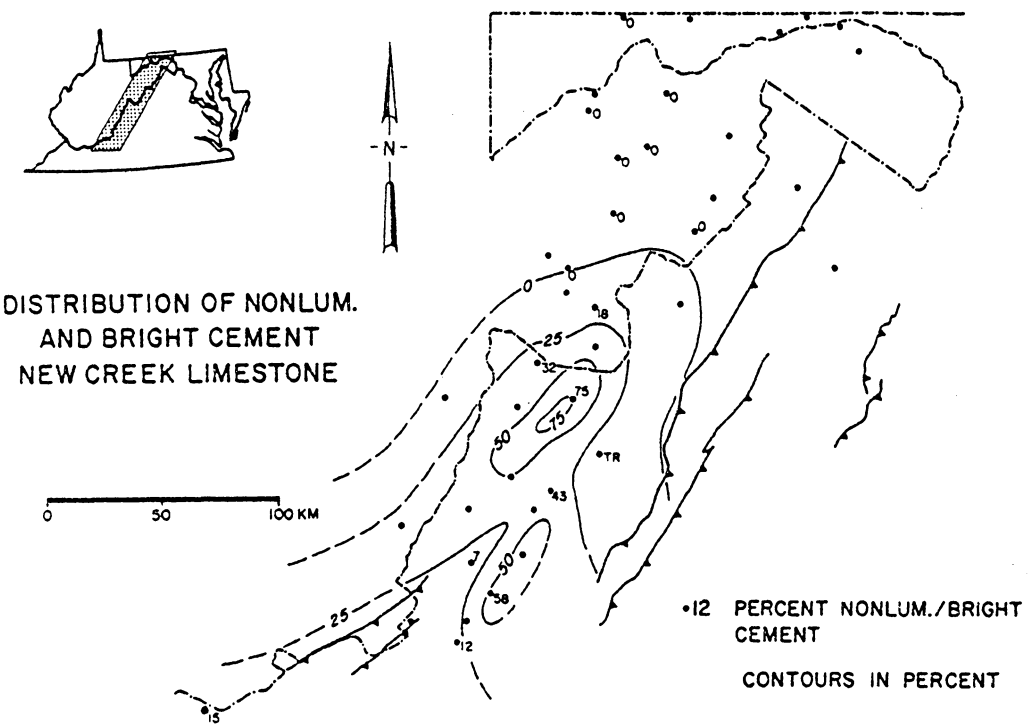
DISTRIBUTION OF NONLUM.
AND BRIGHT CEMENT
NEW CREEK LIMESTONE
N
0
50
100 KM
0
18
25
32
73
75
50
TR
43
7
50
38
12
25
15
•12 PERCENT NONLUM./BRIGHT CEMENT
CONTOURS IN PERCENT

Figure 24. Timing of cements and related diagenetic events, Helderberg Group, Central Appalachians.

Timing of cements and related diagenetic events, Helderberg Group, Central Appalachians

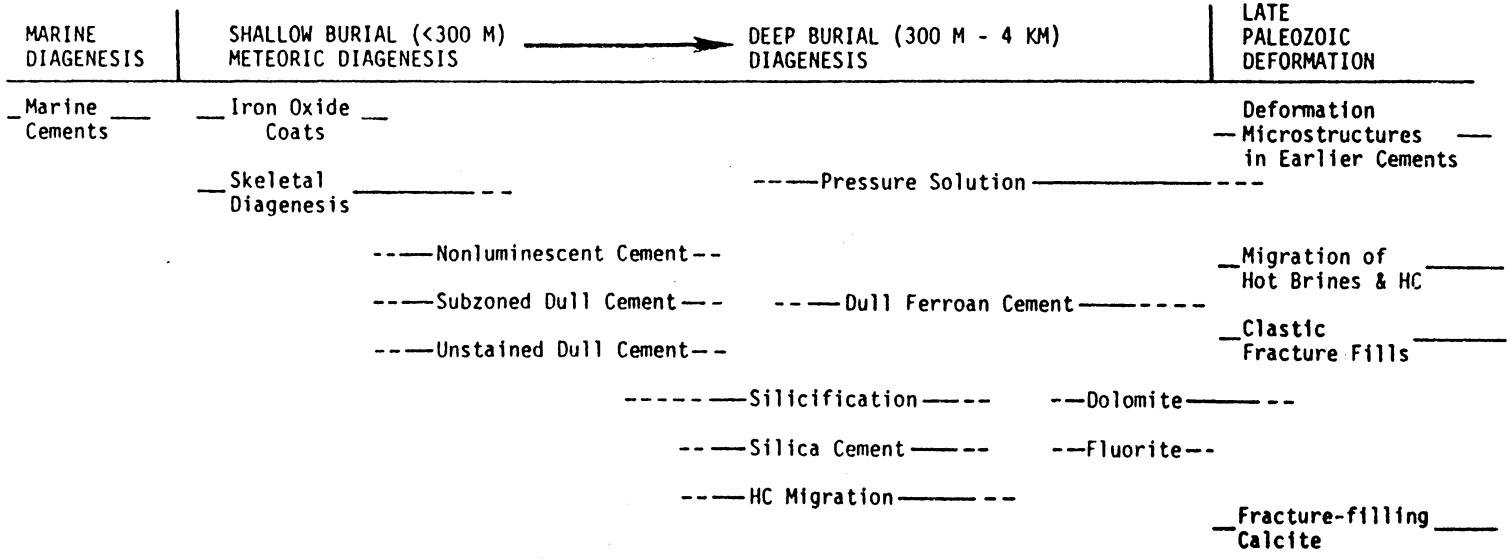

Figure 25. Manganese versus iron contents in various luminescent calcite cement zones (determined by electron microprobe analyses). Values in ppm. Note changes in scale at 2000 ppm on vertical (Mn) scale and at 2000 and 3000 ppm on horizontal (Fe) scale. Symbols: plusses = bright cement; stars = dull; triangles = nonluminescent; squares = slightly luminescent. Overlap of fields at low trace amounts indicates concentrations near the detection limits of the electron microprobe.

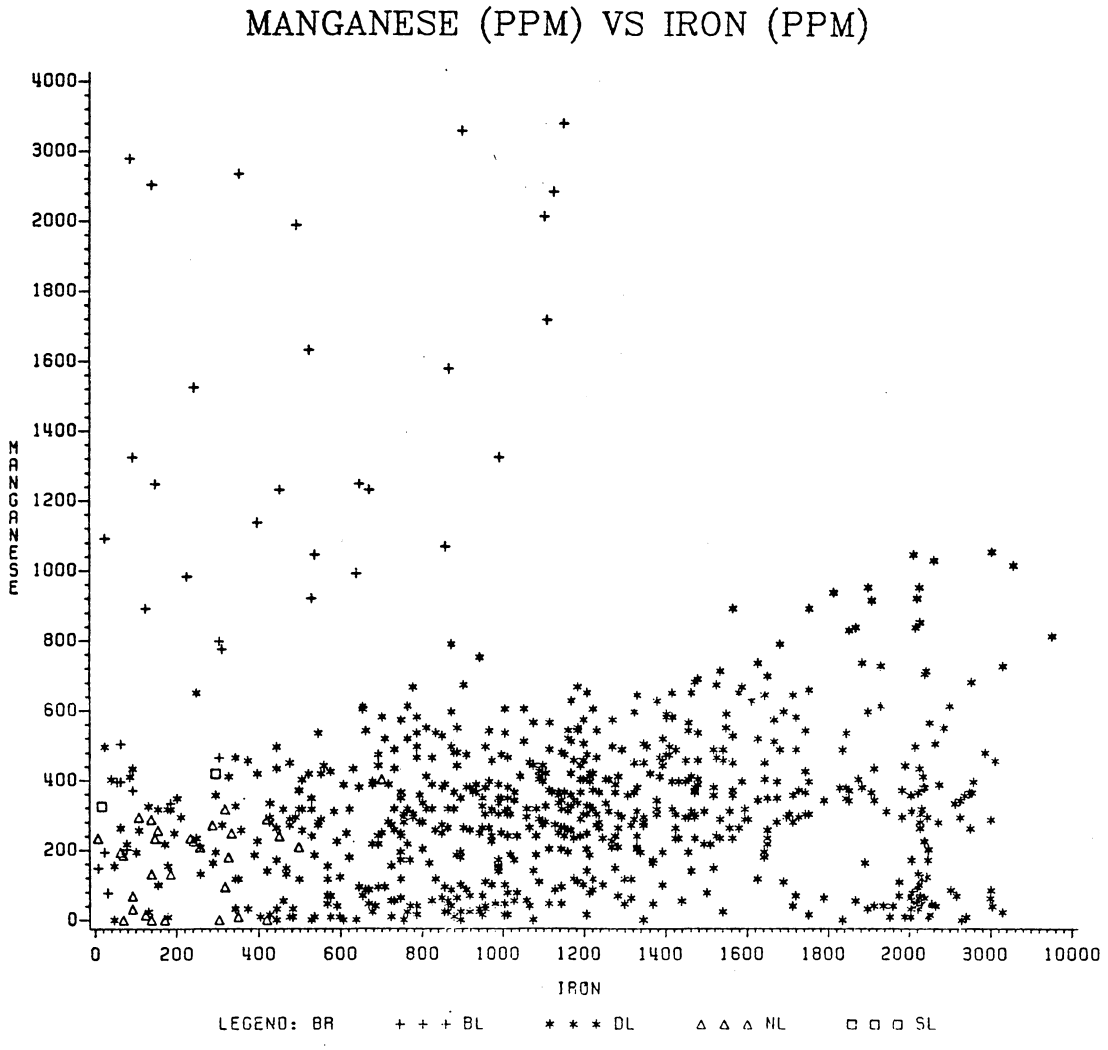
MANGANESE (PPM) VS IRON (PPM)
MANGANESE
4000
3000
2000
1800
1600
1400
1200
1000
800
600
400
200
0
0
200
400
600
800
1000
1200
1400
1600
1800
2000
3000
10000
IRON
LEGEND: BR + + + BL * * * DL △ △ △ NL □ □ □ SL

therefore would not have substituted extensively for calcium in calcite (Meyers, 1974, 1978; Oglesby, 1976). Luminescent interlayers in nonluminescent cement (and downdip, time-correlative, Mn-rich, bright cement, discussed later) suggest that pore fluid redox potential was the major reason for manganese-poor cement and not the lack of manganese in pore fluids (cf. Grover, 1981). Scattered iron oxide coatings on grains in updip portions of aquifers also suggests oxidizing conditions in aquifers prior to precipitation of nonluminescent cement. Iron oxide species (authigenic, particulate, and dissolved) are well-documented in oxidizing, updip portions of modern aquifer systems (Back and Barnes, 1965; Champ et al., 1979).

Nonluminescent equant cements were precipitated from oxidizing meteoric pore fluids (Oglesby, 1976; Frank et al., 1982) derived from recharge areas in tectonic uplands along the eastern flank of the foreland basin. The uplands provided the hydraulic drive to force connate marine fluids from the sediments under shallow burial conditions (cf. Grover and Read, 1983). The basinward decrease in nonluminescent cement from the southeast probably reflects more reducing meteoric pore fluids downdip. The distribution of nonluminescent cement in limestone seaward of quartz sandstone lobes and lack of early nonluminescent cement (except on scattered calcite grains) in sandstone suggests that the sandstones remained "open" during shallow

burial cementation and acted as conduits for upland-sourced, meteoric pore fluids involved in cementation

Very thin interlayered luminescent zones in nonluminescent cement may have developed during temporary stagnation of the aquifer. Temporary stagnation in modern aquifers may develop with seasonal variation in precipitation (Ogden, 1984), convergence or divergence of transient flow systems (Toth, 1980), periodic influxes of dissolved organic carbon into aquifers (Champ et al., 1979), or climatic changes. Periodic undersaturation in updip portions of aquifers probably resulted in corrosion of some early nonluminescent and bright cement.

Bright Cement

Description. Bright cement occurs as thin (submicron to 40 um thick) laminae that have bright yellow to bright orange cathodoluminescence. It postdates or is interlayered with nonluminescent cement (Figs. 15B, 20A) in updip limestone and sandstone. Basinward, bright cement is interlayered with early dull cement (Figs. 15C, D) to form "subzoned dull" cement. Most bright cement uniformly overgrows earlier nonluminescent or dull cement and outlines successive growth morphologies of cement crystals (Figs. 15B, 20A).

Bright cement is locally replaced by microcrystalline quartz or chalcedony. It also contains deformation twins

and cleavage planes and is crosscut by tectonic fractures, stylolites, and secondary fluid inclusion trains.

Trace Elements. Bright cement contains 30-3400 ppm Mn (av. 1170 ppm), 0-1140 ppm Fe (av. 380 ppm), and 0-3500 ppm Mg (av. 800 ppm; Table 1). Levels of Sr, Na, Pb, Zn, Ni, K, and Cl were below microprobe detection limits.

Distribution. Bright cement makes up 0 to 53% of equant calcite cement (Table 1). It postdates nonluminescent cement in updip sections, or occurs immediately downdip from the last occurrence of nonluminescent cement (Fig. 22).

Timing and Origin of Bright Cement. Bright cement is interlayered with and postdates nonluminescent cement; it is interlayered with and predates dull cement (Fig. 24). Bright cement predates quartz cement and silicification, stylolitization, and Late Paleozoic deformation. It precipitated under similar burial regimes (less than 300 m burial depth) as nonluminescent cement.

Bright cement precipitated from meteoric pore fluids that were slightly reducing, allowing manganeses and lesser amounts of iron to be in reduced (2+) valence states and substitute for calcium in calcite cement (Table 1; Figs. 19, 24; Frank et al., 1982). Downdip reduction of groundwater in modern freshwater aquifers is common; manganese species are reduced first, before iron species (Champ et al., 1979; Stumm and Morgan, 1970). Bright cement downdip from

nonluminescent cement and interlayering of bright cement with nonluminescent and dull cement indicate that bright cement formed in transitional redox zones in the aquifers where pore fluid redox potentials fluctuated between oxidizing, slightly reducing, and reducing conditions.

Dull Cement

Description. Dull cement has dull orange to very dull red-orange luminescence. Rare dull laminae are locally interlayered with nonluminescent cement in updip limestone; dull cement is complexly interlayered with bright cement (to form subzoned dull cement) in intermediate portions of aquifer systems (Fig. 15C, D). However, downdip cements have homogeneous, nonzoned dull luminescence (including neomorphosed marine, inclusion-rich, syntaxial rim cement; Figs. 15E, F). Potassium ferricyanide staining of nonzoned dull cements and microprobe data (Fig. 19) show that early dull cement is less ferroan (unstained) than later dull cement (stains blue). Scattered pyrite crystals also occur with dull cement (Figs. 15C, D).

Dull cement is the final void-filling calcite cement. It postdates silicification of skeletal grains and precipitation of quartz overgrowths in quartz sandstone. Dull cement fills molds of siliceous sponge spicules in cherty limestone. Some spicule molds are filled with coexisting megaquartz and dull calcite. Dull calcite

replaces chalcedony botryoids in rare brachiopod shelter voids.

Dull cement is stylolitized and postdates mechanical grain breakage (Fig. 20B). Void-filling dull calcite has deformation twins, cleavage traces, and secondary fluid inclusions in healed microfractures and also occurs in tectonic fractures as equant cement and as fibrous calcite. Dull cement predates dolomite and fluorite.

Trace Elements. Dull cement contains 0-1050 ppm Mn (av. 290 ppm), 0-42500 ppm Fe (av. 1260 ppm), and 0-10,700 ppm Mg (av. 1800 ppm; Table 1; Appendix A). Latest dull cement is more iron-rich (stains with potassium ferricyanide solution) than early dull cement and is locally more magnesium-rich as indicated in some microprobe traverses (Fig. 19) but there is no systematic relation between Fe and Mg in the various calcite zones (Fig. 26). Sr, Na, Pb, Zn, Ni, K, and Cl levels were below microprobe detection limits.

Fluid Inclusions. Primary two-phase fluid inclusions (<15 um diameter) occur only in dull cement and were not found in nonluminescent or bright cement. Several inclusion chips were stained with potassium ferricyanide solution and the host dull cement is ferroan. Eutectic and melting (ice) temperatures suggest fluids are dilute (2.9 wt %) Na-Cl solutions to complex, saline (>23 wt % NaCl) brines (Table 1; Appendix C). Pressure-corrected liquid-vapor

Figure 26. Magnesium versus iron contents in various luminescent calcite cement zones (trace elements determined by electron microprobe analyses). Values in ppm. Symbols: plusses = bright cement; stars = dull cement; open triangles = nonluminescent; solid triangles = slightly luminescent.

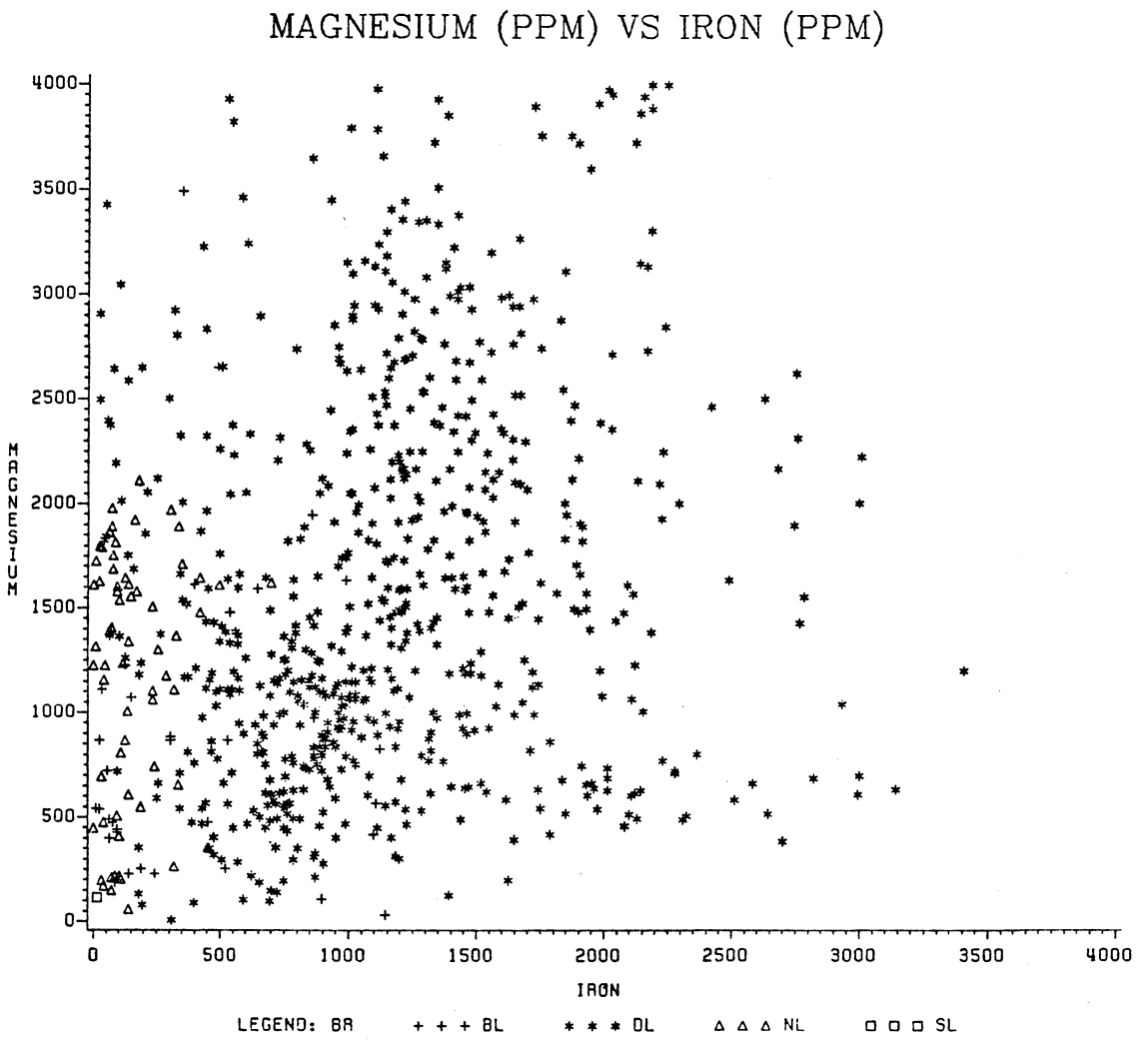
MAGNESIUM (PPM) VS IRON (PPM)
MAGNESIUM
4000
3500
3000
2500
2000
1500
1000
500
0
0
500
1000
1500
2000
2500
3000
3500
4000
IRON
LEGEND: BR + + + BL * * * DL Δ Δ Δ NL □ □ □ SL

homogenization temperatures indicate trapping temperatures between 90 and 200°C (400 bar hydrostatic pressure correction; Table 1). CO_2 or CH_4 hydrate phases were not observed during cooling, indicating that the vapor phase is probably water vapor (Hanor, 1980). Rare, nonfluorescent, dark-colored, primary inclusions that may be hydrocarbons, also occur in some dull cement.

Distribution. Dull cement comprises 23 to 100% of total cement (fracture-filling dull cement excluded; Table 1). It occurs in all lithofacies that have coarse-grained calcite cement and is the last void-filling calcite cement. In nonzoned dull cement, early unstained dull cement was visually estimated as comprising approximately 10-25% of the total cement.

Timing and Origin of Dull Cement. Dull cement is the final void-filling calcite cement and is strained, indicating that Helderberg sediments were lithified prior to Late Paleozoic deformation (Fig. 24). Dull cement precipitated from more reducing pore fluids than nonluminescent or bright cement as suggested by high iron contents (Table 1; Figs. 19, 25) and pyrite inclusions (Frank et al., 1982).

It is difficult to determine the timing of various cement generations in homogeneous, nonzoned dull cement. Interlayered bright and dull laminae ("subzoned" dull

cement; Fig. 15D) and rare dull laminae in nonluminescent cement indicate that some dull cement did precipitate in updip portions of aquifers from meteoric water under shallow burial conditions. Late dull cement is more ferroan (stains in potassium ferricyanide solution) and locally more magnesium-rich than early (unstained) dull cement. In some voids, early unstained dull cement precipitated before quartz cement; final void-filling in these voids is by dull ferroan cement. Silica cements probably formed from hot basinal fluids (see below), as did most dull ferroan cement. Thus, early unstained dull cement is interpreted as dull cement that precipitated from reducing groundwaters under shallow burial conditions (<300 m) in most distal portions of aquifers.

Rare primary two-phase fluid inclusions that occur only in stained dull cement indicate burial temperatures of 90-200°C during precipitation (Table 1). Bodnar and Bethke (1984) have shown that primary fluid inclusion volumes and homogenization temperatures can be re-set if the inclusions are subjected to temperature/pressure conditions greater than those at the time of entrapment. Primary inclusions in this study were selected because they lacked evidence for stretching or necking. Given the small sample size and possibility of inclusion re-setting, the pressure-corrected homogenization temperatures (90-200°C) still suggest precipitation of dull ferroan cement under deep burial

conditions. Possible primary hydrocarbon inclusions in dull cement also suggest that some dull cement precipitated in the oil window (Pusey, 1973) or between 60 and 150°C.

Eutectic and melting (ice) temperatures (Table 1) from primary inclusions indicate burial pore fluids were dilute to saline fluids. Eutectic temperatures indicate that inclusion fluids contain variable concentrations of Na, Ca, and possibly Mg, and K (Crawford, 1981). Thus, void-filling dull cements probably precipitated during progressive burial from 300 m (maximum burial depth for nonluminescent and bright cement) to 4 km (maximum sedimentary overburden; Fig. 16) from dilute to saline fluids that probably were Na-Ca-Cl brines.

Some late dull cement contains more magnesium than nonluminescent, bright, or early dull cement (Fig. 19), although there is no systematic relationship between Fe and Mg in the various cements (Fig. 26). Loucks (1983) has suggested that deep burial calcite cements have lower magnesium contents than shallow burial cements. However, experimentally determined partition coefficients for magnesium in calcite increase with increasing temperature (Katz, 1973; Fuchtbauer and Hardie, 1979). Thus, Mg-enrichment in some dull ferroan cement may reflect this temperature effect on partitioning. Coexisting saddle dolomite and Mg-enriched calcite cement in some vugs and fractures also suggest that pore fluids had sufficient

magnesium to form these phases (probably aided by elevated temperatures; Rosenberg and Holland, 1965).

Stable Isotopes of Calcite Cements

Individual cement components and pelmatozoan grains were sampled for stable isotopic analysis. Preliminary interpretation of stable isotopes is presented here but a more detailed discusion will be presented later (Lohmann and Dorobek, in prep.). All oxygen and carbon isotopic values are expressed relative to PDB, unless stated otherwise. Stable isotopic fractionation curves from Friedman and O'Neil (1977) were used to calculate $\delta^{18}O$ values for pore waters involved in cementation. in cementation. Equilibrium $\delta^{13}C$ values for dissolved HCO_3- in pore waters were calculated using the isotopic fractionation equations of Bottinga (1968) and Mook et al. (1974).

Shallow Burial Cements

Average $\delta^{18}O$ and $\delta^{13}C$ compositions for shallow burial cement components are: nonluminescent cement (-5.8‰, +2.6‰), subzoned dull cement (-6.0‰, +2.4‰), early dull cement (-5.4‰, +3.5‰), and pelmatozoan grains (-6.0‰, +3.5‰; Table 1; Appendix B). Together, the shallow burial cements vary between -8.7 to -4.7‰ $\delta^{18}O$ and +0.4 to +4.7‰ $\delta^{13}C$ (Fig. 27). The average difference

Figure 27. Stable isotopic compositions of various cement components and pelmatozoan grains. Isotopic values relative to PDB standard. Solid symbols are early meteoric cement components and pelmatozoan grains; open symbols are late dull ferroan cement and fracture-filling calcite. Large symbols are mean values for each component. Note overlap of fields for early and late cement components but most early cement components plot between -6.5 to -4.5 $\delta^{18}O$.

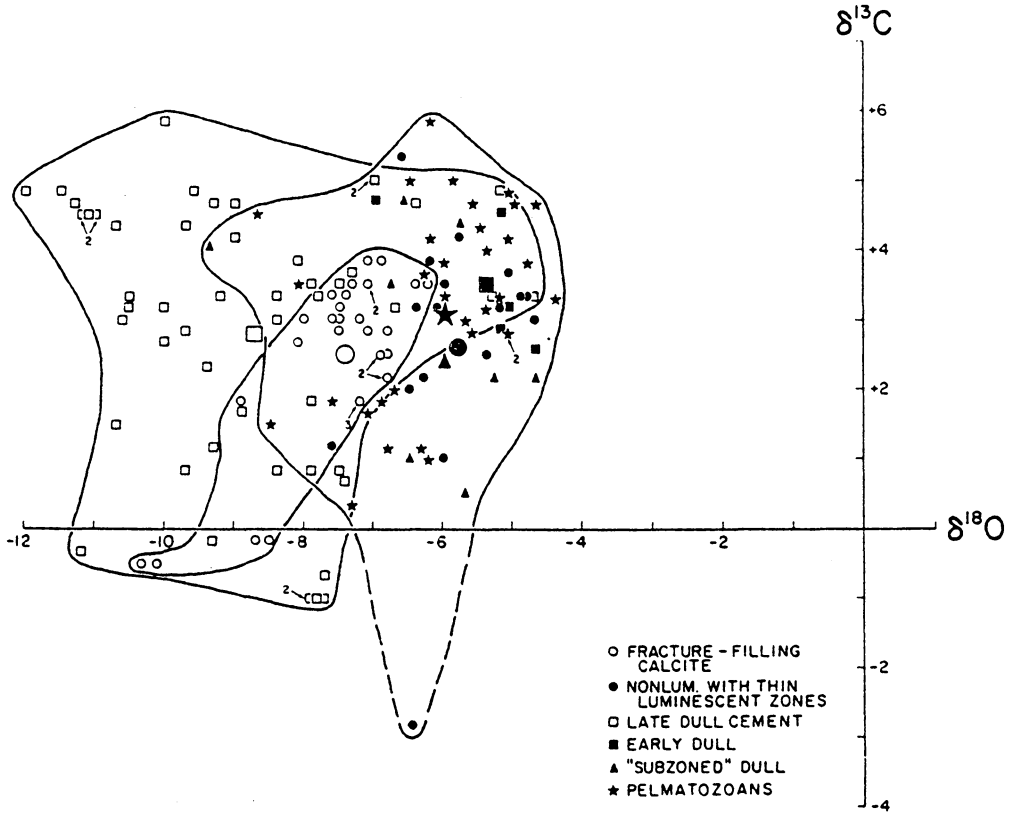
δ13C
+6
+4
+2
-2
-4
δ18O
-12
-10
-8
-6
-4
-2
FRACTURE - FILLING CALCITE
NONLUM. WITH THIN LUMINESCENT ZONES
LATE DULL CEMENT
EARLY DULL
"SUBZONED" DULL
PELMATOZOANS

between the isotopic compositions of pelmatozoan grains and earliest clear equant calcite cement from the same samples is -0.3‰ $\delta^{18}O$ and +0.2‰ $\delta^{13}C$ (Table 1; Appendix B).

Early cement generations (nonluminescent, subzoned dull, and unstained dull) and pelmatozoan grains are significantly lighter in both ^{18}O and ^{13}C in the Lower Keyser than in the Upper Keyser and New Creek Limestones (Fig. 28). $\delta^{18}O$ values also tend to be heavier downdip and upsection in oxidizing to slightly reducing portions of Helderberg aquifers (Fig. 28), while $\delta^{13}C$ values show no obvious trends. No obvious stratigraphic trends in isotopic composition exist in early cements and pelmatozoan grains in basinward sections.

Average $\delta^{18}O$ values from early cement components (-6.0 to -5.4‰) indicate shallow burial pore fluids (at 20 to 30°C) had $\delta^{18}O$ values of about -35 to -33‰ (-5 to -3‰ SMOW). Average $\delta^{13}C$ values from early cement components (2.4 to 3.5‰) indicate that dissolved HCO_3- in pore fluids (at 20 to 30°C) had equilibrium $\delta^{13}C$ values of about -1.3 to +2.3‰.

Discussion.

Average stable isotopic compositions of nonluminescent, subzoned dull, and early dull cements are very similar (Table 1; Fig. 27) suggesting precipitation from related pore fluids. The similarity in stable isotopic composition and luminescence of early cements and pelmatozoan grains

Figure 28. Stratigraphic variation in stable isotopic compositions of early cement components, cross-section E-E'. Note $\delta^{18}O$ and $\delta^{13}C$ values generally lighter in cements from Lower Keyser Limestone compared to cements from Upper Keyser/New Creek Limestones. No obvious stratigraphic variation in isotopes in sections basinward (to the right) of Oak Flat section.

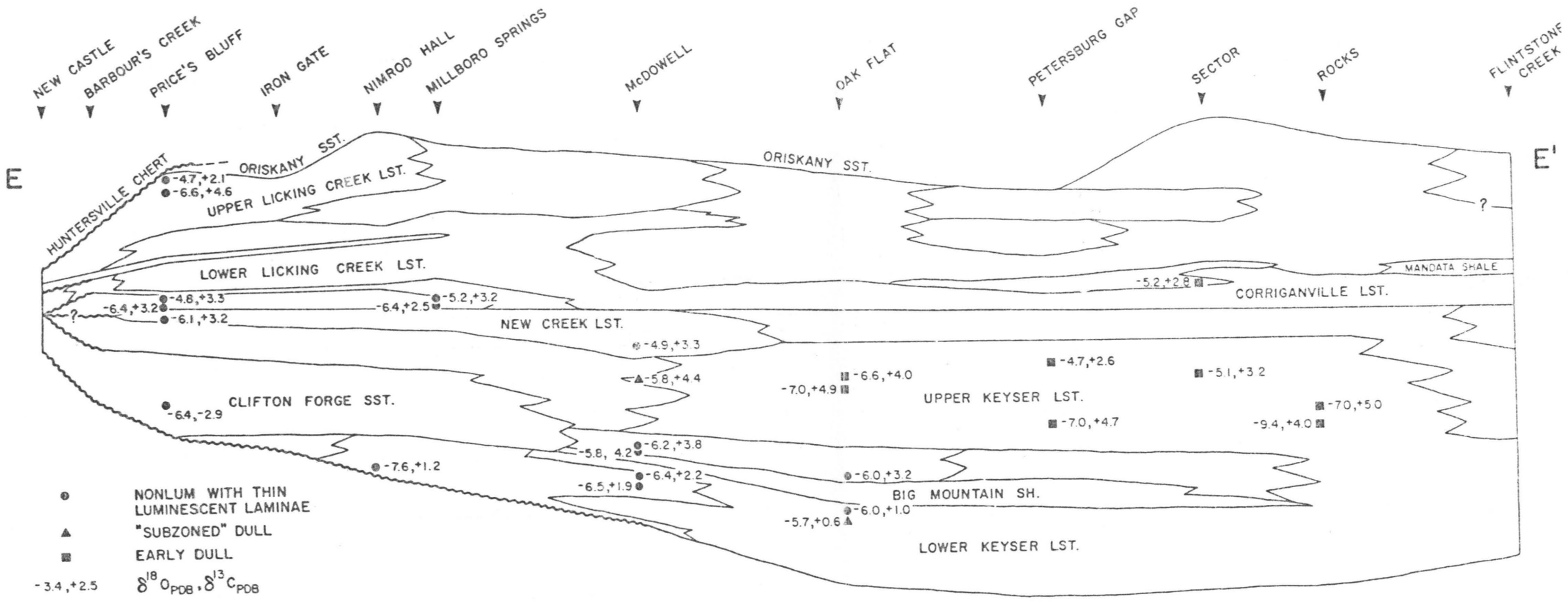
NEW CASTLE
BARBOUR'S CREEK
PRICE'S BLUFF
IRON GATE
NIMROD HALL
MILLBORO SPRINGS
McDOWELL
OAK FLAT
PETERSBURG GAP
SECTOR
ROCKS
FLINTSTONE CREEK
E
E'
HUNTERSVILLE CHERT
ORISKANY SST.
UPPER LICKING CREEK LST.
LOWER LICKING CREEK LST.
NEW CREEK LST.
CLIFTON FORGE SST.
CORRIGANVILLE LST.
MANDATA SHALE
UPPER KEYSER LST.
BIG MOUNTAIN SH.
LOWER KEYSER LST.
-4.7,+2.1
-6.6,+4.6
-4.8,+3.3
-6.4,+3.2
-6.1,+3.2
-6.4,+2.5
-5.2,+3.2
-5.2,+2.8
-4.9,+3.3
-5.8,+4.4
-6.6,+4.0
-7.0,+4.9
-4.7,+2.6
-5.1,+3.2
-7.0,+5.0
-9.4,+4.0
-7.0,+4.7
-6.4,-2.9
-7.6,+1.2
-5.8, 4.2
-6.2,+3.8
-6.4,+2.2
-6.5,+1.9
-6.0,+3.2
-6.0,+1.0
-5.7,+0.6
NONLUM WITH THIN LUMINESCENT LAMINAE
"SUBZONED" DULL
EARLY DULL
-3.4,+2.5
δ18OPDB, δ13CPDB

suggests these components isotopically equilibrated with the first pore fluids to flow through the sediments and precipitate clear equant calcite cement.

The $\delta^{18}O$ of calcite precipitated from modern coastal/island meteoric groundwater should be about -4 $(\pm 2)^{0}/oo$ PDB when average monthly temperatures are 20 to 25°C (Anderson and Arthur, 1983). The Central Appalachian Basin during Helderberg time was at about 10 to 20° S latitude (Scotese et al., 1979) so 20 to 25°C average surface temperatures are reasonable. Assuming the $\delta^{18}O$ composition of seawater (the ultimate source for rainfall) has not changed significantly since the Devonian, the $\delta^{18}O$ values for early Helderberg cements and neomorphosed pelmatozoans are similar to predicted values for calcites precipitated from modern, meteoric-derived, coastal groundwaters (Anderson and Arthur, 1983). Additionally, the calculated $\delta^{18}O$ values of Helderberg paleogroundwaters (-5 to $-3^{0}/oo$ SMOW) obtained from early Helderberg cements are close to $\delta^{18}O$ values of precipitation from modern coastal/island stations with average monthly temperatures of 20 to 25°C ($\delta^{18}O$ = -4 to $-3^{0}/oo$ SMOW; Yurtsever, 1975).

Slightly lighter average $\delta^{18}O$ values (-5.4 to $-6.0^{0}/oo$ versus the predicted $-4^{0}/oo$) from early cements may reflect a temperature effect on oxygen isotope fractionation due to slightly higher temperatures in aquifers compared to surface temperatures. Limited sampling suggests that $\delta^{18}O$ values in

early cements become heavier downdip and upsection (probable groundwater flowpath directions; Fig. 28). Groundwater temperatures would have increased by no more than 10°C from recharge areas (20°C surface temperature) to distal portions of aquifers (about 30°C maximum temperature at 250 m burial, assuming 35°C/km geothermal gradient; aquifer burial depths discussed later) which would have resulted in downdip calcite cements that are about -2‰ $\delta^{18}O$ lighter than updip calcite cement. Therefore, contribution of dissolved heavy marine carbonate may have been important in offsetting increased temperature effects.

$\delta^{13}C$ values from early cement components are relatively heavy compared to commonly accepted values for freshwater carbonate cements (-8 to -4‰; Keith and Weber, 1964). However, if dissolution of heavy, marine, high magnesium-calcite was an important source for ^{13}C in paleogroundwaters (supported by updip dissolution of pelmatozoan grains), cements precipitated downflow could have positive $\delta^{13}C$ values (cf. Allan and Matthews, 1977; Wigley et al., 1978). $\delta^{13}C$ values from groundwaters in shallow carbonate aquifers are positive and heaviest in discharge areas, which is attributed to dissolution of marine carbonate in the aquifers (Smith et al., 1976). Bacterial fermentation of organic matter also may have contributed heavy carbon to the groundwaters (Curtis, 1978).

Deep Burial Cements

Late dull ferroan cement varies between -12.0 to -4.7‰ $\delta^{18}O$ (av. -8.7‰) and -1.0 to +5.8‰ $\delta^{13}C$ (av. +2.8‰; Fig. 27). Late cement components show no stratigraphic variation in isotopic composition.

Two dull ferroan cement-filled brachiopod shelter voids were chosen for multiple stable isotopic analyses because temperature data from primary fluid inclusions in the dull cement had already been obtained and the voids were easy to sample. These data (Table 2) can be used to estimate stable isotopic compositions of deep formation waters responsible for deep burial cementation. Formation waters with salinities of 14 to 22 wt % NaCl and temperatures between 150 and 200°C (obtained from primary fluid inclusions) would have had $\delta^{18}O$ values of -17.8 to -20.4‰ PDB (+9.8 to +12.5‰ SMOW). Dissolved HCO_3- in the pore fluids would have had $\delta^{13}C$ values of -5.7 to +1.3‰.

Alternatively, if dull ferroan calcite precipitated from formation waters with similar $\delta^{18}O$ composition as meteoric water involved in precipitation of early zoned cements (-5 to -3‰ $\delta^{18}O$ SMOW), the waters would have to have been at 45°C in order to get the observed isotopic values for dull ferroan calcite, which is far below the temperatures determined from primary fluid inclusions. Average $\delta^{13}C$ values for early and late dull calcites overlap, so temperature estimates are not possible.

Table 2. Paired stable isotopic analyses and primary fluid inclusion data from dull cement.

Sample	Primary Fluid Inclusions* T_{HP-C}	Salinity		Stable Isotopes** δ18O	δ13C
W11	182°C	21.8		-7.5	+2.9
				-9.0	+2.1
				-7.0	+1.6
				-7.9	+2.0
				-8.0	+2.1
			MEAN	-7.9	+2.1
FC6	154°C	13.8		-7.9	-0.9
				-7.8	-0.9
	195°C	15.9		-7.7	-0.7
				-7.8	-0.9
				-7.9	-1.0
			MEAN	-7.8	-0.9

*Primary fluid inclusions: T_{HP-C} = 400 bar hydrostatic pressure corrected homogenization temperature; salinity expressed as wt % NaCl.

**Stable isotopes relative to PDB standard.

Discussion.

Void-filling, dull ferroan calcite is, on average, lighter in ^{18}O than early cement components and neomorphosed pelmatozoan grains, but $\delta^{13}C$ values are similar. However, there is overlap of all fields. Lower $\delta^{18}O$ values for late, deeper burial cements can be explained by less fractionation of ^{18}O into cements at higher burial temperatures. If dull ferroan cement precipitated from fluids of similar isotopic composition as meteoric fluids involved in shallow burial cementation, but at 150 to 200°C (from primary fluid inclusion filling temperatures), then the cements should have $\delta^{18}O$ values of -25 to -20‰ PDB (about 11 to 16‰ lighter than the average observed value). If primary fluid inclusion temperatures are accepted, then deep Helderberg formation waters had to have a source(s) for ^{18}O in order to compensate for temperature effects on oxygen isotope fractionation. ^{18}O could have been derived from local pressure-solution of marine carbonate or shallow burial cements or possibly from interstitial fluids expelled from compacting evaporite beds in the Silurian Tonoloway-Salina Formation which directly underlie the Helderberg Group. If fluids were expelled from Silurian evaporites, they probably would be saline, which could account for the relatively high salinities observed in primary fluid inclusions in dull cement (Table 1; Appendix C). Calculated $\delta^{18}O$ values for burial pore fluids (+9.8 to +12.5‰ SMOW; using primary

fluid inclusion filling temperatures) for deep burial pore fluids are remarkably similar to $\delta^{18}O$ values from 150 to 200°C formation waters of the Edwards Group, Texas (Land and Prezbindowski, 1981). Calculated $\delta^{13}C$ values for dissolved HCO_3- (-5.7 to +1.3‰ PDB) are similar to observed values in oil-field waters (Carothers and Kharaka, 1980).

Alternatively, minimum burial temperatures of 45°C are required to get average $\delta^{18}O$ values in dull ferroan cement, if burial fluids had similar ^{18}O composition as meteoric fluids involved in shallow burial diagenesis. This still puts precipitation of "average" dull ferroan cement at burial depths of about 1 km, but implies that primary fluid inclusions have been altered after entrapment. Considering all of the data and because of the similarity of calculated isotopic composition of Helderberg deep burial fluids with modern oil field waters, the first explanation for isotopic compositon of dull ferroan cement is favored.

Fracture-filling Dull Calcite Cement

Fracture-filling calcite varies between -10.3 to -5.2‰ (av. -7.4‰, +2.5‰) $\delta^{18}O$ and -0.5 to +4.8‰ $\delta^{13}C$ (Fig. 27).

Discussion.

Fracture-filling dull calcite cements have stable isotopic compositions that are intermediate between late

dull cement and early cement components (Fig. 27). The shift towards more positive ^{18}O may reflect mixing of deep burial fluids with cooler waters when tectonic fractures were cemented. Alternatively, the intermediate isotopic compositions for fracture-filling calcite may reflect contribution of both early, shallow burial calcite and late, deep burial calcite to the isotopic compositions of fluids involved in cementing fractures. Temperature determinations from primary fluid inclusions in fracture-filling cements were not obtained, so the temperature at which fracture-filling cements formed is not known. Therefore, it is difficult to evaluate the effects of cooling (by mixing with cooler, surface? waters) or the contribution of stable isotopes from all cements and grains ("whole rock") on the isotopic composition of fracture-filling calcite.

Silica Replacement

Silicification of calcareous grains is common in basinal/deep ramp siliceous shale, cherty limestone, and nodular-bedded limestone and skeletal grainstone/packstone. The silica occurs as microcrystalline quartz, fibrous chalcedony, and megaquartz crystals (Fig. 29A).

Microcrystalline quartz and chalcedony have a "spongy" texture at the contact between silicified and unreplaced skeletal grains (Fig. 29B). Partially silicified pelmatozoan grains have rhombohedral calcite crystals

Figure 29. Silica replacement fabrics.

A. Megaquartz replacing brachiopod valve (B). Arrows indicate euhedral terminations on quartz crystals.

B. SEM photomicrograph of acid-etched silicified pelmatozoan grain. Note spongy interface between unreplaced pelmatozoan grain (P) and silica (S) and crystallographically oriented molds from leached calcite surrounded by silica in lower part of photograph (1000X, secondary electron mode).

C. Cathodoluminescent photomicrograph of early zoned calcite cement with sponge spicule molds (M) filled with dully luminescent cement. Note truncation of early zoned calcite cements against dull cement-filled molds indicating early zoned cements encased spicules before they were dissolved and filled with calcite. Also note calcite filling molds has same luminescence as last generation of dull calcite cement. Final void-filling is by nonluminescent silica (S) which probably came from dissolved sponge spicules.

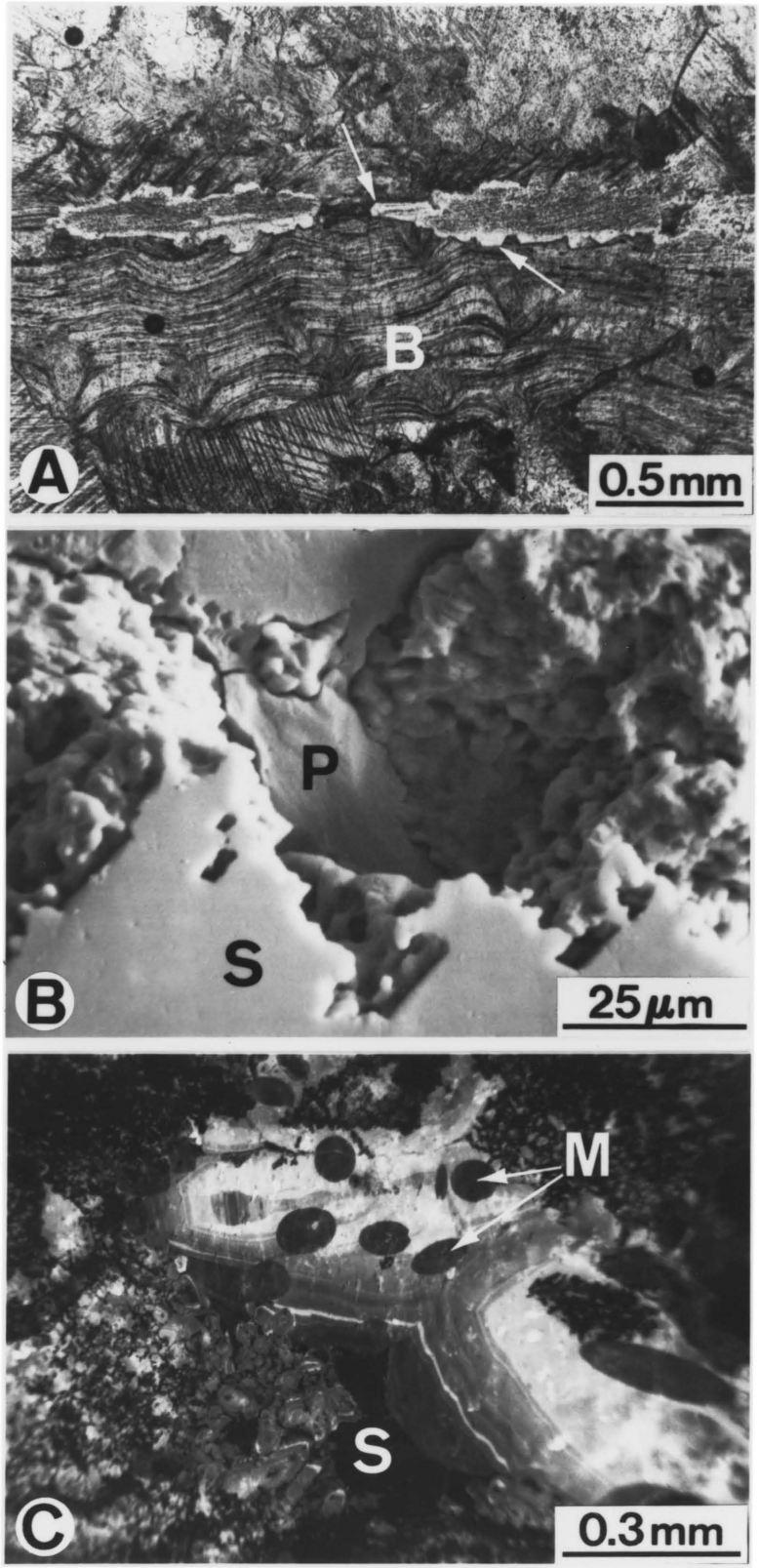
B
A
0.5mm
P
S
B
25μm
M
S
C
0.3mm

surrounded by microcrystalline quartz (cf. Kuslansky and Friedman, 1981). Early calcite cements locally are replaced by silica (Figs. 20E, F). The silica crosscuts nonluminescent and bright calcite cement. Some chert nodules have stylolitized contacts with host limestone and silicified grains may be broken by mechanical compaction. Replacement silica is crosscut by trains of secondary hydrocarbon inclusions.

Timing of Silicification and Source of Silica

Silica replacement occurred prior to some pressure-solution and mechanical compaction. Tectonic fractures through chert nodules and silicified grains indicate that silicification predates Late Paleozoic deformation. Replacement of early zoned cements indicates that some silicification postdated early cementation, but silicification most likely occurred during all stages of burial diagenesis.

Much of the replacement silica may be remobilized biogenic silica. Calcitized sponge spicules are abundant in siliceous shale and some fine-grained limestone, but appear to be absent in cherty limestone under plane light. However, under cathodoluminescence, abundant calcitized sponge spicules are present. These spicules are filled with dull ferroan calcite. Locally, early zoned cement grew around sponge spicules before silica dissolution (Fig. 29C).

After silica dissolution, spicule molds in zoned cement and remaining pore spaces were filled with dull ferroan calcite. Some spicule molds are filled with dull calcite and megaquartz, indicating that quartz and calcite precipitation occurred at nearly the same time in some molds. Homogenization temperatures from primary fluid inclusions in dull cement elsewhere suggest that dissolution of amorphous biogenic silica and precipitation of ordered silica and dull calcite occurred at temperatures between 90 and 200°C.

Silica Cements

Description

Silica cement occurs as: 1) fibrous, commonly botryoidal, chalcedony in intraskeletal and shelter voids; 2) megaquartz crystals in intraskeletal voids and tectonic fractures; and, 3) euhedral quartz overgrowths in sandstone (Fig. 30).

Overgrowths on quartz grains grew into open voids and also replaced surrounding calcareous material (Fig. 30B). Quartz overgrowths postdate nonluminescent, bright, and unstained dull calcite cement.

Quartz crystals occur in many tectonic fractures (Fig. 30C). In some fractures in calcareous quartz sandstone, quartz cement nucleates only on quartz grains, while calcite fracture-filling cements nucleate only on calcareous skeletal grains.

Figure 30. Silica cements.

A. Crossed nicols photomicrograph of microcrystalline quartz and chalcedony filling brachiopod shelter void and partially replacing internal sediments and brachiopod valve.

B. Plane light photomicrograph of euhedral quartz overgrowths on two adjacent quartz grains. Note overgrowths are replacive as indicated by inclusions of host rock calcite within overgrowth.

C. Crossed nicols photomicrograph of tectonic fracture through quartz sandstone. Fracture filled with euhedral quartz (Q) and twinned calcite.

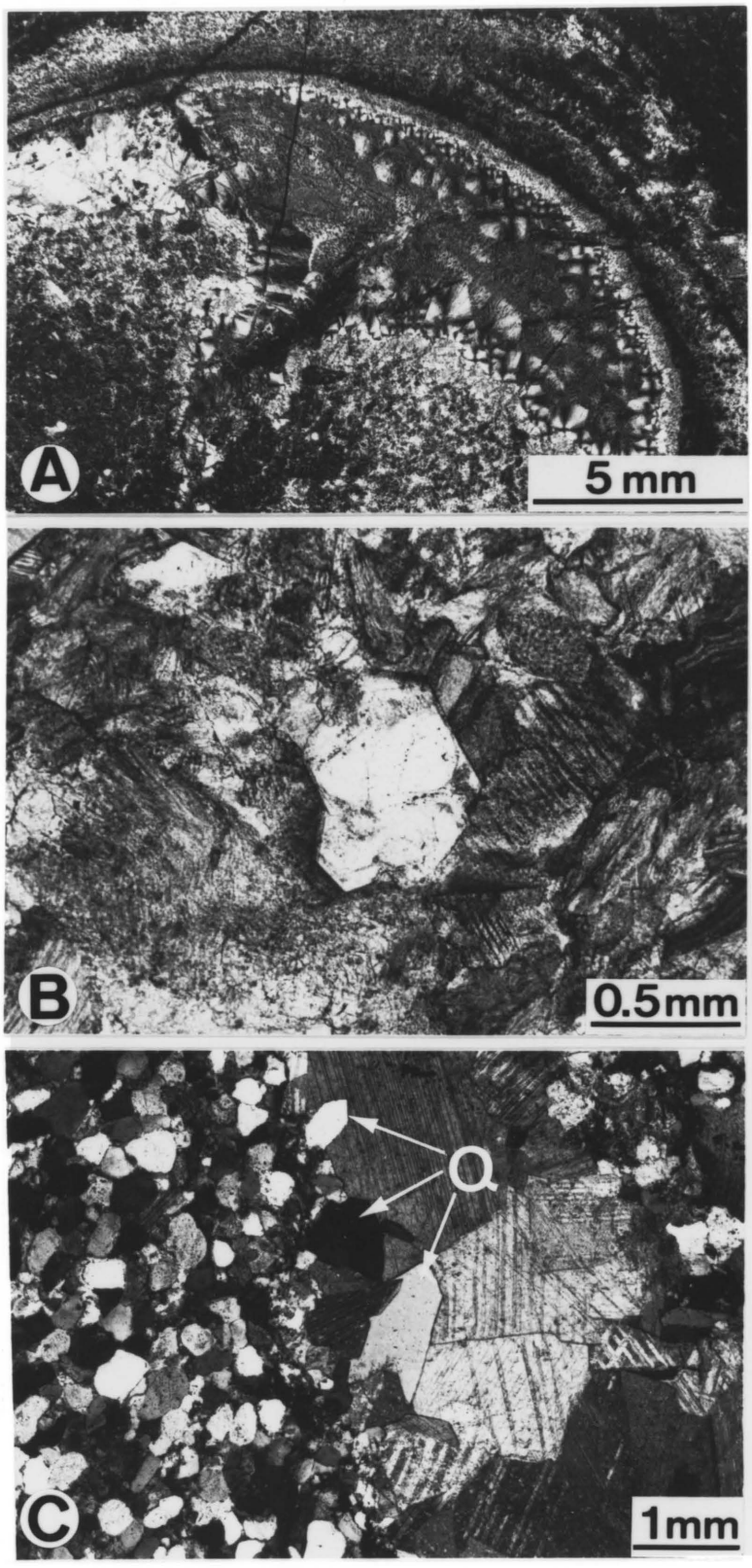
A
5 mm
B
0.5mm
Q
C
1mm

Megaquartz and chalcedony cements in intraskeletal voids locally have hydrocarbon(?) films on crystal terminations (Fig. 31A). Primary hydrocarbon inclusions define crystal growth faces in some quartz overgrowths (Fig. 31B). Secondary hydrocarbon and two-phase fluid inclusions occur in healed microfractures that crosscut quartz cements (Fig. 31C).

Discussion

Silica cements formed during several stages of deeper burial diagenesis. Some quartz overgrowths and megaquartz cement in intragranular voids formed after early zoned calcite cements, but before precipitation of dull ferroan calcite cement. Primary hydrocarbon inclusions in some quartz overgrowths suggest precipitation of quartz overgrowths in the "oil window" (60-150°C; Pusey, 1973). Rare primary two-phase fluid inclusions indicate that some quartz cement formed from dilute Na-Cl fluids at burial temperatures of 180-220°C (400 bar hydrostatic pressure correction; Appendix C).

Much silica may have come from biogenic sources. Cathodoluminescent petrography shows that biogenic silica was remobilized just prior to formation of ferroan dull calcite cement. Sutured quartz grains are rare, but indicate that some silica cement may have come from pressure solution of quartz grains. Clay mineral recrystallization

Figure 31. Hydrocarbons in silica cement.

A. Hydrocarbon films (HC) define megaquartz crystal terminations filling intraskeletal pore space in Favositid coral.

B. Plane light photomicrograph of primary hydrocarbon inclusions (HC) defining crystal growth faces in euhedral quartz overgrowths. See Figure 36C,D for color photomicrograph of this same region.

C. Crossed nicols photomicrograph of quartz cements filling brachiopod shelter void. Arrow indicates secondary fluid inclusion trains that are trapped in healed microfractures that crosscut cements.

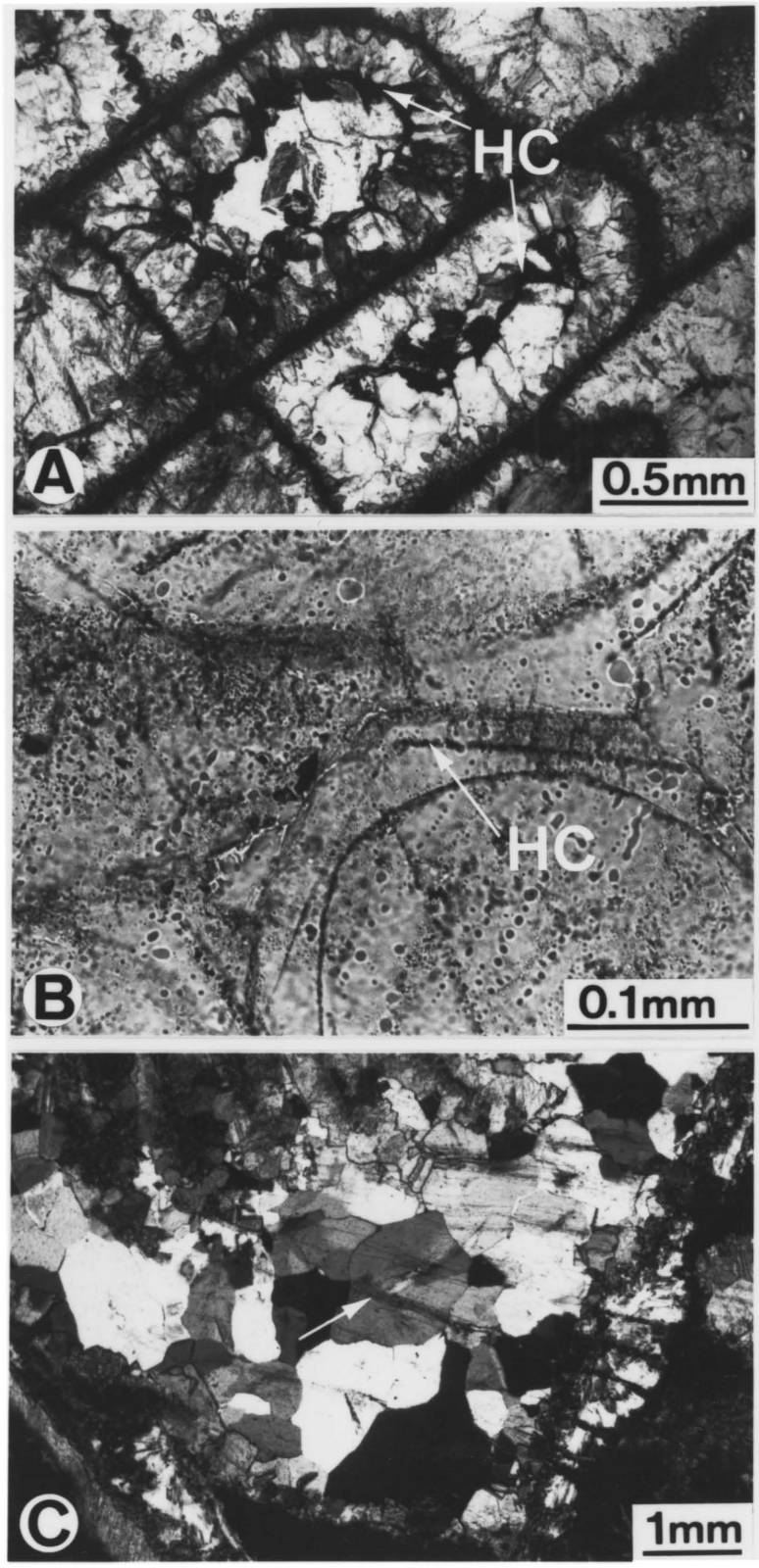
HC
A
0.5mm
HC
B
0.1mm
C
1mm

during burial diagenesis of Helderberg shale and later Devonian shales also may have provided some silica for cementation (Hower et al., 1976; Boles and Franks, 1979).

Dolomite and Fluorite

Dolomite occurs as: 1) void-filling and locally replacive coarse-grained, iron-rich dolomite with curved crystal faces and cleavage planes (Fig. 32A, B) that is similar to "saddle dolomite" (Radke and Mathis, 1980); and 2) small euhedral dolomite rhombs (5-30 um) concentrated along pressure-solution seams in fine-grained argillaceous limestone (Figs. 32C, D).

Saddle dolomite postdates dull ferroan calcite cement and quartz cement. Some ferroan dull cement has irregular contacts with saddle dolomite (Figs. 32E, F) indicating calcite dissolution prior to dolomite precipitation. Saddle dolomite also replaces skeletal grains and lime mud, especially in mud mound lithologies (Fig. 32A). Saddle dolomite coexists with calcite in some voids and tectonic fractures (Fig. 32B). Rare fracture-filling saddle dolomite is refractured and healed by more saddle dolomite.

Much saddle dolomite is extensively dedolomitized, leaving residual calcite and iron oxides (Figs. 33A, B). X-ray maps (Figs. 33C, D, E) of dedolomite show iron oxide and calcite zones are magnesium-deficient. Under cathodoluminescence, dedolomitized areas are brightly

Figure 32. Dolomite fabrics.

A. Crossed nicols photomicrograph of void-filling and partially replacive saddle dolomite (D) in mud mound facies. Note sweeping extinction and curved crystal faces.

B. Coexisting saddle dolomite (D) and calcite (C) in stromatoporoid framestone. Calcite predates and locally postdates saddle dolomite.

C,D. Paired plane light (C) and cathodoluminescent (D) photomicrographs of euhedral dolomite rhombs concentrated along stylolitic seams. Note dolomite rhombs are zoned under cathodoluminescence, with some early zones appearing corroded.

E,F. Paired plane light (E) and cathodoluminescent (F) photomicrographs of saddle dolomite (D) postdating earlier zoned cements. Arrow in F indicates irregular contact between saddle dolomite and dull calcite cement, suggesting corrosion of calcite cement prior to precipitation of saddle dolomite.

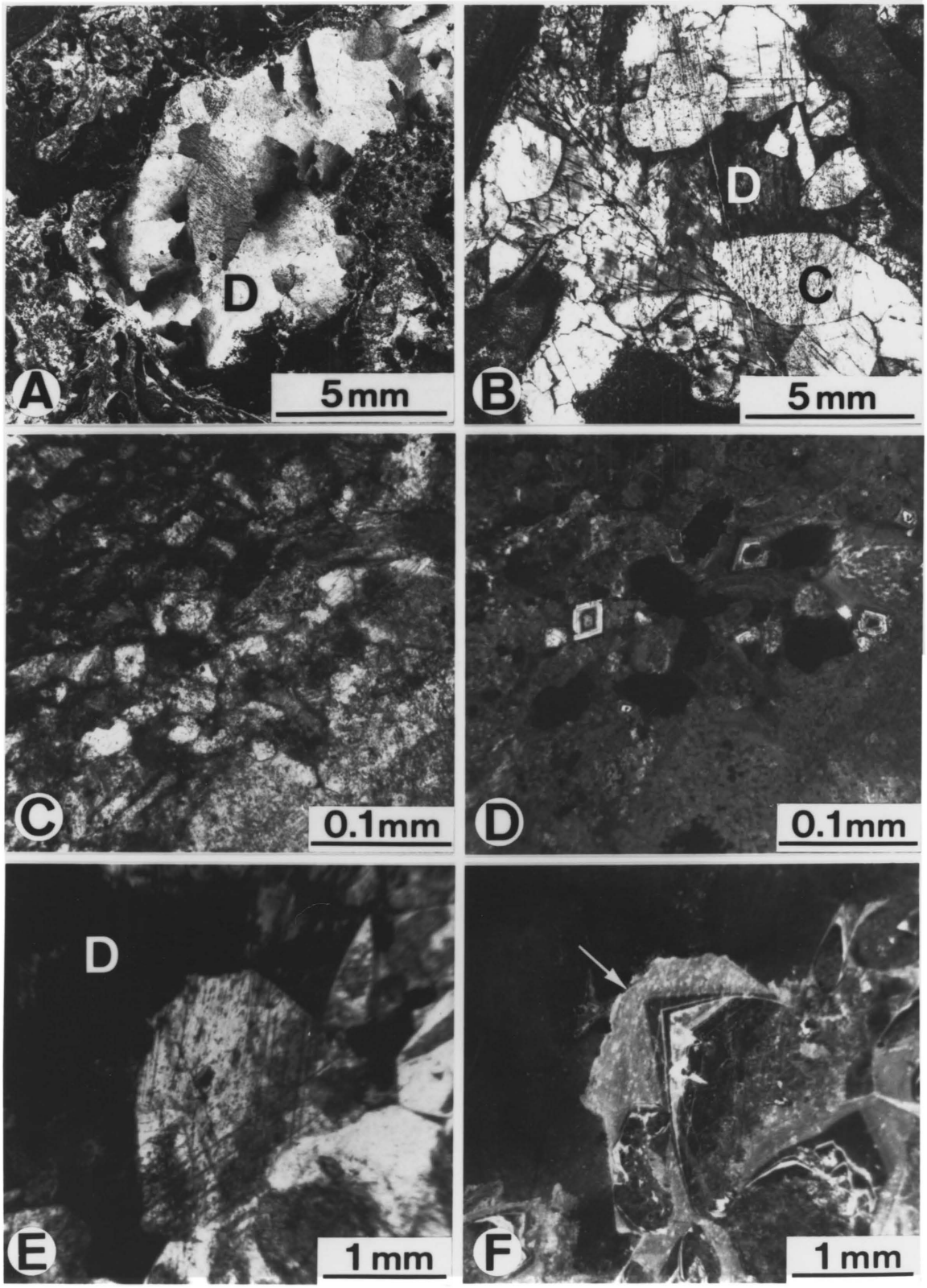
A
D
5mm
B
D
C
5mm
C
0.1mm
D
0.1mm
E
D
1mm
F
1mm

Figure 33. Dedolomite fabrics.

A,B. Paired plane light (A) and cathodoluminescent (B) photomicrographs of saddle dolomite (D). Brightly luminescent patches in B are regions where saddle dolomite has been dedolomitized.

C,D,E. X-ray maps of dedolomite (DE) and saddle dolomite (D) showing qualitative abundance of Mg (33C), Fe (33D), and Mn (33E). Dark regions are deficient in the particular element, light regions are rich in the element. Dedolomitized regions are Mg-deficient (dark areas in 33C), have local Fe-rich patches (where Fe in saddle dolomite formed iron oxides, 33D) and have Mn levels similar to unaltered saddle dolomite (homogeneous distribution in 33E).

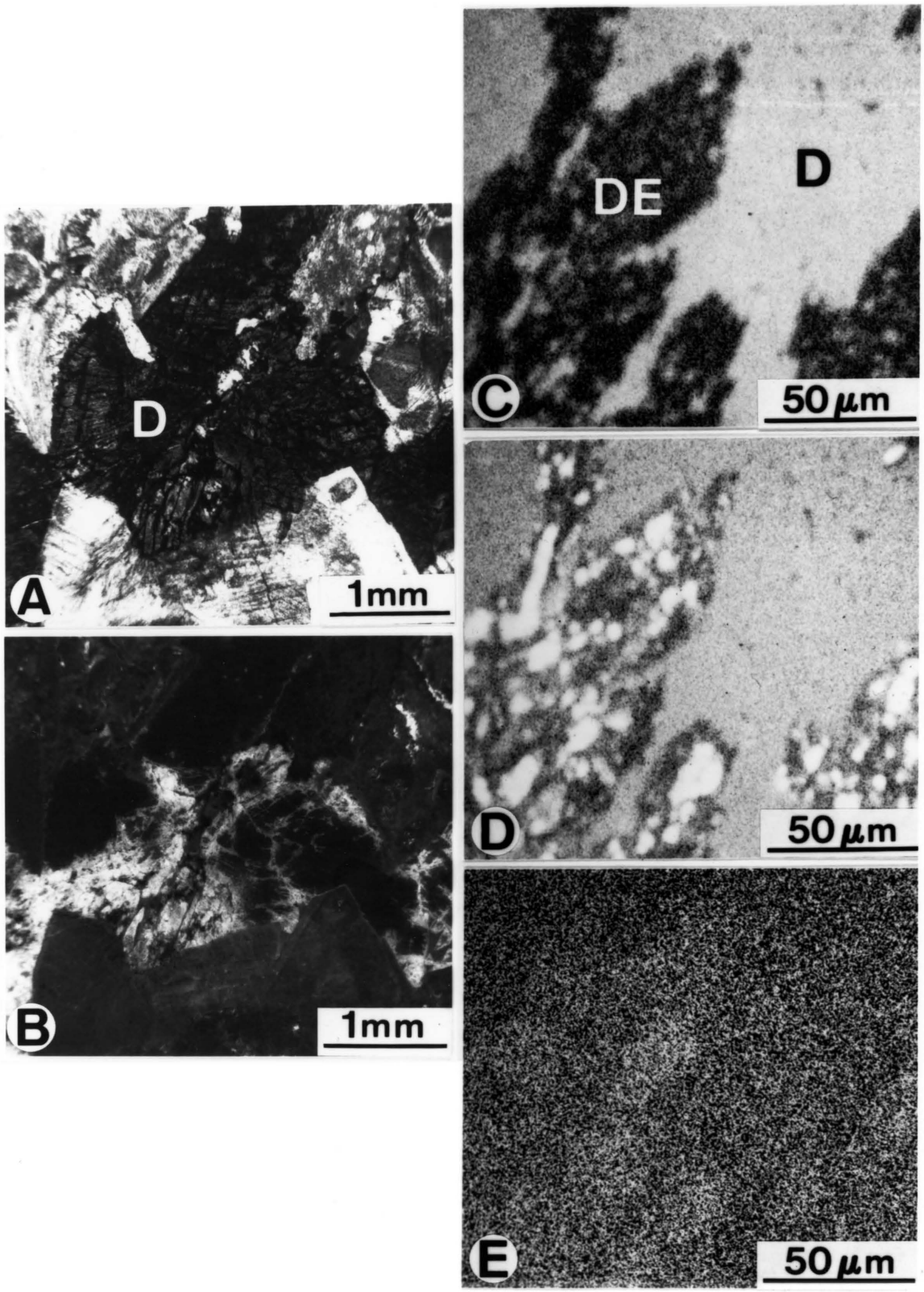
D
A
1mm
B
1mm
DE
D
C
50 μm
D
50 μm
E
50 μm

luminescent, whereas unaltered saddle dolomite has very dull luminescence (Fig. 33B).

Euhedral dolomite crystals concentrated along pressure solution seams in fine-grained argillaceous limestone are zoned under cathodoluminescence (Figs. 32C, D). Early zones appear corroded.

Rare fluorite fills voids and locally replaces host limestone. It postdates void-filling dull cement, appears to have nearly co-precipitated with saddle dolomite in some vugs, and locally is fractured and filled with fibrous calcite.

Discussion

"Saddle" dolomite probably formed during deepest burial from hot brines (about 150°C). Dissolution of calcite cement and grains indicates fluids were undersaturated with respect to calcite prior to formation of saddle dolomite. Fracturing and re-healing of saddle dolomite-filled tectonic fractures indicates that some saddle dolomite formed during Late Paleozoic deformation. Dedolomitization probably occurred by oxidation and alteration of ferroan saddle dolomite in Recent near-surface weathering zones (cf. Frank, 1981). Unaltered saddle dolomite has very dull luminescence, but where it is dedolomitized, iron from saddle dolomite formed iron oxides. Iron thus does not quench Mn-activated cathodoluminescence in dedolomite, even

though Mn levels probably are not significantly different in unaltered saddle dolomite compared to dedolomite (Fig. 33E). Corroded zones in dolomite rhombs in argillaceous limestone suggest that fluids fluctuated between dolomite supersaturation and understauration. Concentration along pressure-solution seams suggests that ions were derived from host limestone, with clay minerals and microdolomite-rich grains and cement possibly supplying magnesium ions for dolomite. Elevated burial temperatures also would have favored dolomite precipitation and calcite dissolution (Rosenberg and Holland, 1965).

Fluorite formed at about the same time as saddle dolomite. Fractured fluorite indicates formation prior to some phases of tectonic fracturing. Fluorite and saddle dolomite are common authigenic phases found in Mississippi Valley-Type ore deposits that may form from deep, basinal brines (Radke and Mathis, 1980; Anderson and Macqueen, 1982).

Regional Distribution of Cement Zones

The regional distribution of cathodoluminescent cement zones (Fig. 22) indicates that meteoric groundwaters, derived from eastern tectonic uplands that bordered the basin were responsible for shallow burial cementation of Helderberg sediments. The downdip gradation of interlayered nonluminescent and luminescent cement to "subzoned dull"

(interlayered bright and dull) cement to nonzoned dull cement reflects progressive downdip reduction of groundwaters. The updip occurrence of early authigenic iron oxides also suggests oxidizing pore waters in updip portions of aquifers. Pyrite occurs with interlayered bright and dull cement and indicates reducing pore fluids downdip.

Downdip reduction is typical of most modern aquifer systems and results from utilization of dissolved oxygen and later reduction of NO_3^- and SO_4^{2-} in pore fluids during the oxidation of particulate and dissolved organic carbon (Champ et al., 1979). Oxidation of reduced inorganic species along aquifer flow paths also may have subordinate effects on oxygen content of groundwaters.

In updip areas of aquifers, groundwaters were undersaturated with respect to high magnesium calcite (indicated by leached pelmatozoans), while downdip, fluids were near-saturation with respect to high magnesium calcite after water-rock reactions along groundwater flow paths (indicated by neomorphosed pelmatozoans).

The regional distribution of nonluminescent and subzoned dull cements coincides with the distribution of sandstone tongues (Figs. 21) suggesting that sandstones acted as permeable conduits for upland-sourced meteoric groundwaters. Scarcity of nonluminescent and bright cement in Helderberg sandstones indicates that they remained permeable during shallow burial diagenesis, when oxidizing

pore fluids, oversaturated with respect to calcite, migrated through sandstones, precipitating early zoned cements only on calcareous substrates. Flushing of sandstone lobes by oxidizing groundwaters had ceased prior to quartz cementation, as indicated by hydrocarbon inclusions in overgrowths on quartz grains (Fig. 31B).

Nonluminescent and bright cements decrease in abundance downdip (Figs. 21, 22, 23), reflecting progressively more reducing conditions in distal portions of aquifers.

Aquifer Evolution

During the Middle Devonian, Helderberg aquifers would have had the necessary conditions for meteoric groundwaters to flow laterally through them and discharge out on the marine shelf. This would have required that the aquifers had hydrologic communication with meteoric recharge areas, groundwaters had sufficient hydraulic head, and the aquifers were confined. Helderberg quartz sandstone lobes that acted as the main conduits for meteoric groundwaters pinch out towards eastern tectonic uplands that were their probable source areas. These uplands were also meteoric recharge areas and provided the necessary gravity-driven hydraulic head for long distance, lateral flow of groundwaters beneath the Appalachian Basin.

Helderberg aquifer(s) must have been confined, otherwise a Ghyben-Herzberg interface would have developed

and meteoric groundwaters would have discharged near the shoreline. However, in layered, confined coastal aquifers, freshwaters can flow offshore up to tens to hundreds of kilometers offshore even under relatively low hydraulic heads, providing that permeability is sufficient (Collins and Gelhar, 1971; Frind, 1982). Submarine discharge occurs on the Atlantic continental shelf,United States (Manheim and Horn, 1968; Manheim and Paull, 1981; Johnston, 1983) and in the Persian Gulf (Chiarelli, 1973, cited in Toth, 1980) only because the discharge is channeled seaward through confined aquifers.

During Helderberg deposition, coastal aquifers largely were unconfined, thus they developed freshwater wedges that probably extended less than a few tens of meters from the paleoshoreline (Fig. 34) and there was little freshwater discharge out on the shelf. In unconfined coastal aquifers, freshwater wedges generally will not extend greater than a few tens of meters offshore (Freeze and Cherry, 1979). However, by the Middle Devonian, Helderberg aquifers were confined by underlying shaly and dolomitic, fine-grained limestone (Tonoloway Formation) and overlying shales and siliceous shale (Huntersville Chert-Needmore Shale, Millboro-Marcellus Shale; Fig. 34). Additional aquitards occur within the Helderberg Group (Big Mountain Shale, Mandata Shale, Shriver Chert). These confining beds allowed meteoric groundwater lenses to extend at least 150 km

Figure 34. Development of Helderberg aquifers. Simplified Helderberg stratigraphy and lithofacies distribution shown. Cross-sections approximately 200 km across; no vertical scale intended. C.F. = Clifton Forge Sandstone; B.M.S. = Big Mountain Shale; H.S. = Healing Springs Sandstone; R.G. = Rocky Gap Sandstone.

A. Development of local freshwater-seawater mixing zone in coastal aquifer where meteoric groundwaters discharged near shoreline because aquifer (Clifton Forge Sandstone) was unconfined.

B. Development of laterally extensive meteoric groundwater systems in Helderberg aquifers during deposition of Huntersville Chert/Needmore Shale. Helderberg aquifers were cofnined at this time, allowing gravity-driven flow of meteoric groundwaters with recharge areas in tectonic uplands. Meteoric groundwaters flowed laterally, expelled connate marine pore fluids, precipitated shallow burial cements, and discharged on the sea floor.

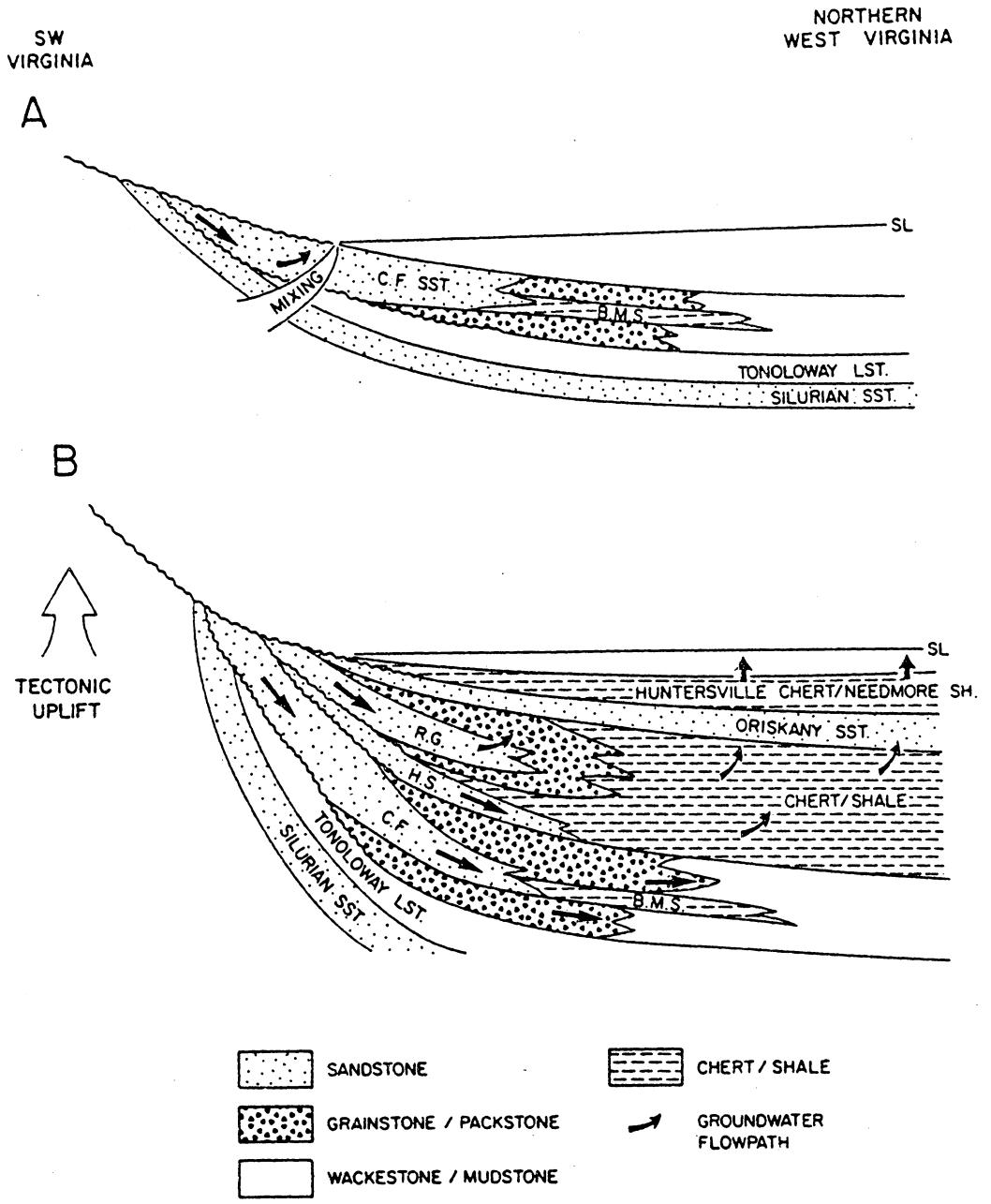
SW
VIRGINIA
NORTHERN
WEST VIRGINIA
A
SL
MIXING
C.F. SST.
B.M.S.
TONOLOWAY LST.
SILURIAN SST.
B
TECTONIC
UPLIFT
SL
HUNTERSVILLE CHERT/NEEDMORE SH.
ORISKANY SST.
R.G.
H.S.
C.F.
CHERT/SHALE
TONOLOWAY LST.
SILURIAN SST.
B.M.S.
SANDSTONE
GRAINSTONE / PACKSTONE
WACKESTONE / MUDSTONE
CHERT / SHALE
GROUNDWATER
FLOWPATH

offshore (minimum palinspastic distance from present eastern outcrop limit to most basinward occurrence of bright cement).

Freshwater tongues must have had sufficient time to develop and completely expel connate marine fluids, for shallow burial cementation of Helderberg carbonates to have occurred. Extensive freshwater tongues in the Helderberg Group probably developed during post-Helderberg/pre-Middle Devonian erosion along the basin margin. During this time fossiliferous marine Oriskany Sandstone and parts of the Helderberg Group were subaerially exposed and eroded in southwest Virginia (Fig. 34). Similar erosional relationships between the Helderberg, Oriskany, and Middle Devonian beds cannot be documented elsewhere (except on the western side of the basin; Dennison and Head, 1975) because of Late Paleozoic erosion and/or overthrusting, but probably can be inferred. The unconformity was exposed for 3-4 m.y. (estimated from Dennison and Head, 1975).

If a conservative flow rate of 1 cm/day (hydraulic conductivity of silt/silty sand; Freeze and Cherry, 1979) is assumed throughout the aquifer, it would take 55,000 years for a parcel of freshwater to flow 200 km through the aquifer. Studies of modern aquifers have shown that even poorly permeable marine clays and marls can be flushed by meteoric waters within a few thousand years (Lusczynski and Swarzenski, 1966; Manheim, 1967). Thus, 3-4 m.y. probably

would have been sufficient time for laterally extensive freshwater tongues to develop in Helderberg sediments and completely flush connate marine pore fluids.

Meteoric groundwaters must have had sufficient hydraulic head to migrate laterally for long distances in the aquifer and be able to expel denser, connate marine pore fluids onto the floor of the Appalachian Basin. Groundwater lenses developed during post-Oriskany erosion when Huntersville Chert-Needmore Shale beds acted as confining beds (Fig. 34).

The contact between the Oriskany Sandstone and Huntersville Chert-Needmore Shale is conformable basinward indicating that deposition was continuous in the basin while the Oriskany Sandstone was being eroded along the basin margin. Less than 60 m of Huntersville Chert-Needmore Shale (maximum thickness; Woodward, 1943) were deposited before the unconformity was buried beneath thick Middle Devonian marine sediments. Water depths during Huntersville-Needmore deposition were probably less than 60 m (using estimated slopes from Huntersville-Needmore isopach maps). Therefore, assuming hydrostatic pressures, Helderberg groundwaters would have had to displace a 250 m (maximum) column of seawater, measured from the base of the Helderberg Group to sea level during Huntersville-Needmore deposition. Using the Ghyben-Herzberg relation, the groundwater table would have been at least 6 to 7 m above sea level in order to

expel connate seawater and discharge on the sea floor (Appendix D). This value is the minimum calculated freshwater head in the coastal zone and was probably much higher because recharge areas were in tectonic uplands bordering the eastern side of the basin. Higher heads also were probably necessary for "fresh" groundwaters to flow laterally for several hundred kilometers and then flow upward through fine-grained aquitards and discharge on the floor of the Appalachian Basin.

Recharge of oxidizing meteoric groundwaters to Helderberg aquifers probably ceased when upland recharge areas were drowned and buried. In southwest Virginia, windows through the Pulaski Thrust Sheet that expose Saltville Thrust Sheet rocks have Middle Devonian clastics overlying Silurian Sandstone. Therefore, by the Middle Devonian, subaerial outcrops of porous Helderberg rocks were buried beneath thick Middle Devonian clastics; additional burial beneath these clastics also helped remove Helderberg sediments from oxidizing groundwaters.

Assuming groundwater flow through Helderberg aquifers was continuous for at least 3 m.y. and using a flow rate of 1 cm/day (3.65 m/year), nearly 1.1 billion pore volumes would have been exchanged in a hypothetical cubic centimeter of porous aquifer (Fig. 35). Assuming 35% initial porosity (reasonable for skeletal limestone at 250 m burial depth; Schmoker and Halley, 1982; Halley and Schmoker, 1983), then

Figure 35. Calculated rates of shallow burial calcite cementation in a hypothetical cubic centimeter of porous Helderberg aquifer material.

FLOW RATE
1 CM/DAY
OR 365 CM/YEAR

1 CM OF UNCEMENTED
AQUIFER MATERIAL
WITH INITIAL POROSITY
OF 35%

$\times$ 3 M.Y. $\cong$ 1.1×10^9 PORE VOLUMES EXCHANGED

AVE. 32%
NONLUMINESCENT
& BRIGHT CEMENT

$\times$ 35% INITIAL POROSITY $\times$ DENSITY OF CALCITE ($2.71 g/cm^3$) = 0.3g NONLUMINESCENT & BRIGHT CEMENT PER CM^3 OF AQUIFER MATERIAL

$$\frac{0.3g \text{ OF CEMENT}}{1.1 \times 10 \text{ PORE VOLUME}} = \frac{2.7 \times 10^{-10} g \text{ OF CEMENT}}{\text{PRECIPITATED PER PORE VOLUME}}$$

0.35 cc of the hypothetical cube initially would have been open void space. Multiplying the average amount of nonluminescent and bright cement from 85 samples (determined by image analysis and normalized to percent of total cement; 32%), total "primary" porosity (0.35 cc), and the density of pure calcite (2.71 g/cc) gives the average total amount, 0.30 g, of nonluminescent and bright cement that precipitated per cubic centimeter of initially uncemented aquifer material. If all 1.1 billion pore volumes precipitated equal amounts of calcite cement, then 2.7×10^{-10} g of calcite cement were precipitated from each pore volume. However, cementation was more likely episodic and this low value suggests that pore fluids, on average, only needed to be slightly supersaturated over the 3 to 4 m.y. period of aquifer development for cementation to have occurred. The calculated rates of cementation for the Helderberg (converted to 2.5×10^{-3} mmol/l of H_2O/year) are similar to calculated rates of calcite cementation in the modern Mississippian Pahasapa Limestone aquifer, Black Hills (3.4×10^{-4} mmol/l of H_2O/year; Back et al., 1983).

Post-cementation Migration of High Temperature, High Pressure Fluids

Fluid inclusion data and fracture-filling cements suggest that migration of high temperature and high pressure fluids occurred during or after Late Paleozoic deformation of tightly cemented Helderberg sediments.

Secondary Two-phase Fluid Inclusions

Secondary two-phase fluid inclusions occur along healed microfractures that cross cut grains and cement and along cleavage planes in strained calcite crystals (Figs. 31C, 36A). Some secondary inclusion trains are crosscut by later tectonic fractures.

Temperature data from 46 secondary two-phase fluid inclusions indicate that fluids were complex, high temperature brines (Figure 37; Appendix C). Eutectic temperatures (appearance of first melt) are -50.1 to -24.0°C and indicate the presence of ions (Ca, Mg, K, SO_4) other than Na and Cl in the trapped brines (Crawford, 1981). Freezing temperatures (last occurrence of ice) are -25.1 to -11.3°C and indicate brine salinities of 15.3 to >23 wt % NaCl. No CO_2 or CH_4 hydrates were observed during cooling (Hanor, 1980; Buruss, 1981). Also, five inclusion chips were placed in several drops of vacuum pump oil and fractured between glass thin section slides under a petrographic microscope; no escaping gas bubbles or effervescence of gas phases were observed. Therefore, in the inclusions selected, the vapor phase is assumed to be water vapor and the liquid phase did not contain significant quantities of dissolved CH_4 or CO_2.

Vapor bubbles occupy the same proportion of the total inclusion volume in inclusions from the same secondary inclusion train (Fig. 36A). This is an indication that

Figure 36. Plane light photomicrographs of secondary fluid inclusions and clastic fracture fills.

A. Secondary two-phase (liquid and vapor) fluid inclusions in quartz cement crystal. Note vapor bubbles occupy the same proportion of total inclusion volume in various inclusions, suggesting fluids were not boiling at time of entrapment.

B. Secondary hydrocarbon inclusions in calcite cement. Arrow indicates hydrocarbon inclusion train trapped along line of intersection of several cleavage planes. Cleavages probably developed during Late Paleozoic deformation, therefore hydrocarbons were trapped during or after Late Paleozoic time.

C. Secondary hydrocarbon trains in quartz sandstone that crosscut quartz grains and overgrowths.

D. Secondary hydrocarbon inclusions in calcite cement. Hydrocarbons trapped along cleavage traces (indicated by arrow) were fed from hydrocarbons migrating through microfracture (F, now healed) to the right.

E. Clastic fracture fill through cemented sandstone. Note Mud (M) along fracture walls between host rock and fracture-filling cement. Also note clasts (C) of recemented fracture-filling cement and assorted detrital fragments in cemented fracture fill.

F. Clastic fracture fill through limestone. Note clasts of former fracture-filling cement and skeletal fragments (indicated by arrows) in fracture fill.

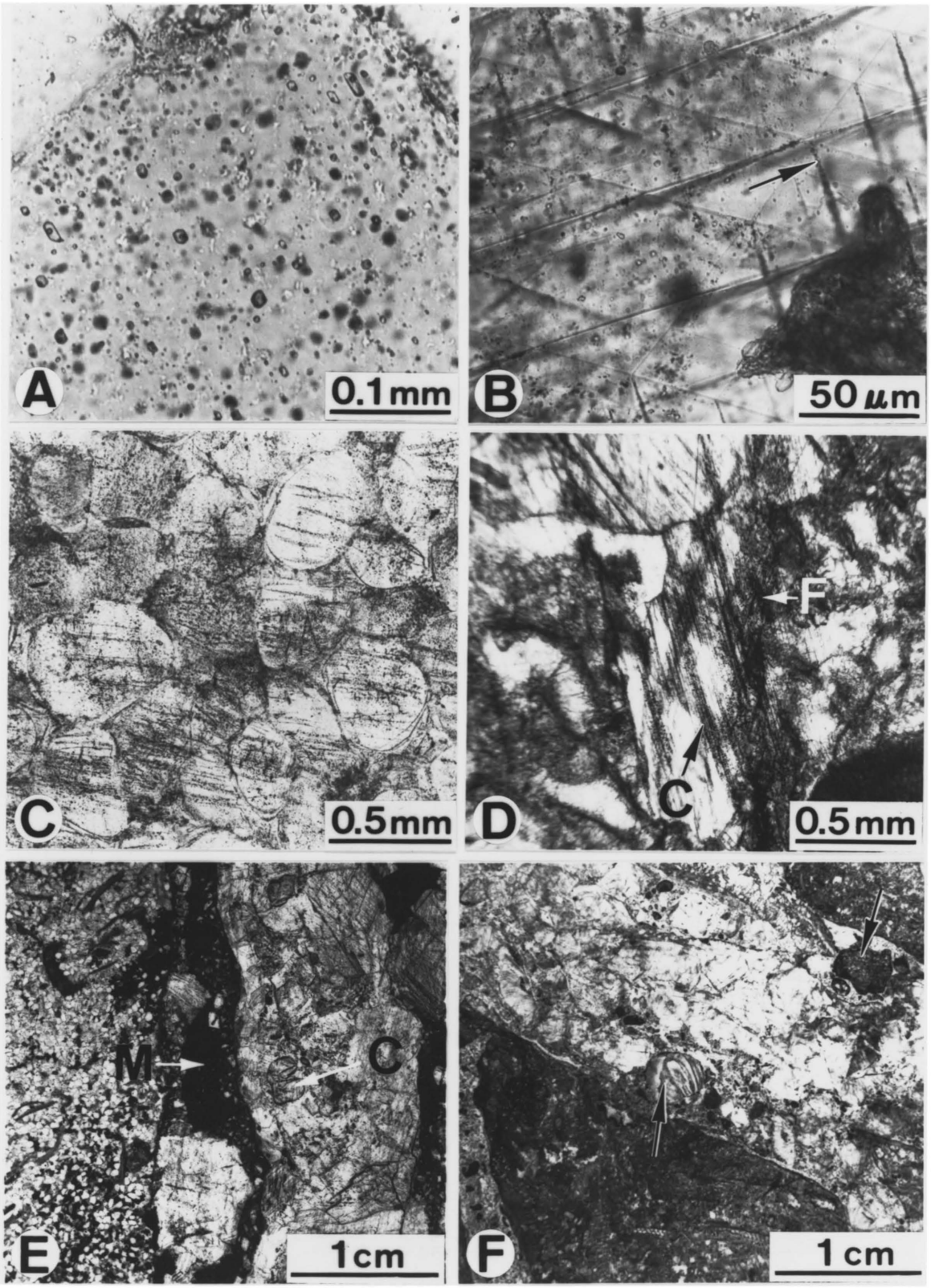
A
0.1mm
B
50 μm
C
0.5mm
D
F
C
0.5mm
M
C
E
1cm
F
1 cm

Figure 37. Summary of fluid inclusion data. T_e = eutectic temperature; T_m = melting temperature of ice; T_h = homogenization temperature of liquid and vapor phases in fluid inclusions. 400 bar hydrostatic pressure correction and 880 bar lithostatic pressure correction applied to observed homogenization temperatures. See Appendix C for complete listing of secondary fluid inclusion data.

SECONDARY FLUID INCLUSIONS

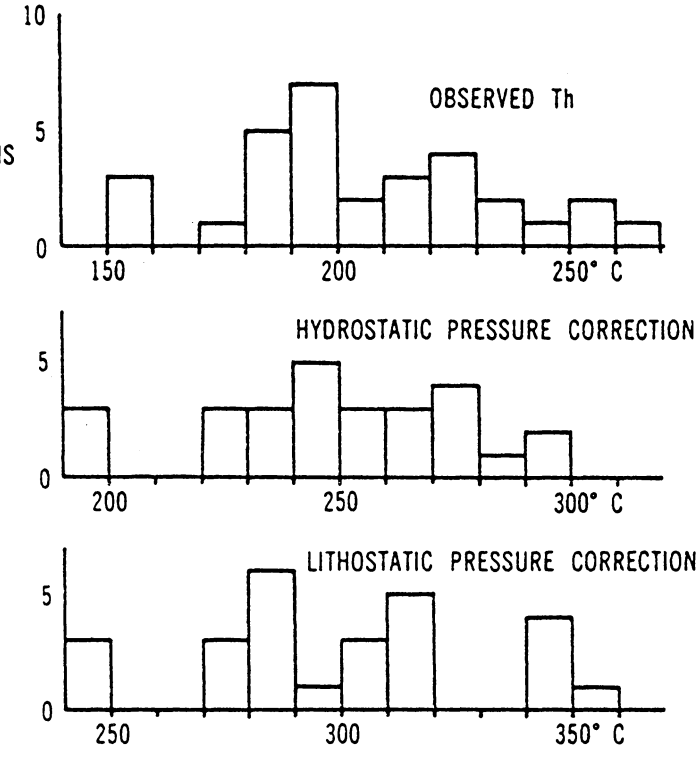

Te = −50.1° TO −24.0° C

Tm = −25.1° TO −11.3° C

WT% NaCl 15.3% TO 23%

COMPLEX,
HI TEMPERATURE BRINES

fluids were not boiling at the time of entrapment (Roedder, 1981).

Observed liquid-vapor homogenization temperatures (disappearance of vapor bubble into liquid phase) are 150 to 270°C (Fig. 37). Inclusions where both salinity and homogenization temperature are known were hydrostatic and lithostatic pressure-corrected (400 and 880 bars, respectively; pressure corrections after Potter, 1977). The temperatures greatly exceed maximum Helderberg paleotemperatures (125 to 190°C) given by conodont color alteration index values (CAI = 3 to 4; Harris, 1979) or paleotemperatures of 120 to 160°C calculated from known sedimentary overburden.

Secondary Hydrocarbon Inclusions

Secondary hydrocarbon inclusions occur along deformation microstructures that cross cut completely cemented host rock. Under ultraviolet light they are nonfluorescent, bright blue-white fluorescent, or bright yellow-green fluorescent (Fig. 38).

Nonfluorescent and blue-white hydrocarbon inclusions occur along healed microfractures and along deformation twins, cleavage planes, and cleavage intersections (Fig. 36) in strained calcite. Nonfluorescent hydrocarbons may be thermally overmatured (Buruss, 1981). Blue-white fluorescence indicates higher API gravity oils or possibly

Figure 38. Plane light and fluorescence photomicrographs of primary and secondary hydrocarbon inclusions.

A. Primary hydrocarbon inclusions defining euhedral crystal terminations in quartz overgrowths. White boxed-in area shown in 38C and 38D.

B. Same sample as in 38A,C,D, but different region, under ultraviolet light. Yellow-green fluorescent hydrocarbons (YG) occur in microfractures that roughly follow grain boundaries.

C,D. Paired plane light (C) and fluorescent (D) photomicrographs of boxed-in area of 38A. Hydrocarbon inclusions define quartz overgrowth (OG) and edge of detrital quartz grain. Under ultraviolet light, primary hydrocarbon inclusions are mostly nonfluorescent with some bright blue-white inclusions (BW). Later, secondary yellow-green hydrocarbons (YG) fill microfractures that roughly follow grain and cement boundaries.

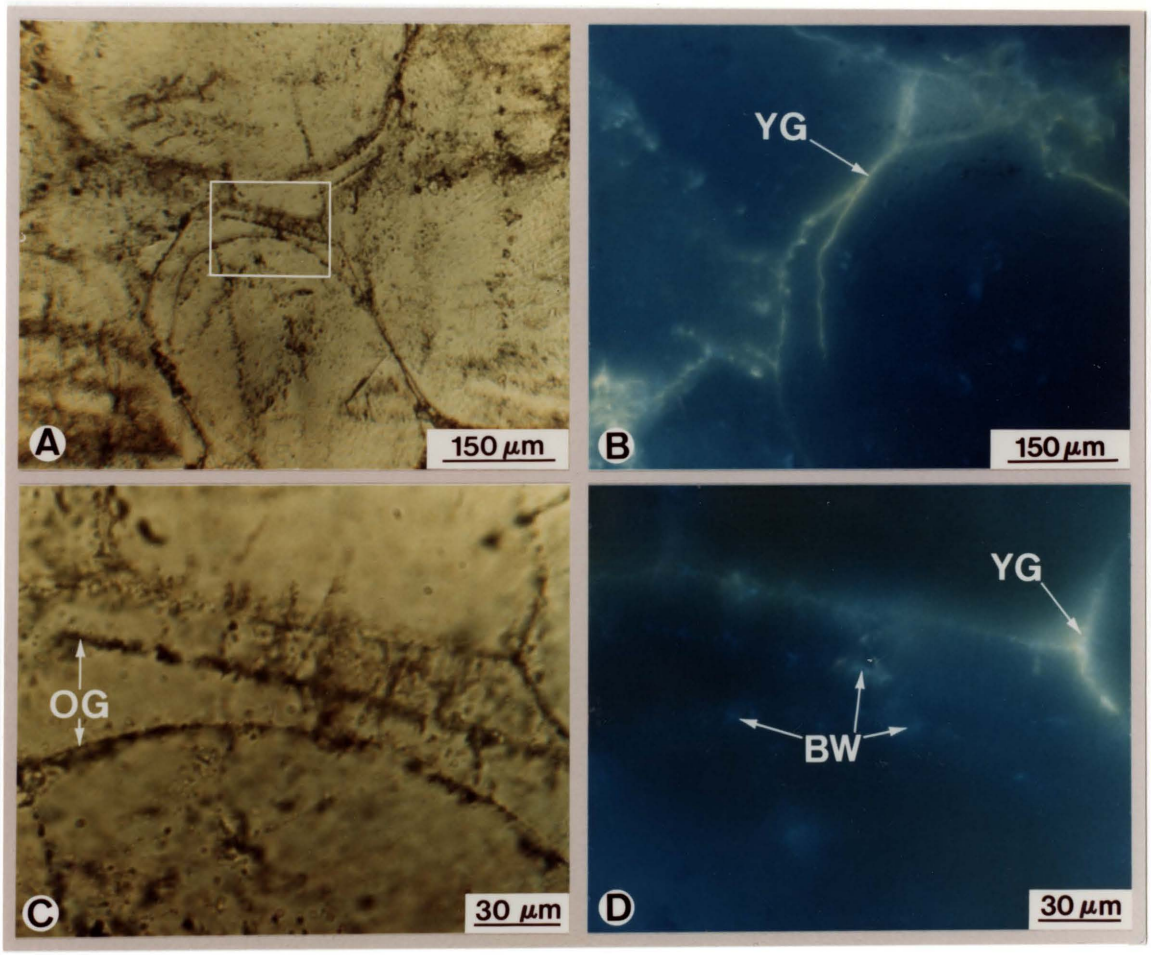
A
150 μm
B
YG
150 μm
C
OG
30 μm
D
YG
BW
30 μm

condensate (Buruss et al., 1983). Yellow-green hydrocarbons are rare and occur in irregular microfractures that roughly follow grain boundaries in quartz sandstone and locally crosscut younger, more linear microfractures filled with nonfluorescent and blue-white hydrocarbons (Fig. 38B). Yellow-green hydrocarbons were trapped after blue-white and nonfluorescent hydrocarbon inclusions and probably are medium API gravity oils (Buruss et al., 1983).

Clastic Fracture Fills

Some fractures through completely cemented Helderberg rocks crosscut stylolites and contain transported skeletal grains, "exotic" clasts of lithologies different from host rock, recemented clasts of earlier fracture-filling cement, and mud (Figs. 36E, F). Cement clasts contain solid inclusions of mud and skeletal grains. Two primary(?) two-phase fluid inclusions in cement clasts give homogenization temperatures of 120 to 150°C. Nonfluorescent hydrocarbons(?) occur as primary inclusions that define crystal growth faces in cement clasts. Hydrocarbons also fill micropore spaces between silt-sized calcite crystals in matrix material surrounding larger clasts.

Discussion

Source of High Temperature Brines

The Helderberg Group was subjected only to Late Paleozoic deformation, therefore, secondary inclusions located along deformation microstructures were trapped during or after the Late Paleozoic. Pressure-temperature constraints can be put on the possible origin of fluids trapped as secondary two-phase fluid inclusions (Fig. 39). A hydrostatic pressure correction of 400 bars applied to the observed homogenization temperature gives a pressure-corrected, minimum trapping temperature of 275°C. The hydrostatic pressure correction is probably a minimum correction with actual trapping temperatures between hydrostatic and lithostatic pressure corrected values. Occurrence of secondary inclusions along deformation microstructures and lack of evidence for boiling implies that fluid pressures during entrapment were probably greater than hydrostatic.

This pressure-corrected temperature implies that at least local and probably short-term average geothermal gradients of about 65°C/km would be required at maximum burial (4 km), as indicated by the intersection of the 65°C/km gradient, the 21 wt % NaCl isochore, and the 400 bar pressure corrected homogenization temperature. The 25, 30, and 35°C/km gradients (typical of most sedimentary basins) intersect the isochore at approximately 9, 12, and 17 km

Figure 39. Pressure-temperature constraints on origin of fluids trapped as secondary two-phase fluid inclusions. Actual inclusion with intermediate salinity (21 wt % NaCl) and homogenization temperature (225°C) plotted on temperature versus burial depth (or pressure) diagram. Isochore for 21 wt % NaCl brine constructed from data of Potter and Brown (1977). Liquid-vapor curve for water terminated for simplicity. Lines of average geothermal gradients (25, 30, 35, and 65°C/km) converge back to horizontal axis at surface temperature of 20°C. Dashed lines indicate 400 bar hydrostatic pressure correction applied to observed two-phase fluid inclusion homogenization temperature. See text for more complete discussion.

P-T CONSTRAINTS ON FLUID ORIGIN

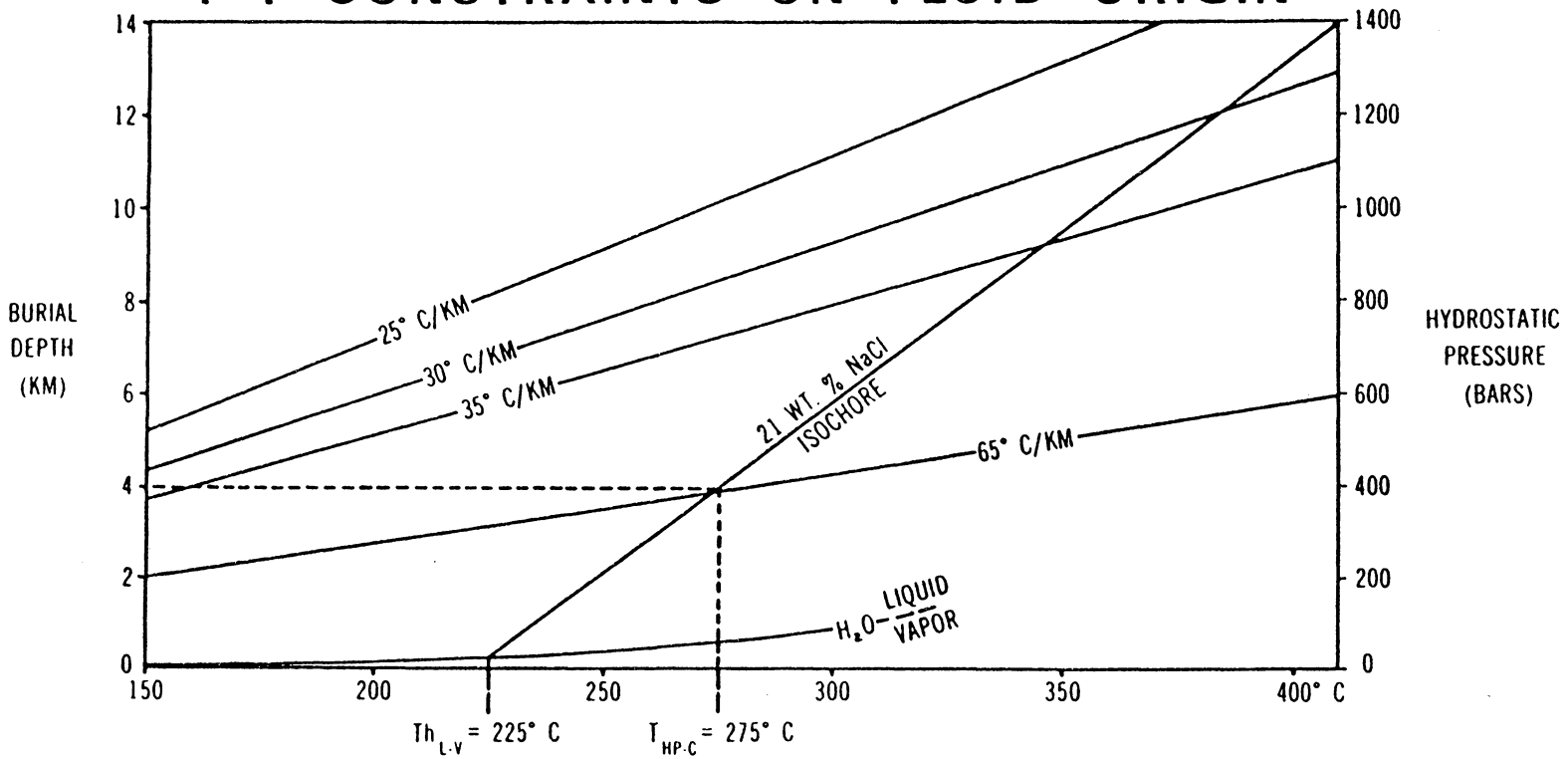

burial depths, respectively. There are <8.5 km of sediments overlying Precambrian crystalline basement rocks. Therefore, if the brines trapped in secondary two-phase fluid inclusions came from immediately downsection, they would have to be derived from Precambrian crystalline rocks, which is unlikely. It seems more likely that the fluids were derived from beneath overthrusted sedimentary rocks to the east.

Hot brines could have come from the Piedmont terrane to the east that was undergoing upper amphibolite grade metamorphism during Late Paleozoic deformation (Glover et al., 1983). Minimum lateral migration distances (non-palinspastic) of 100 km are required (distance from sample localities to western limit of the Piedmont) assuming that metamorphic fluids migrated along detachment surfaces during or after thrusting.

Brines also may have come from Paleozoic sediments beneath thick thrust sheets east of the folded Valley and Ridge. Overburden would have increased by 4 to 6 km by emplacement of a single thrust sheet (stratigraphic thickness within single thrust sheets), with even greater overburden caused by several overriding sheets. Hot brines could have come from any part of the Paleozoic section, but more likely sources for large amounts of fluids during burial by thrust sheets are thick shale sequences. These include the Lower Cambrian Hampton Formation (in eastern

belts), the Lower Cambrian Rome Formation, Ordovician shales and graywackes, and perhaps Devonian shales.

The Rome Formation is the major detachment horizon for Valley and Ridge thrust sheets (Bartholomew et al., 1980) and was probably overpressured during thrusting (Schultz, 1983). Major decollements in active fold-and-thrust belts occur only within overpressured horizons (Suppe and Wittke, 1977). Chlorite and muscovite in Rome "phyllitic" breccia at the base of the Pulaski Thrust Sheet indicate regional burial metamorphism of the Rome Formation at 300-400°C (Schultz, 1983). These data suggest that Rome shales may have been expelling high-temperature, high-pressure fluids during Late Paleozoic thrusting. Overpressured Rome fluids could have migrated along major detachment surfaces and out into the foreland along blind thrusts. Tectonic deformation probably caused microfracturing of well-cemented sediments, including the Helderberg Group, which allowed further migration of fluids. Brines would have migrated westward several tens of kilometers from beneath thrust sheets before being trapped in healed microfractures in foreland basin rocks. Potentially, Ordovician and Devonian shales also could have been expelling overpressured, hot brines during thrusting, if these units extend to the east beneath overthrusted rocks.

Migration of hot brines must have been of sufficiently short duration so that conodont color alteration indices

were not affected by increased burial temperatures. To change maximum conodont CAI values of 4 from the Helderberg Group to 4.5 would require burial temperatures of 250°C for 10 m.y., 300°C for 50,000 years, or 350°C for 500 years (Harris, 1979). This implies that ambient, basinwide burial temperatures were not raised by the hot brines because total fluid volume was too small to heat the entire basin fill and/or migration events were of short duration.

Clastic fracture fills may provide further evidence that high-pressure fluids migrated through tightly cemented Helderberg rocks. Fabrics of clastic fracture fills suggest transport of sediment through fracture conduits as poorly sorted slurries of silt to gravel-sized material. When fluid pressures abated, slurries "froze" and clasts were left floating in silt-sized matrix. Multiple migration events are suggested by refractured fills. Fracturing occurred under deep burial conditions as indicated by fluid inclusion homogenization temperatures, crosscut stylolites, and clasts of cemented sandstone, limestone, and chert. These fractures may have formed when fluid pressures exceeded rock strength, resulting in abrupt fracturing and fluid release (cf. Murphy, 1984).

Source of Secondary Hydrocarbon Inclusions

Secondary hydrocarbon inclusions occur along deformation microstructures that developed during Late Paleozoic deformation. Tectonic fractures that crosscut secondary hydrocarbon inclusion trains suggest that at least some hydrocarbon migration events occurred during Late Paleozoic deformation.

Lopatin modeling was done on the burial history plot (Fig. 16) for Pendleton County, West Virginia in order to determine potential hydrocarbon source beds during Alleghenian deformation. This technique accounts for the accumulative effects of both time and temperature on organic maturation (Lopatin, 1971). Waples (1980) summarized the Lopatin Method and correlated other organic maturation scales with Time-Temperature Index (TTI) values obtained from the Lopatin Method. TTI values of 15 to 160 indicate the onset of generation and destruction, respectively, of liquid hydrocarbons from source beds (Waples, 1980).

During Late Paleozoic deformation, only Lower to Middle Devonian beds were within the "oil generative window"; sediments older than Lower Devonian siliciclastics to Lower Silurian beds had finished generating liquid hydrocarbons but had not yet reached the "oil preservation deadline" for 50° API gravity oil (Waples, 1980). Therefore, potential source beds for hydrocarbons trapped as secondary inclusions could have been Lower Silurian through Middle Devonian beds.

Occurrence of nonfluorescent and blue-white hydrocarbons in deformation microstructures that are crosscut by later microfractures filled with yellow-green hydrocarbons indicates that the different hydrocarbons migrated during different episodes of microfracturing and that they may have come from different source rocks. The difference in fluorescence suggests that the hydrocarbons are of different thermal maturity (yellow-green hydrocarbons may be less mature than blue-white/nonfluorescent hydrocarbons) and that yellow-green hydrocarbons may have come from stratigraphically higher source rocks than blue-white/nonfluorescent hydrocarbons.

Conclusions

Regional diagenetic patterns in the Siluro-Devonian Helderberg Group, Central Appalachians, were determined using cathodoluminescent petrography and trace element, stable isotope, and fluid inclusion studies, within a well-defined stratigraphic framework and geologic history. The data show that:

1. Marine cements in the Helderberg Group occur as: isopachous cements with bladed or relict rhombohedral fabrics, inclusion-rich syntaxial rim cement, and microcrystalline hardground cement. Fabric neomorphism and chemical re-equilibration of marine cements occurred following flushing of connate marine pore fluids by meteoric

fluids. Marine cementation is more prevalent in shallow ramp, wave-agitated, deposits which consequently show less effects of mechanical compaction than deeper ramp deposits which lack sparry marine cements.

2. Leaching and neomorphism of high magnesium-calcite pelmatozoan fragments occurred when meteoric groundwaters flowed through Helderberg sediments during shallow burial. Much dissolved carbonate probably was precipitated as early cement downdip. Similarity in cathodoluminescence and stable isotopic composition between pelmatozoan grains and earliest clear calcite cement suggests pelmatozoans re-equilibrated with early meteoric groundwaters involved in shallow burial cementation. Lack of leached, former aragonite skeletal grains and limited occurrence of leached pelmatozoans to updip limestone/sandstone suggests early updip pore fluids were undersaturated with respect to very high magnesium-calcite (>12 mole % $MgCO_3$), but not aragonite.

3. Early, clear cathodoluminescent zoned cements precipitated from meteoric groundwaters under shallow burial conditions. Early zoned cements consist of updip nonluminescent cements with thin luminescent laminae in limestone/sandstone, that pass downdip into "subzoned" dull cements (interlayered bright and dull laminae), and then into nonzoned dull cement in basinward limestone. Regional distribution of cement zones suggests that nonluminescent

cement precipitated from oxidizing meteoric groundwaters in updip portions of paleoaquifers, subzoned dull cement in transitional redox portions of paleoaquifers, and early dull cement in most reducing, distal portions of paleoaquifers. The regional distribution, stable isotopic compositions, and timing of early zoned cements relative to other diagenetic events suggests that all of these early zoned cements formed synchronously from meteoric groundwaters that became progressively more reducing as they flowed downdip. Helderberg sandstone tongues probably were preferential conduits for meteoric groundwaters because early calcite cements formed only on scattered skeletal grains in sandstones.

4. Meteoric groundwaters flowed laterally for at least 150 km through Helderberg paleoaquifers and precipitated early zoned cements during a 3-4 m.y. period when recharge areas were subaerially exposed in tectonic uplands bordering the eastern side of the Appalachian Basin, and porous aquifer facies were confined by underlying and overlying aquitards. The tectonic uplands provided the necessary elevation for gravity-driven flow of meteoric groundwaters out under the Appalachian Basin. Paleoaquifers were at <300 m burial depth when early cements formed. Calculated rates of early cementation are similar to cementation rates in the modern Pahaspa Limestone aquifer, Black Hills.

5. Void-filling dull cement formed from deep burial pore fluids at burial depths of >300 m to 4 km. Deep burial pore fluids ranged from dilute to saline Na-Ca-Cl brines with stable isotopic compositions that probably were similar to formation waters from modern oil fields. Dull calcite cements occluded nearly all remaining porosity before Late Paleozoic deformation because dull cement is cross-cut by tectonic fractures and deformation microstructures. Fracture-filling dull cements indicate that some dull cements formed during and after tectonic deformation.

6. Silica replacement of calcite probably occurred during all stages of burial diagenesis and most silica probably came from dissolved sponge spicules, although some silica may have come from clay mineral diagenetic reactions or pressure-solution of detrital quartz grains. Quartz overgrowths postdate early zoned cements and have primary hydrocarbon inclusions that define crystal growth faces which indicate multiple oil migration episodes during quartz cementation. Rare primary fluid inclusions in quartz cement suggest pore fluids were dilute Na-Cl brines with temperatures of 180-220°C.

7. Dolomite and fluorite were the last diagenetic phases to form under deep burial conditions and probably formed just prior to and during Late Paleozoic deformation.

8. After complete lithification of Helderberg sediments, late stage fluids migrated along microfractures

and microstructures that formed during Late Paleozoic deformation. High-temperature, complex brines probably were sourced from overthrusted rocks to the east of the nonoverthrusted, folded Helderberg rocks. Brines were trapped as secondary fluid inclusions with trapping temperatures that are twice the maximum calculated burial temperatures (125 to 190°C) for the Helderberg Group. Conodont CAI values were unaffected by these high-temperature brines, suggesting brine volumes and/or migration events were not of large enough magnitude to raise ambient burial temperatures so that conodonts were altered. Secondary hydrocarbon inclusions occur as distinct populations (based on occurence and fluorescence) that were trapped during discrete episodes of microfracturing during Late Paleozoic deformation; different hydrocarbons probably came from different source rocks but only Lower Silurian to Middle Devonian beds were generating liquid hydrocarbons or still had preserved liquid hydrocarbons during Late Paleozoic deformation. Late stage fluids probably were overpressured (> hydrostatic pressure) as suggested by poorly-sorted, clastic fracture fills that probably moved through fractures as slurries.

CHAPTER 3. IMAGE ANALYSIS OF CATHODOLUMINESCENT-ZONED CALCITE CEMENTS USING THE GENERAL IMAGE PROCESSING SYSTEM (GIPSY)[1]

Introduction

Most studies of carbonate diagenesis have relied on time consuming point counting to determine area volumetric abundances of grains versus cement and there has been little effort to quantitatively assess the volumetric abundance of specific cement generations. Computer-assisted image analysis provides a rapid quantitative method for determining grain size, shape, orientation and cement abundance and porosity. In this study, one such image analysis software sytem (the General Image Processing System or GIPSY), has been used to determine abundance of grains versus total cement in carbonate rocks, and also uses cathodoluminescence to quantitatively document porosity loss at specific stages of the carbonate rocks history.

Cementation of carbonate rocks is amenable to study using cathodoluminescence, especially where vadose to shallow phreatic meteoric fluids were involved in cementation (Grover et al., 1983). Settings favoring this include humid zone tidal flats and islands (where wedges or

[1]This chapter will be published as a separate publication at a later date with the following authors: S.L. Dorobek, J.F. Read, R.M.Haralick, and Ting-chuen Pong.

lenses of meteoric water may develop; Grover and Read, 1983), unconformity-capped platforms (where meteoric fluids are recharged from the unconformity; Meyers, 1974, 1978) and carbonate platforms bordering tectonic highlands (which provide the hydraulic drive for forcing meteoric fluids along confined aquifers into the subsurface; Grover and Read, 1983; Dorobek, 1983).

A common sequence of cathodoluminescent calcite cement that forms where carbonate rocks were influenced by meteoric fluids is nonluminescent cement (Fe and Mn poor, deposited from oxidizing pore waters), brightly luminescent calcite (Mn rich, deposited from more reducing pore waters), and latest dully luminescent cements (moderate Mn, high Fe, deposited from highly reducing waters, either following stagnation of the aquifer or following burial (Meyers, 1978; Frank et al., 1982; Grover and Read, 1983). This commonly developed cement sequence, when analyzed using GIPSY, provides rapid determination of abundance of specific cement zones deposited under the various diagenetic environments. The cathodoluminescent zonation provides a framework for stable isotope sampling, fluid inclusion studies, and trace element studies on the cements. Furthermore, because the nonluminescent cements develop in the near surface to shallow burial diagenetic regime, image analysis of the cathodoluminescent zones allows shallow burial versus deep burial cementation and accompanying porosity loss to be

Figure 40. Image analysis procedure. All figures same scale, approximately 3 mm wide. See text for complete discussion of image analysis procedure.

A. Plane light photomicrograph of skeletal grainstone.

B. Thresholded image of A showing grains (black areas) versus cement (white areas).

C. Cathodoluminescent photomicrograph of same area as A.

D. Thresholded image of C.

E. Resultant image after "multiplying" images B and D. Bright cement zones are shown as white regions on image.

F. Inverted cathodoluminescent photomicrograph. Nonluminescent cements are now brightest areas, bright cements are darkest areas.

G. Thresholded image of F.

H. Resultant image after "multiplying" images B and G. Nonluminescent cement is shown as white regions on image.

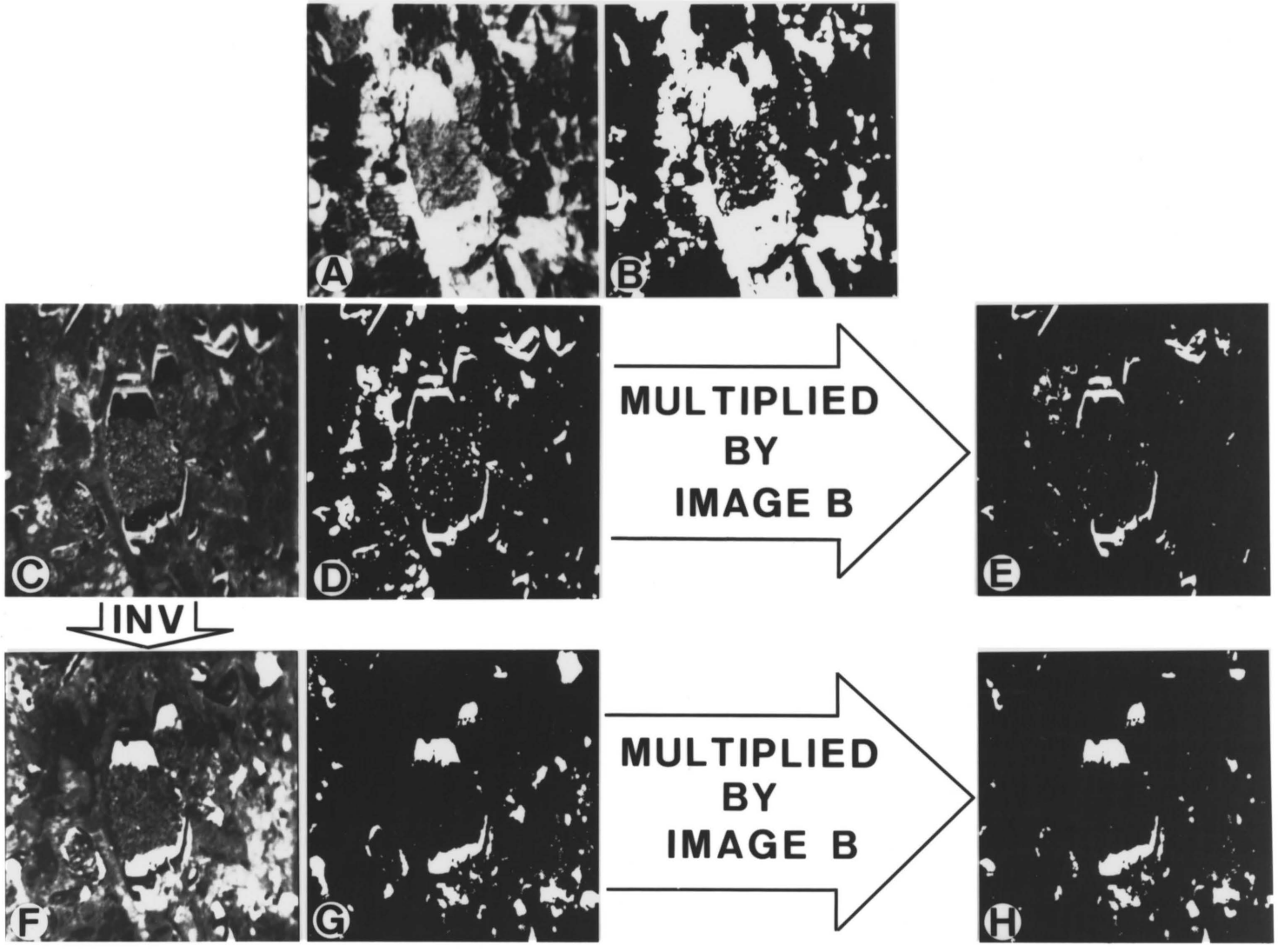
A
B
C
D
MULTIPLIED
BY
IMAGE B
E
INV
F
G
MULTIPLIED
BY
IMAGE B
H

is due to their their having been reproduced electronically several times. Digitized images analyzed actually are of high resolution and quality.

1. The plane light image of the limestone thin section is thresholded to determine abundance of grains versus total cement (Fig. 40A,B). The plane light image is digitized and stored in "image plane 1" (Fig. 40A). A threshold value is selected (between 0.01 and 1.00) that allows maximum differentiation beteen grains and cement. The computer thresholds the plane light image, calculates percent grains and percent cement, and the thresholded image (Fig. 40B) is stored in "image plane 2" for later use. The plane light image stored in image plane 1 subsequently is destroyed in Step 2.

2. The cathodoluminescent image of the same area of the thin section (Fig. 40C) is digitized and stored in "image plane 1", deleting the previously stored image.

3. Next the amount of bright cement is calculated in the following manner. Threshold values are chosen that differentiate bright luminescent zones from other cement types. The computer thresholds the cathodoluminescent image and the thresholded luminescent image is stored in "image plane 3" (Fig. 40D). It is preferable to remove skeletal grains from the thresholded luminescent image because skeletal grains commonly have luminescent characteristics that are similar to some of the cements. This is done by

"multiplying" the thresholded luminescent image (in image plane 3) by the thresholded grains-versus-cement image (in image plane 2). Only pixels that have designated values of "1" in both image planes will be reproduced after multiplication. Therefore, skeletal grains which are designated as "0" in the grains-versus-cement image (black areas in Fig. 40B) will not be be counted in the calculation of abundance of bright cement. The multiplied image (Fig. 40E) is stored in image plane 1, destroying the digitized cathodoluminescent image. Abundance of bright cement is then determined from the "multiplied" image.

4. Abundance of nonluminescent cement is determined by first digitizing the cathodoluminescent image and storing it in image plane 1. Because of the difficulaty of choosing threshold values for the non-luminescent cement, it is easiest to have GIPSY invert the image to form a negative image. By using the inversion operator on the luminescent image, nonluminescent cements will appear as "bright" regions and bright cements will become "dark." The inverted image (Fig. 40F) is then stored in image plane 3. The inverted image is thresholded and the thresholded image (Fig. 40G) stored in image plane 1. The same multiplication procedure described for bright cement (Step 3) is done on the thresholded inverted nonluminescent cement image. Abundance of nonluminescent cement is then determined on the multiplied image.

5. Abundance of dull calcite cement is calculated by adding the determined values for nonluminescent and bright cement and subtracting this from the "total cement" value determined in Step 1.

Values for nonluminescent, bright, and dull cement are expressed as unit fraction of total rock volume. However, they may be be recalculated as percent of total cement if required. Once the user is familiarized with this procedure, all of the steps can be performed in about five minutes.

The cement abundance data (expressed as percent of total rock volume) for each cement zone, along with porosity data, may be graphically plotted alongside stratigraphic columns, providing a picture of vertical variation of cementation and porosity occlusion or preservation through the section.

For correlation of relatively complex sequences of cements throughout stratigraphic sections, plots of individual cement zones expressed as percent of total primary void space (both filled and unfilled) have been found to be best. This removes the effect of stratigraphic variation in primary void space, and lays out the cement zones on a constant width band alongside the stratigraphic column; the total width of the band represents 100% which equals the amount of cement plus porosity in the rock.

Cement abundance data also may be plotted on maps by time-slicing selected intervals of rock units of interest throughout the region, averaging the abundance of each cement zone within each interval, plotting abundance of each cement zone on separate maps, and then contouring the data. This provides a map view of cement variation throughout the region, and clarifies lateral relations of the cements with such features as recharge areas, permeable conduits for meteoric fluid flow, and allows assessment of the stratigraphic section's position with respect to regional paleoaquifer systems. The maps also might be useful for prediction of possible porosity occlusion or preservation in less studied adjacent areas.

Conclusions

Image analysis of cathodoluminescent cement zones using the General Image Processing System (GIPSY) provides a rapid method for determining abundance of various calcite cements deposited under different diagenetic regimes. Because the nonluminescent-bright-dull luminescent sequence is common in rocks that have been influenced by vadose to shallow phreatic diagenesis and reflects change from oxidizing meteoric pore fluids to reducing pore fluids as aquifers stagnate or the sequence is buried, the cement zones provide a means for obtaining minimum estimates of porosity

occlusion under near surface conditions and prior to hydrocarbon migration into reservoirs.

BIBLIOGRAPHY

Ahr, W.M., 1973, The carbonate ramp: an alternative to the shelf model: Gulf Coast Assoc. Geol. Soc. Trans., v. 23, p. 221-225.

Allan, J.R. and Matthews, R.K., 1977, Carbon and oxygen isotopes as diagenetic and stratigraphic tools: Surface and subsurface data, Barbados, West Indies: Geology, v. 5, p. 16-20.

Anderson, G.M. and Macqueen, R.W., 1982, Ore deposits models - 6. Mississippi Valley-type lead-zinc deposits: Geoscience Canada, v. 9, p. 108-117.

Anderson, T.F. and Arthur, M.A., 1983, Stable isotopes of oxygen and carbon and their application to sedimentological and paleoenvironmental problems: Ch. 1 in M.A. Arthur, et al., eds., Stable Isotopes in Sedimentary Geology, Soc. Econ. Paleontologists Mineralogists, Short Course Notes 10.

Back, W. and Barnes, I., 1965, Relation of electrochemical potentials and iron content of ground-water flow patterns: U.S. Geol. Survey Prof. Paper 498-C, 16 p.

Back, W., Hanshaw, B.B., Plummer, L.N., Rahn, P.H., Rightmire, C.T., and Rubin, M., 1983, Process and rate of dedolomitization: mass transfer and ^{14}C dating in a regional carbonate aquifer: Bull. Geol. Soc. Amer., v. 94, p. 1415-1429.

Bartholomew, M.J., Milici, R.C., and Schultz, A.P., 1980, Geologic structure and hydrocarbon potential along the Saltville and Pulaski thrusts in southwestern Virginia and northeastern Tennessee: Virginia Division of Mineral Resources, Publ. 23, Part A, Sheet 1.

Barwis, J.H. and Makurath, J.H., 1978, Recognition of ancient tidal inlet sequences: an example from the Upper Silurian Keyser Limestone in Virginia: Sedimentology, v. 28, p. 61-82.

Blake, D.F., Peacor, D.R., and Wilkinson, B.H., 1982, The sequence and mechanism of low-temperature dolomite formation: calcian dolomites in a Pennsylvania echinoderm: Sed. Petrol., v. 52, p. 59-70.

Bodnar, R.J. and Bethke, P.M., 1984, Systematics of stretching of fluid inclusions I: fluorite and sphalerite at 1 atmosphere confining pressure: Econ. Geology, v. 79, p. 141-161.

Boersma, J.R., 1969, Internal structure of some tidal megaripples on a shoal in the Westerschelde Estuary, The Netherlands: Geologic Mijnb., v. 48, p. 409-414.

Boersma, J.R. and Terwindt, J.H.J., 1981, Berms on an intertidal shoal: shape and internal structure, in S.-D. Nio, R.T.E. Shuttenhelm and Tj.C.E. Van Weering, eds., Holocene Marine Sedimentation in the North Sea Basin: Int'l Assoc. of Sedimentologists Spec. Publ. 5, p. 39-49.

Boles, J.R. and Franks, S.G., 1979, Clay diagenesis in Wilcox sandstones of southwest Texas: implications of smectite diagenesis on sandstone cementation: J. Sed. Petrol., v. 49, p. 55-70.

Bottinga, Y., 1968, Calculation of fractionation factors for carbon and oxygen exchange in the system calcite-carbon dioxide-water: J. Chem. Phys., v. 72, p. 800-808.

Bowen, Z.P., 1966, Brachiopods and stratigraphy of the Elbow Ridge Sandstone (Lower Devonian) of Pennsylvania, Maryland and West Virginia: J. Paleontology, v. 40, p. 1051-1062.

Bowen, Z.P., 1967, Brachiopoda of the Keyser Limestone (Silurian-Devonian) of Maryland and adjacent areas: Geol. Soc. Amer., Mem. 102, 103 p.

Burruss, R.C., 1981, Analysis of phase equilibria in C-O-H-S fluid inclusions, in L.S. Hollister and M.L. Crawford, eds., Short Course in Fluid Inclusions: Applications to Petrology: Min. Assoc. Canada Short Course Handbook, v. 6, p. 39-74.

Burruss, R.C., 1981, Hydrocarbon fluid inclusions in studies of sedimentary diagenesis, in, L.S. Hollister and M.L. Crawford, eds., Fluid Inclusions: Applications to Petrology: Min. Assoc. Canada Short Course Handbook, v. 6, p. 138-156.

Burruss, R.C., Cercone, K.R., and Harris, P.M., 1983, Fluid inclusion petrography and tectonic-burial history of the Al Ali No. 2 well: evidence for the timing of diagenesis and oil migration, northern Oman Foredeep: Geology, v. 11, p. 567-570.

Butts, C., 1940, Geology of the Appalachian Valley in Virginia: Virginia Geol. Survey Bull. 52, Part 1, 568 p.

Caless, J.R., 1983, Geology, paragenesis, and geochemistry of sphalerite mineralization at the Young Mine, Mascot-Jefferson City Zinc District, East Tennessee: M.S. thesis, Blacksburg, Virginia, Virginia Polytechnic Institute and State University, 161 p.

Carothers, W.W. and Kharaka, Y.K., 1980, Stable carbon isotopes of HCO_3^- in oil-field waters - implications for the origin of CO_2: Geochim. Cosmochim. Acta, v. 44, p. 323-332.

Champ, D.R., Gulens, J., and Jackson, R.E., 1979, Oxidation-reduction sequences in ground water flow systems: Can. J. Earth Sci., v. 16, p. 12-23.

Chave, K.E., 1952, A solid solution between calcite and dolomite: J. Geol., v. 60, p. 190-192.

Chiarelli, A., 1973, Etude des nappes aquiferes profondes, Contribution de l'hydrogeologie a la connaissance d'un bassin sedimentaire et a l'exploration petroliere: D.Sc. Thesis, no. 401, l'Universite de Bordeaux I, Bordeaux, 187 p.

Collins, M.A. and Gelhar, L.W., 1971, Seawater intrusion in layered aquifers: Water Resources Research, v. 7, p. 971-979.

Colton, G.W., 1970, The Valley and Ridge and Appalachian Plateau; stratigraphy and sedimentation; the Appalachian basin; its depositional sequence and their geologic relationships: in G.W. Fisher et al., eds., Studies of Appalachian Geology: Central and Southern: New York, Intersci. Pubs., p. 5-47.

Cook, E.G., 1981, Conodont biostratigraphy and paleoecology of the Lower Devonian Helderberg Group of Virginia: M.S. thesis, Blacksburg, Va., Virginia Polytechnic Institute and State University, 152 p.

Craig, H., 1957, Isotopic standards for carbon and oxygen and correction factors for mass-spectro-metric analysis of carbon dioxide: Geochim. Cosmochim. Acta, v. 12, p. 133-149.

Crawford, M.L., 1981, Phase equilibria in aqueous fluid inclusions, in L.S. Hollister and M.L. Crawford, eds., Fluid Inclusions: Applications to Petrology: Min. Assoc. Canada Short Course Handbook, v. 6, p. 75-100.

Curtis, C.D., 1978, Possible links between sandstone diagenesis and depth-related geochemical reactions occurring in enclosing mudstones: J. Geol. Soc. London, v. 135, p. 107-117.

Davies, G.R., 1970, Carbonate bank sedimentation, eastern Shark Bay, Western Australia: in Carbonate Sedimentation and Environments, Shark Bay, Western Australia, Am. Assoc. Petroleum Geologists, Mem. 13, p. 85-168.

Dennison, J.M., 1970, Silurian stratigraphy and sedimentary tectonics of southern West Virginia and adjacent Virginia, in Silurian Stratigraphy, Central Appalachian Basin, Field Conf.: Appalachian Geol. Soc., p. 1-33.

Dennison, J.M. and Boucot, A.J., 1974, Little War Gap at Clinch Mountain provides standard reference section for Silurian Clinch Sandstone and most nearly complete Devonian section in eastern Tennessee: Southeastern Geology, v. 16, p. 79-101.

Dennison, J.M. and DeWitt, W., Jr., 1972, Redbed zone produced by sea level drop at beginning of Devonian Cohocton Age delimits Fulton and Augusta Lobes of Catskill delta complex: Guidebook 37th Annual Field Conference of Pennsylvania Geologists, p. 109-114.

Dennison, J.M. and Head, J.W., 1975, Sealevel variations interpreted from the Appalachian Basin Silurian and Devonian: Am. J. Sci., v. 275, p. 1089-1120.

Dickson, J.A.D., 1965, A modified staining technique for carbonates in thin section: Nature, v. 205, p. 587.

Dorobek, S.L., 1983, Regional cathodoluminescent cement zonation related to upland-sourced paleoaquifers: Devonian Helderberg carbonates and clastics, Central Appalachians (abs.): Am. Assoc. Petroleum Geologists Bull., v. 67, p. 452.

Edmundson, R.S., 1958, Industrial limestones and dolomites in Virginia: James River District west of the Blue Ridge: Va. Div. Mineral Resources, Bull. 73, 137 p.

Evamy, B.D. and Shearman, D.J., 1965, The development of overgrowths from echinoderm fragments: Sedimentology, v. 5, p. 211-233.

Evamy, B.D. and Shearman, D.J., 1969, Early stages in development of overgrowths on echinoderm fragments in limestones: Sedimentology, v. 12, p. 317-322.

Frank, J.R., 1981, Dedolomitization in the Taum Sauk Limestone (Upper Cambrian), Southeast Missouri: J. Sed. Petrol., v. 51, p. 7-18.

Frank, J.R., Carpenter, A.B., and Oglesby, T.W., 1982, Cathodoluminescence and composition of calcite cement in the Tom Sauk Limestone (Upper Cambrian), southeast Missouri: J. Sed. Petrol., v. 52, p. 631-638.

Freeze, R.A. and Cherry, J.A., 1979, Groundwater: Englewood Cliffs, N.J., Prentice-Hall, Inc., 604 p.

Friedman, I. and O'Neil, J.R., 1977, Compilation of stable isotope fractionation factors of geochemical interest, M. Fleischer, ed., Data of Geochemistry, 6th ed., U.S. Geol. Survey Prof. Paper 440 KK.

Frind, E.O., 1982, Seawater intrusion in continuous coastal aquifer-aquitard systems: Advances in Water Resources, v. 5, p. 89-99.

Fuchtbauer, H. and Hardie, L.A., 1976, Experimentally determined homogeneous distribution coefficients for precipitated magnesian calcites: application to marine carbonate cements (abs.): Geol. Soc. Am. Abstracts with Programs, v. 8, p. 877.

Glover, L., III, Speer, J.A., Russell, G.S., and Farrar, S.S., 1983, Ages of regional metamorphism and ductile deformation in the central and southern Appalachians: Lithos, v. 16, p. 223-245.

Goldstein, J.I., 1976, Statistics of X-ray analysis, in Proceedings of 11th Annual Conference, Microbeam Analysis Society, p. T1A-T1H.

Grover, G.A., Jr., 1981, Cement types and cementation patterns of Middle Ordovician ramp-to-basin carbonates, Virginia: Ph.D. thesis, Blacksburg, Va., Virginia Polytechnic Institute and State University, 220 p.

Grover, G., Jr., and Read, J.F., 1983, Paleoaquifer and deep burial related cements defined by regional cathodoluminescent patterns, Middle Ordovician carbonates, Virginia: Am. Assoc. Petroleum Geologists, v. 67, p. 1275-1303.

Grover, G.A., Dorobek, S.L., and Read, J.F., 1983, Tidal flat-, unconformity-, and upland-sourced paleoaquifers and associated cathodoluminescent zoned cements in Appalachian carbonates (abs.): Geol. Soc. Amer. Abstracts with Programs, v. 15, p. 587.

Halley, R.B. and Schmoker, J.W., 1983, High-porosity Cenozoic carbonate rocks of South Florida: progressive loss of porosity with depth: Am. Assoc. Petroleum Geologists Bull., v. 67, p. 191-200.

Hanor, J.S., 1980, Dissolved methane in sedimentary brines: potential effect on the PVT properties of fluid inclusions: Econ. Geol., v. 75, p. 603-609.

Haralick, R.M., 1983, GIPSY users manual, Volume I: Spatial Data Analysis Laboratory, Virginia Polytechnic Institute and State University, Blacksburg, Virginia 24061.

Harms, J.C., Southard, J.B., Spearing, D.R., and Walker, R.G., 1975, Depositional environments as interpreted from primary sedimentary structures and stratification sequences: Soc. Econ. Paleontologists Mineralogists, Short Course no. 2, Dallas, Texas, 161 p.

Harris, A.G., 1979, Conodont color alteration, an organo-mineral metamorphic index, and its application to Appalachian Basin geology, in P.A. Scholle and P.R. Schluger, eds., Aspects of Diagenesis: Soc. Econ. Paleontologists Mineralogists, Spec. Pub. 26, p. 3-16.

Head, J.W., 1969, An integrated model of carbonate depositional basin evolution: Late Cayugan (Upper Silurian) and Helderbergian (Lower Devonian) of the central Appalachians: Ph.D. dissertation, Providence, R.I., Brown University, 390 p.

Head, J.W., 1974, Correlation and paleogeography of upper part of Helderberg Group (Lower Devonian) of Central Appalachians: Am. Assoc. Petroleum Geologists Bull., v. 58, p. 247-259.

Helfrich, C.T., 1975, Silurian conodonts from Wills Mountain Anticline, Virginia, West Virginia, Maryland: Geol. Soc. America Spec. Paper 161, 82 p.

Hollister, L.D., Crawford, M.L., Roedder, E., Burruss, R.C., Spooner, E.T.C., and Touret, J., 1981, Practical aspects of microthermometry, in L.S. Hollister and M.L. Crawford, eds., Fluid Inclusions: Applications to Petrology: Min. Assoc. Canada Short Course Handbook, v. 6, p. 278-304.

Hower, J., Eslinger, E.V., Hower, M.E., and Perry, E.A., 1976, Mechanism of burial metamorphism of argillaceous sediments: 1. Mineralogical and chemical evidence: Bull. Geol. Soc. Amer., v. 87, p. 725-737.

James, N.P. and Choquette, P.W., 1983, Limestones - The sea floor diagenetic environment: Geoscience Canada, v. 10, p. 162-179.

James, N.P., Ginsburg, R.N., Marszalek, D.S., and Choquette, P.W., 1976, Facies and fabric specificity of early subsea cements in shallow Belize (British Honduras) reefs: J. Sed. Petrol., v. 46, p. 523-544.

James, N.P. and Ginsburg, R.N., 1979, The seaward margins of Belize Barrier and Atoll Reefs: Int'l Assoc. of Sedimentologists Spec. Publ. 3, 197 p.

Johnston, R.H., 1983, The saltwater-freshwater interface in the Tertiary limestone aquifer, southeast Atlantic outer-continental shelf of the U.S.A.: J. Hydrology, v. 61, p. 239-249.

Jones, S.E., 1982, Stratigraphy and petrology of the Wildcat Valley Sandstone (Lower Devonian), Southwestern Virginia: M.S. thesis, Chapel Hill, North Carolina, University of North Carolina, 127 p.

Katz, A., 1973, The interaction of magnesium with calcite during crystal growth at 25-90°C and one atmosphere: Geochim. Cosmochim. Acta, v. 37, p. 1563-1586.

Keith, M.L. and Weber, J.N., 1964, Carbon and oxygen isotopic composition of selected limestones and fossils: Geochim. Cosmochim. Acta, v. 28, p. 1787-1816.

Kreisa, R.D., 1981, Storm-generated sedimentary structures in subtidal marine facies with examples from the Middle and Upper Ordovician of southwestern Virginia: J. Sed. Petrol., v. 51, p. 823-848.

Kuslansky, G.H. and Friedman, G.M., 1981, Chertification of crinoids may yield a product resembling "dedolomite": J. Sed. Petrol., v. 51, p. 795-798.

Land, L.S., 1970, Phreatic versus vadose meteoric diagenesis of limestones: evidence from a fossil water table: Sedimentology, v. 14, p. 175-185.

Land, L.S. and Prezbindowski, D.R., 1981, The origin and evolution of saline formation water, Lower Cretaceous carbonates, South-Central, Texas, U.S.A.: J. Hydrology, v. 51, p. 51-74.

Laporte, L.F., 1969, Recognition of a transgressive carbonate sequence within an epeiric sea: Helderberg Group (Lower Devonian) of New York State, in G.M. Friedman, ed., Depositional Environments in Carbonate Rocks: Soc. Econ. Paleontologists Mineralogists Spec. Publ. 14, p. 98-119.

Lesure, F.G., 1957, Geology of the Clifton Forge Iron District, Virginia: Va. Eng. Expt. Station Series no. 118, 130 p.

Logan, B.W., Read, J.F., Hagan, G.M., Hoffman, P., Brown, R.G., Woods, P.J., and Gebelein, C.D., 1974, Evolution and diagenesis of Quaternary carbonate sequences, Shark Bay, Western Australia: Am. Assoc. Petroleum Geologits, Memoir 22.

Lohmann, K.C. and Meyers, W.J., 1977, Microdolomite inclusions in cloudy prismatic calcites - a proposed criterion for former high-magnesium calcites: J. Sed. Petrol., v. 47, p. 1078-1088.

Lopatin, N.V., 1971, Temperature and geologic time as factors in coalification (in Russian): Akad. Nauk. SSSR Izv. Ser. Geol., no. 3, p. 95-106.

Loucks, R.G., 1983, Distinguishing diagenetic environments of equant calcite cementation: example from Lower Cretaceous Pearsall Formation in South Texas (abs.): Am. Assoc. Petroleum Geologists, v. 67, p. 506.

Lusczynski, N.J. and Swarzenski, W.V., 1966, Salt-water encroachment in southern Nassau and southeastern Queens counties, Long Island, N.Y.: U.S. Geol. Survey Water-Supply Paper 1613-F, 76 p.

Mackenzie, F.T., Bischoff, W.D., Bishop, F.C., Loijens, M., Schoonmaker, J., and Wollast, R., 1983, Magnesian calcites: low-temperature occurrence, solubility and solid-solution behavior, in R.J. Reeder, ed., Carbonates: mineralogy and chemistry: Reviews in Mineralogy, v. 11, Mineral. Soc. Amer., p. 97-144.

Makurath, J.H., 1975, The sedimentology and palaeoecology of the Keyser Limestone (Silurian-Devonian) of the Central Appalachians: Ph.D. dissertation, Baltimore, Md., The Johns Hopkins University, 101 p.

Makurath, J.H., 1977, Marine faunal assemblages in the Silurian-Devonian Keyser Limestone of the central Appalachians: Lethaia, v. 10, p. 235-256.

Manheim, F.T., 1967, Evidence for submarine discharge of water on the Atlantic continental slope of the southern United States, and suggestions for further search: Trans. N.Y. Acad. Science, Ser. II, v. 29, p. 839-853.

Manheim, F.T. and Horn, M.K., 1968, Composition of deeper subsurface waters along the Atlantic continental margin: Southeast Geology, v. 9, p. 215-236.

Manheim, F.T. and Paull, C.K., 1981, Patterns of groundwater salinity changes in a deep continental-oceanic transect off the southeastern Atlantic Coast of the U.S.A.: J. Hydrology, v. 54, p. 95-105.

Meyers, W.J., 1974, Carbonate cement stratigraphy of the Lake Valley Formation (Mississippian), Sacramento Mountains, New Mexico: J. Sed. Petrol., v. 44, p. 837-861.

Meyers, W.J., 1978, Carbonate cements: their regional distribution and interpretation in Mississippian limestones of southwestern New Mexico: Sedimentology, v. 25, p. 371-400.

Miller, R.L., Back, W., and Deike, R.G., 1977, Wildcat Valley Sandstone in southwest Virginia - possible reservoir sandstone: Am. Assoc. Petroleum Geologists Bull., v. 61, p. 416-430.

Montgomery, C.W., 1967, The Clifton Forge Sandstone: distribution, lithology, and paleocurrents: unpublished report, Lexington, Va., Washington and Lee Univesity, 38 p.

Mook, W.G., Bommerson, J.C., and Staverman, W.H., 1974, Carbon isotope fractionation between dissolved bicarbonate and gaseous carbon dioxide: Earth Planet. Sci. Lett., v. 22, p. 169-176.

Moore, C.H. and Druckman, Y., 1981, Burial diagenesis and porosity evolution, Upper Jurassic Smackover, Arkansas and Louisiana: Am. Assoc. Petroleum Geologists Bull., v. 65, p. 597-628.

Murphy, F.C., 1984, Fluidized breccias: A record of brittle transitions during ductile deformation: Tectonophysics, v. 104, p. 325-349.

Ogden, A.E., 1984, Discharge and seasonal effects on the water chemistry of the San Marcos Springs, Edwards Aquifer, Texas (abs.): Geol. Soc. Amer. Abstracts with Programs, v. _, p. 111.

Oglesby, T.W., 1976, A model for the distribution of manganese, iron and magnesium in authigenic calcite and dolomite cements in the Upper Smackover Formation in eastern Mississippi: M.S. Thesis, Columbia, University of Missouri, 122 p.

Plummer, L.N. and Back, W., 1980, The mass balance approach: application to interpreting the chemical evolution of hydrologic systems: Am. J. Sci., v. 280, p. 130-142.

Plummer, L.N., Vacher, H.L., Mackenzie, F.T., Bricker, O.P., and Land, L.S., 1976, Hydrogeochemistry of Bermuda: A case history of ground-water diagenesis of biocalcarenites: Bull. Geol. Soc. Amer., v. 87, p. 1301-1316.

Potter, R.W., II, 1977, Pressure corrections for fluid-inclusion homogenization temperatures based on the volumetric properties of the system NaCl-H_2O: J. Research U.S. Geol. Survey, v. 5, p. 603-607.

Potter, R.W., II, and Brown, D.L., 1977, The volumetric properties of aqueous sodium chloride solutions from 0° to 500°C at pressures up to 2000 bars based on a regression of available data in the literature: U.S. Geol. Survey, Bull. 1421-C, 36 p.

Prezbindowski, D.R., 1981, Carbonate ro[illegible]water diagenesis Lower Cretaceous, Stuart City Trend, [illegible]th Texas: Ph.D. dissertation, Austin, Texas, The Univ[illegible]sity of Texas at Austin, 236 p.

Pryor, W., 1975, Biogenic sedimentation and alteration of argillaceous sediments in shallow marine environments: Bull. Geol. Soc. Amer., v. 86, p. 1244-1254.

Purser, B.H., ed., 1973, The Persian Gulf: Holocene Carbonate Sedimentation and Diagenesis in a Shallow Epicontinental Sea: New York, N.Y., Springer-Verlag, 471 p.

Pusey, W.C., III, 1973, Paleotemperatures in the Gulf Coast using the ESR-kerogen method: Gulf Coast Assoc. Geol. Soc. Transactions, v. 23, p. 195-202.

Radke, B.M. and Mathis, R.L., 1980, On the formation and occurrence of saddle dolomite: J. Sed. Petrol., v. 50, p. 1149-1168.

Read, J.F., 1980, Carbonate ramp-to-basin transitions and foreland basin evolution, Middle Ordovician, Virginia Appalachians: Am. Assoc. Petroleum Geologists Bull., v. 64, p. 1575-1612.

Roedder, E., 1981, Origin of fluid inclusions and changes that occur after trapping, in L.S. Hollister and M.L. Crawford, eds., Fluid inclusions: applications to petrology: Min. Assoc. Canada Short Course Handbook, v. 6, p. 101-137.

Rosenberg, P.E. and Holland, H.D., 1964, Calcite-dolomite-magnesite stability relations in solutions at elevated temperatures: Science, v. 145, p. 700-701.

Sartain, R.R., 1981, Stratigraphy and conodont paleontology of Late Silurian-Early Devonian strata of western Virginia: M.S. thesis, Blacksburg, Va., Virginia Polytechnic Institute and State University, 142 p.

Schlager, W. and James, N.P., 1978, Low-magnesium calcite limestones forming at the deep sea floor, Tongue of the Ocean, Bahamas: Sedimentology, v. 15, p. 675-702.

Schmoker, J.W. and Halley, R.B., 1982, Carbonate porosity versus depth: a predictable relation for South Florida: Am. Assoc. Petroleum Geologists Bull., v. 66, p. 2561-2570.

Schultz, A.P., 1983, Broken-formations of the Pulaski Thrust Sheet near Pulaski, Virginia: Ph.D. dissertation, Blacksburg, Va., Virginia Polytechnic Institute and State University, 99 p.

Scotese, C., Bambach, R.K., Barton, C., Van der Voo, R., and Ziegler, A., 1979, Paleozoic base maps: J. Geology, v. 87, p. 217-277.

Shinn, E.A., Halley, R.B., Hudson, J.H., and Lidz, B.H., 1977, Limestone compaction: An enigma: Geology, v. 5, p. 21-24.

Smith, D.B., Downing, R.A., Munkhouse, R.A., Otlet, R.L., and Pearson, F.J., 1976, The age of groundwater in the chalk of the London Basin: Water Resources Res., v. 12, p. 392-404.

Smosna, R. and Patchen, D., 1978, Silurian evolution of Central Appalachian Basin: Am. Assoc. Petroleum Geologists Bull., v. 62, p. 2308-2328.

Smosna, R. and Warshauer, S.M., 1979, A very early Devonian patch reef and its ecological setting: J. Paleontology, v. 53, p. 142-152.

Stumm, W. and Morgan, J.J., 1970, Aquatic Chemistry: New York, John Wiley and Sons, 583 p.

Suppe, J. and Wittke, J.H., 1977, Abnormal pore-fluid pressures in relation to stratigraphy and structure in the active fold-and-thrust belt of northwestern Taiwan: Petroleum Geology of Taiwan, no. 14, p. 11-24.

Swartz, F.M., 1929, The Helderberg Group of parts of West Virginia and Virginia: U.S. Geol. Survey Prof. Paper, no. 158-C, p. 27-75.

Tillman, C.G., 1963, Late Silurian and Early Devonian positive area, Salem Syncline, Virginia, in R.V. Dietrich, ed., Geologic Excursions in southwest Virginia: Virginia Polytechnic Institute and State University, Department of Geological Sciences Geologic Guidebook, v. 6, p. 23-68.

Toth, J., 1980, Cross-formational gravity-flow of groundwater: a mechanism of the transport and accumulation of petroleum (the generalized theory of petroleum migration), in W.H. Roberts, III and R.J. Cordell, eds., Problems of petroleum migration: Am. Assoc. Petroleum Geologists Studies in Geology, no. 10, p. 121-167.

Usdowski, H.-E., 1967, Die Genese Von Dolomit in Sedimenten: Berlin, Springer-Verlag, 95 p.

Walter, L.M., 1983, New data on relative stability of carbonate minerals: implications for diagenesis and cementation (abs.): Am. Assoc. Petroleum Geologists, v. 67, p. 566.

Walter, L.M. and Morse, J.W., 1984, Magnesian calcite stabilities: a reevaluation: Geochim. Cosmochim. Acta, v. 48, p. 1059-1069.

Wanless, H.R., 1979, Limestone response to stress: pressure solution and dolomitization: J. Sed. Petrol., v. 49, p. 437-462.

Waples, D.W., 1980, Time and temperature in petroleum formation: application of Lopatin's Method to petroleum exploration: Am. Assoc. Petroleum Geologists Bull., v. 64, p. 916-926.

Wigley, T.M.L., Plummer, L.N., and Pearson, F.J., Jr., 1978, Mass transfer and carbon isotope evolution in natural water systems: Geochim. Cosmochim. Acta, v. 42, p. 1117-1139.

Wilkinson, B.H., 1979, Biomineralization, paleoceanography, and the evolution of calcareous marine organisms: Geology, v. 7, p. 524-527.

Woods, T.L., Bethke, P.M., Bodnar, R.J., and Werre, R.W., Jr., 1981, Supplementary components and operation of the U.S.G.S. gas-flow heating/freezing stage: U.S. Geol. Survey Open-file Report 81-954.

Woodward, H.P., 1943, Devonian System of West Virginia: West Virginia Geol. Survey, v. XV, 665 p.

Yurtsever, Y., 1975, Worldwide survey of stable isotopes in precipitation: Report Sect. Isotope Hydrol., IAEA, November 1975, 40 p.

Appendix A

TRACE ELEMENT ANALYSES FOR VARIOUS CEMENT COMPONENTS AND SKELETAL GRAINS

Electron microprobe analyses.

Data reported in wt % oxide in this table; converted to ppm for text figures by multiplying data in table by the following factors:

Mn: 7745

Fe: 7774

Mg: 6031

Type of luminescence in fourth column.

NL: Nonluminescent cement

BL: Bright cement

DL: Dull cement

CR: Crinoid fragments

```
TEST     SAS      A1  07/31/84 14:29

//                          'CEMENTS',REGION=700K
/*JOBPARM LINES=3
/*LONGKEY
/*PRIORITY  S
/*ROUTE PRINT MVS1
//STEP1 EXEC SAS
//SYSIN DD *
DATA LUM;
INPUT NO $ 1-8 REC $ 10-15 MN 16-22 FE 25-31 ;
MG=MG*6031;
MN=MN*7745;
FE=FE*7774;
CARDS;                    Mn        Fe        Mg
M3 CRI    A40    -0.010    0.017     0.167     NL
M3 CRI    A42    0.119     0.068     0.144     BL
M3 CRI    A43    0.008     0.114     0.139     DL
M3 CRI    A44    0.000     0.138     0.100     DL
M3 CRI    A45    0.003     0.198     0.103     DL
M3 CRI    A46    0.006     0.293     0.118     DL
M3 CRI    A47    0.008     0.385     0.101     DL
M3 CRI    A48    0.011     0.386     0.116     DL
M3 CRI    A49    -0.002    0.363     0.114     DL
M3 CRI    A50    0.009     0.332     0.110     DL
M3 CRI    A51    0.004     0.259     0.114     DL
M3 CRI    A52    0.005     0.246     0.124     DL
M3 CRI    A53    -0.003    0.248     0.109     DL
M3 CRI    A54    0.001     0.259     0.122     DL
M3 CRI    A55    0.001     0.287     0.128     DL
M3 CRI    A56    0.005     0.293     0.120     DL
M3 CRI    A57    0.004     0.271     0.100     DL
M3 CRI    A58    -0.009    0.208     0.097     DL
M3 CRI    A59    0.008     0.230     0.069     DL
M3 CRI    A60    0.009     0.165     0.132     DL
M3 CRI    A61    -0.000    0.068     0.184     DL
M3 CRI    A62    0.006     0.086     0.147     DL
M3 CRI    A63    0.011     0.086     0.134     DL
M3 CRI    A64    0.008     0.096     0.166     DL
M3 CRI    A65    0.012     0.091     0.191     DL
M3 CRI    A66    0.011     0.112     0.186     DL
M3 CRI    A67    0.011     0.117     0.179     DL
M3 CRI    A68    0.014     0.123     0.189     DL
M3 CRI    A69    0.004     0.121     0.181     DL
M3 CRI    A70    0.010     0.130     0.202     DL
M3 CRI    A71    0.005     0.112     0.166     DL
M3 CRI    A72    0.003     0.118     0.158     DL
M3 CRI    A73    0.003     0.111     0.129     DL
M3 CRI    A74    -0.000    0.115     0.134     DL
M3 CRI    A75    0.003     0.115     0.120     DL
M3 CRI    A76    0.001     0.113     0.125     DL
M3 CRI    A77    0.003     0.121     0.142     DL
M3 CRI    A78    0.006     0.111     0.132     DL
M3 CRI    A79    0.005     0.088     0.092     DL
M3 CRI    A80    -0.006    0.090     0.101     DL
M3 CRI    A81    -0.001    0.091     0.096     DL
M3 CRI    A82    0.002     0.101     0.126     DL
```

TEST SAS A1 07/31/84 14:29

M3 CRI	A83	0.004	0.123	0.155	DL
M3 CRI	A84	0.006	0.126	0.161	DL
M3 CRI	A85	0.013	0.115	0.148	DL
M3 CRI	A86	0.002	0.129	0.177	DL
M3 CRI	A87	-0.000	0.078	0.078	DL
M3 CRI	A88	0.007	0.093	0.082	DL
M3 CRI	A89	0.006	0.147	0.165	DL
M3 CRI	A90	0.011	0.157	0.223	DL
M3 CRI	A91	0.002	0.130	0.152	DL
M3 CRI	A92	-0.001	0.131	0.159	DL
M3 CRI	A93	0.007	0.136	0.175	DL
M3 CRI	A94	0.007	0.132	0.180	DL
M3 CRI	A95	0.005	0.099	0.094	DL
M3 CRI	A96	0.006	0.073	0.047	DL
M3 CRI	A97	0.003	0.098	0.072	DL
M3 CRI	A98	0.009	0.122	0.139	DL
M3 CRI	A99	0.004	0.123	0.154	DL
M3 CRI	A100	0.007	0.106	0.123	DL
M3 CRI	A101	-0.001	0.116	0.145	DL
M3 CRI	A102	0.013	0.125	0.171	DL
M3 CRI	A103	0.007	0.111	0.138	DL
M3 CRI	A104	0.009	0.118	0.150	DL
M3 CRI	A105	0.000	0.097	0.196	DL
M3 CRI	A106	-0.003	0.071	0.198	DL
M3 CRI	A107	-0.001	0.132	0.125	DL
M3 CRI	A108	0.006	0.268	0.076	DL
M3 CRI	A109	0.011	0.323	0.097	DL
M3 CRI	A110	0.007	0.276	0.104	DL
M3 CRI	A111	0.007	0.270	0.085	DL
M3 CRI	A112	0.008	0.273	0.102	DL
M3 CRI	A113	0.009	0.254	0.089	DL
M3 CRI	A114	0.005	0.252	0.106	DL
M3 CRI	A115	0.001	0.251	0.110	DL
M3 CRI	A116	0.000	0.236	0.112	DL
M3 CRI	A117	0.005	0.249	0.100	DL
M3 CRI	A118	0.005	0.299	0.084	DL
M3 CRI	A119	-0.000	0.340	0.086	DL
M3 CRI	A120	0.005	0.404	0.105	DL
M3 CRI	A121	0.001	0.347	0.064	DL
M3 CRI	A122	0.009	0.274	0.082	DL
M3 CRI	A123	0.002	0.225	0.090	DL
M3 CRI	A124	0.007	0.185	0.081	DL
M3 CRI	A125	0.006	0.176	0.127	DL
M3 CRI	A126	0.006	0.143	0.148	DL
PG2 DU	A168	0.000	0.006	0.568	DL
PG2 DU	A169	0.008	0.109	0.374	DL
PG2 DU	A170	0.006	0.129	0.629	DL
PG2 DU	A171	-0.002	0.119	0.406	DL
PG2 DU	A172	0.011	0.145	0.607	DL
PG2 DU	A173	0.000	0.173	0.652	DL
PG2 DU	A174	0.006	0.167	0.556	DL
PG2 DU	A175	0.005	0.220	0.824	DL
PG2 DU	A176	0.013	0.154	0.263	DL
PG2 DU	A177	0.014	0.217	0.381	DL
PG2 DU	A178	0.010	0.262	0.665	DL

TEST SAS A1 07/31/84 14:29

PG2 DU	A179	-0.001	0.250	0.597	DL
PG2 DU	A180	0.008	0.275	0.699	DL
PG2 DU	A181	0.001	0.256	0.670	DL
PG2 DU	A182	0.008	0.259	0.659	DL
PG2 DU	A183	0.014	0.254	0.648	DL
PG2 DU	A184	0.004	0.244	0.617	DL
PG2 DU	A185	0.009	0.221	0.494	DL
PG2 DU	A186	0.006	0.277	0.678	DL
PG2 DU	A187	0.007	0.240	0.623	DL
PG2 DU	A188	0.013	0.272	0.670	DL
PG2 DU	A189	0.009	0.261	0.656	DL
PG2 DU	A190	0.012	0.270	0.670	DL
PG2 DU	A191	0.007	0.264	0.681	DL
PG2 DU	A192	0.015	0.277	0.654	DL
PG2 DU	A193	0.002	0.289	0.663	DL
PG2 DU	A194	0.017	0.271	0.677	DL
PG2 DU	A195	0.008	0.281	0.644	DL
S5 DUL	A201	0.005	0.137	0.227	DL
S5 DUL	A202	0.022	0.099	0.182	DL
S5 DUL	A203	0.029	0.125	0.215	DL
S5 DUL	A204	0.022	0.127	0.230	DL
S5 DUL	A205	0.023	0.115	0.352	DL
S5 DUL	A206	0.051	0.141	0.489	DL
S5 DUL	A207	0.044	0.238	0.708	DL
S5 DUL	A208	0.044	0.246	0.302	DL
S5 DUL	A209	0.034	0.354	0.435	DL
S5 DUL	A210	0.044	0.338	0.415	DL
FR1 ZO	A213	0.048	0.064	0.292	DL
FR1 ZO	A214	0.257	0.063	0.439	BL
FR1 ZO	A216	0.012	0.083	0.141	DL
FR1 ZO	A217	-0.008	0.064	0.184	DL
FR1 ZO	A218	0.000	0.082	0.156	DL
FR1 ZO	A220	0.138	0.110	0.323	BL
FR1 ZO	A221	0.345	0.045	0.579	BL
FR1 ZO	A222	0.097	0.121	0.473	DL
FR1 ZO	A223	0.063	0.094	0.384	DL
FR1 ZO	A224	0.074	0.214	0.488	DL
FR1 ZO	A225	0.062	0.147	0.451	DL
DP 27	A252	-0.008	0.030	0.176	NL
DP 27	A253	-0.014	0.013	0.068	NL
DP 27	A254	-0.019	0.011	0.036	NL
DP 27	A255	-0.011	0.013	0.036	NL
DP 27	A257	0.115	0.016	0.203	BL
DP 27	A259	-0.019	0.014	0.134	NL
DP 27	A260	-0.014	0.004	0.033	NL
DP 27	A261	-0.015	0.009	0.025	NL
DP 27	A263	0.159	0.058	0.079	BL
DP 27	A264	0.086	0.152	0.095	DL
DP 27	A265	0.084	0.188	0.165	DL
DP 27	A266	0.089	0.190	0.205	DL
DP 27	A267	0.065	0.173	0.162	DL
DP 27	A268	0.075	0.221	0.186	DL
DP 27	A269	0.083	0.171	0.166	DL
DP 27	A270	0.102	0.216	0.174	DL
DP 27	A271	0.135	0.263	0.239	DL

TEST SAS A1 07/31/84 14:29

DP 27	A272	0.110	0.273	0.204	DL
DP 27	A273	0.059	0.186	0.153	DL
DP 27	A274	0.077	0.217	0.208	DL
DP 27	A275	0.047	0.224	0.188	DL
DP 27	A276	0.045	0.212	0.164	DL
DP 27	A277	0.034	0.111	0.051	DL
DP 27	A278	0.022	0.096	0.032	DL
DP 27	A279	0.005	0.076	0.017	DL
DP 27	A280	0.023	0.080	0.036	DL
DP 27	A281	0.012	0.089	0.016	DL
DP 27	A282	0.034	0.147	0.092	DL
DP 27	A283	0.036	0.220	0.136	DL
DP 27	A284	0.030	0.189	0.107	DL
DMC5 C	B15	-0.009	0.008	0.394	DL
DMC5 C	B16	-0.002	0.058	0.264	DL
DMC5 C	B17	-0.002	0.086	0.163	DL
DMC5 C	B18	0.001	0.074	0.157	DL
DMC5 C	B19	0.001	0.077	0.209	DL
DMC5 C	B20	0.009	0.073	0.193	DL
DMC5 C	B21	-0.000	0.057	0.185	DL
DMC5 C	B22	-0.005	0.060	0.197	DL
DMC5 C	B23	-0.005	0.064	0.222	DL
DMC5 C	B24	-0.002	0.073	0.227	DL
NH9 CR	B30	0.040	0.192	0.152	DL
NH9 CR	B31	0.041	0.277	0.167	DL
NH9	B44	0.171	0.127	0.271	BL
NH9	B45	0.084	0.155	0.359	DL
NH9	B46	0.025	0.187	0.326	DL
NH9	B47	0.032	0.079	0.387	DL
NH9	B48	0.003	0.110	0.605	DL
NH9	B49	-0.006	0.026	0.308	DL
NH9	B50	-0.002	0.045	0.255	DL
NH9	B51	-0.015	0.013	0.226	DL
NH9	B52	-0.026	0.004	0.723	DL
NH9	B53	-0.011	-0.002	0.333	DL
NH9	B54	-0.007	0.000	0.664	DL
NH9	B55	-0.024	0.003	0.414	DL
NH9	B56	-0.003	0.007	0.397	DL
NH9	B57	-0.017	0.016	0.209	DL
DMC5 A	B93	0.004	-0.002	0.186	BL
DMC5 A	B94	-0.005	0.006	0.203	NL
DMC5 A	B96	0.009	0.012	0.262	NL
DMC5 A	B98	0.010	0.004	0.184	BL
DMC5 A	B99	-0.005	0.024	0.205	DL
DMC5 A	B100	0.001	0.023	0.196	DL
DMC5 A	B101	-0.006	0.034	0.228	DL
DMC5 A	B102	-0.001	0.047	0.252	DL
DMC5 A	B103	0.007	0.059	0.192	DL
DMC5 A	B104	0.004	0.048	0.194	DL
DMC5 A	B105	-0.003	0.069	0.221	DL
DMC5 A	B106	0.001	0.052	0.201	DL
DMC5 A	B107	0.001	0.061	0.237	DL
DMC5 A	B108	-0.001	0.070	0.184	DL
DMC5 A	B109	0.001	0.062	0.171	DL
DMC5 A	B110	-0.003	0.066	0.110	DL

TEST SAS A1 07/31/84 14:29

DMC5	A	B111	0.001	0.069	0.180	DL
DMC5	A	B112	0.003	0.087	0.273	DL
DMC5	A	B113	-0.002	0.072	0.230	DL
DMC5	A	B114	0.004	0.057	0.238	DL
DMC5	A	B115	-0.006	0.084	0.187	DL
DMC5	A	B116	0.005	0.101	0.271	DL
DMC5	A	B117	-0.005	0.041	0.485	DL
DP27	B	B139	-0.000	0.018	0.222	NL
DP27	B	B140	-0.018	0.013	0.255	NL
DP27	B	B141	-0.017	0.016	0.273	NL
DP27	B	B142	-0.014	0.009	0.233	NL
DP27	B	B143	-0.018	0.023	0.350	NL
DP27	B	B144	-0.013	0.030	0.183	NL
DP27	B	B145	-0.010	0.043	0.109	NL
DP27	B	B146	-0.015	0.005	0.192	NL
DP27	B	B153	0.025	0.003	0.144	BL
DP27	B	B154	0.141	0.003	0.089	BL
DP27	B	B155	0.043	0.024	0.042	BL
DP27	B	B156	0.002	0.016	0.144	NL
DP27	B	B157	-0.010	-0.000	0.074	NL
DP27	B	B158	-0.022	0.005	0.028	NL
DP27	B	B159	0.004	0.012	0.084	NL
DP27	B	B160	-0.012	0.005	0.079	NL
DP27	B	B161	0.065	0.008	0.066	BL
DP27	B	B162	0.326	0.018	0.038	BL
DP27	B	B163	0.159	0.086	0.164	BL
DP27	B	B164	0.014	0.152	0.052	DL
DP27	B	B165	0.011	0.085	0.135	DL
DP27	B	B166	0.041	0.068	0.093	DL
DP27	B	B167	0.079	0.098	0.093	DL
DP27	B	B168	0.078	0.084	0.083	DL
DP27	B	B169	0.075	0.101	0.190	DL
DP27	B	B170	0.059	0.125	0.155	DL
DP27	B	B171	0.064	0.163	0.236	DL
DP27	B	B172	0.070	0.158	0.264	DL
DP27	B	B173	0.088	0.189	0.245	DL
DP27	B	B174	0.074	0.154	0.159	DL
DP27	B	B175	0.066	0.135	0.147	DL
DP27	B	B176	0.059	0.151	0.183	DL
DP27	B	B177	0.087	0.196	0.277	DL
DP27	B	B178	0.115	0.225	0.269	DL
DP27	B	B179	0.123	0.244	0.246	DL
DP27	B	B180	0.118	0.245	0.276	DL
DP27	B	B181	0.123	0.272	0.260	DL
DP27	B	B182	0.119	0.269	0.267	DL
DP27	B	B183	0.108	0.267	0.245	DL
DP27	B	B184	0.094	0.248	0.261	DL
DP27	B	B185	0.079	0.248	0.248	DL
DP27	B	B186	0.070	0.224	0.240	DL
DP27	B	B187	0.063	0.216	0.253	DL
DP27	B	B188	0.068	0.201	0.259	DL
DP27	B	B189	0.063	0.195	0.214	DL
DP27	B	B190	0.067	0.098	0.086	DL
DP27	B	B191	0.053	0.104	0.082	DL
DP27	B	B192	0.045	0.096	0.092	DL

TEST SAS A1 07/31/84 14:29

DP27	B	B193	0.060	0.106	0.105	DL
DP27	B	B194	0.050	0.092	0.093	DL
DP27	B	B195	0.031	0.096	0.103	DL
DP27	B	B196	0.074	0.096	0.074	DL
DP27	B	B197	0.044	0.230	0.143	DL
DP24	Z	C8	-0.016	0.018	0.268	NL
DP24	Z	C9	-0.017	0.021	0.319	NL
DP24	Z	C10	-0.000	0.022	0.262	NL
DP24	Z	C12	0.000	0.009	0.314	NL
DP24	Z	C14	-0.025	0.010	0.280	NL
DP24	Z	C15	-0.012	0.001	0.286	NL
DP24	Z	C16	-0.015	-0.002	0.254	NL
DP24	Z	C17	-0.011	0.008	0.231	NL
DP24	Z	C18	-0.009	0.003	0.270	NL
DP24	Z	C19	0.020	-0.003	0.216	BL
DP24	Z	C20	-0.028	0.015	0.205	NL
DP24	Z	C21	-0.014	0.004	0.115	NL
DP24	Z	C23	0.051	0.008	0.081	BL
DP24	Z	C24	0.060	-0.001	0.082	BL
DP24	Z	C25	0.019	0.001	0.090	BL
DP24	Z	C26	0.048	0.012	0.071	BL
DP24	Z	C27	0.011	-0.003	0.081	BL
DP24	Z	C28	0.026	0.010	0.079	BL
DP24	Z	C29	0.171	0.012	0.073	BL
DP24	Z	C30	0.051	0.007	0.120	BL
DP24	Z	C31	-0.012	0.018	0.101	NL
DP24	Z	C32	0.060	0.039	0.147	BL
DP24	Z	C33	0.041	0.125	0.178	DL
DP24	Z	C34	0.008	0.169	0.145	DL
DP24	Z	C35	0.002	0.055	0.162	DL
DP24	Z	C36	0.004	0.062	0.182	DL
DP24	Z	C37	0.069	0.129	0.250	DL
DP24	Z	C38	0.073	0.187	0.263	DL
DP24	Z	C39	0.115	0.201	0.351	DL
DP24	Z	C40	0.121	0.233	0.261	DL
DP24	Z	C41	0.133	0.295	0.332	DL
DP24	Z	C42	0.136	0.386	0.332	DL
DP24	E	C68	0.001	0.045	0.284	NL
DP24	E	C69	0.000	0.039	0.327	NL
DP24	E	C70	-0.012	0.003	0.298	NL
DP24	E	C71	-0.012	0.010	0.291	NL
DP24	E	C72	-0.013	0.011	0.301	NL
DP24	E	C73	-0.011	-0.004	0.324	NL
DP24	E	C74	-0.010	0.009	0.328	NL
DP24	E	C75	-0.003	0.004	0.297	NL
DP24	E	C76	-0.004	-0.000	0.203	NL
DP24	E	C78	-0.001	0.012	0.266	NL
DP24	E	C79	-0.013	-0.000	0.267	NL
DP24	E	C80	0.003	0.017	0.291	DL
DP24	E	C81	0.013	0.020	0.280	DL
DP24	E	C82	0.004	0.044	0.276	DL
DP24	E	C83	0.003	0.517	0.552	DL
DP24	E	C84	0.015	0.064	0.375	DL
DP24	E	C85	0.016	0.077	0.340	DL
DP24	E	C86	0.009	0.074	0.276	DL

TEST SAS A1 07/31/84 14:29

DP24 E	C87	0.108	0.240	0.398	DL
W12 DU	C100	0.021	-0.002	0.283	DL
W12 DU	C101	0.025	0.013	0.505	DL
W12 DU	C102	0.045	0.068	0.652	DL
W12 DU	C103	0.047	0.119	0.572	DL
W12 DU	C104	0.024	0.069	0.339	DL
W12 DU	C105	0.030	0.032	0.352	DL
W12 DU	C106	-0.007	0.012	0.119	DL
W12 DU	C107	0.020	0.006	0.306	DL
W12 DU	C108	0.022	0.057	0.326	DL
W12 DU	C109	0.028	0.010	0.438	DL
W12 DU	C115	0.016	0.285	0.348	DL
W12 DU	C116	0.022	0.287	0.373	DL
W12 DU	C117	0.002	0.101	0.104	DL
W12 DU	C118	0.012	0.110	0.213	DL
W12 DU	C119	0.002	0.155	0.482	DL
W12 DU	C120	-0.001	0.102	0.229	DL
W12 DU	C121	0.010	0.133	0.331	DL
W12 DU	C122	0.010	0.156	0.446	DL
W12 DU	C123	0.015	0.151	0.444	DL
W12 DU	C124	0.013	0.160	0.449	DL
W12 DU	C125	0.005	0.123	0.282	DL
W12 DU	C126	0.007	0.094	0.193	DL
W12 DU	C127	0.001	0.093	0.189	DL
W12 DU	C128	0.018	0.155	0.557	DL
W12 DU	C129	0.015	0.073	0.220	DL
W8	D55	0.069	0.107	0.122	DL
W8	D56	0.086	0.204	0.188	DL
W8	D57	0.077	0.244	0.368	DL
W8	D58	0.045	0.215	0.418	DL
W8	D59	0.045	0.237	0.304	DL
W8	D60	0.051	0.204	0.357	DL
W8	D61	0.042	0.149	0.565	DL
W8	D62	0.066	0.214	0.542	DL
W8	D63	0.037	0.206	0.388	DL
W8	D64	0.060	0.178	0.639	DL
W8	D65	0.084	0.182	0.430	DL
W8	D66	0.085	0.225	0.455	DL
W8	D67	0.084	0.203	0.705	DL
W8	D68	0.053	0.178	0.742	DL
W8	D69	0.063	0.198	0.696	DL
W8	D70	0.067	0.179	0.496	DL
W8	D71	0.071	0.152	0.688	DL
W8	D72	0.070	0.149	0.675	DL
W8	D73	0.057	0.141	0.520	DL
W8	D74	0.058	0.173	0.553	DL
W8	D75	0.050	0.120	0.219	DL
DMC26	D95	0.147	0.051	0.268	BL
DMC26	D96	0.034	0.122	0.098	DL
DMC26	D97	0.040	0.250	0.232	DL
DMC26	D98	0.046	0.345	0.360	DL
DMC26	D99	0.059	0.438	0.199	DL
DMC26	D100	0.051	0.358	0.258	DL
DMC26	D101	0.037	0.387	0.369	DL
DMC26	D102	0.047	0.353	0.315	DL

TEST SAS A1 07/31/84 14:29

W10	D178	0.049	0.189	0.503	DL
W10	D179	0.031	0.133	0.309	DL
W10	D180	0.041	0.104	0.304	DL
W10	D181	0.053	0.140	0.316	DL
W10	D182	0.033	0.107	0.216	DL
W10	D183	0.047	0.153	0.185	DL
W10	D184	0.054	0.067	0.230	DL
W10	D185	0.024	0.114	0.182	DL
W10	D186	0.032	0.109	0.186	DL
W10	D187	0.028	0.098	0.199	DL
W10	D188	0.043	0.127	0.172	DL
W10	D189	0.073	0.138	0.161	DL
W10	D190	0.040	0.125	0.289	DL
W10	D191	0.040	0.129	0.180	DL
W10	D192	0.025	0.115	0.132	DL
W10	D193	0.031	0.125	0.121	DL
W10	D194	0.035	0.158	0.229	DL
W10	D195	0.034	0.137	0.177	DL
W10	D196	0.047	0.245	0.316	DL
W10	D197	0.091	0.281	0.230	DL
W10	D198	0.079	0.320	0.271	DL
W10	D199	0.071	0.311	0.409	DL
W10	D200	0.063	0.221	0.198	DL
W10	D201	0.063	0.236	0.422	DL
W10	D202	0.051	0.225	0.623	DL
W7	D206	0.077	0.112	0.675	DL
W7	D207	0.064	0.181	0.535	DL
W7	D208	0.061	0.155	0.247	DL
W7	D209	0.057	0.138	0.252	DL
W7	D210	0.071	0.199	0.246	DL
W7	D211	0.032	0.121	0.317	DL
W7	D212	0.041	0.106	0.313	DL
W7	D213	0.063	0.183	0.560	DL
W7	D214	0.063	0.143	0.394	DL
W7	D215	0.070	0.124	0.443	DL
W7	D216	0.054	0.157	0.253	DL
W7	D217	0.073	0.289	1.412	DL
W7	D218	0.039	0.131	0.489	DL
W7	D219	0.090	0.212	0.318	DL
W7	D220	0.073	0.143	0.537	DL
W7	D221	0.049	0.123	0.456	DL
W7	D222	0.031	0.171	0.396	DL
W7	D223	0.059	0.179	0.712	DL
W7	D224	0.063	0.166	0.420	DL
W7	D225	0.044	0.132	0.325	DL
W7	D226	0.025	0.096	0.226	DL
W7	D227	0.041	0.113	0.207	DL
W7	D228	0.041	0.098	0.302	DL
W7	D229	0.071	0.114	0.340	DL
W7	D230	0.052	0.154	0.365	DL
W7	D231	0.055	0.140	0.190	DL
W7	D232	0.061	0.181	0.389	DL
CR1	D286	0.056	0.246	0.314	DL
CR1	D287	0.039	0.219	0.293	DL
CR1	D288	0.049	0.242	0.248	DL

TEST SAS A1 07/31/84 14:29

DMC26	D103	0.047	0.271	0.177	DL
DMC26	D104	0.038	0.255	0.199	DL
DMC26	D105	0.030	0.184	0.164	DL
DMC26	D106	0.033	0.212	0.065	DL
DMC26	D107	0.053	0.188	0.149	DL
DMC26	D108	0.314	0.144	0.137	BL
DMC26	D109	0.204	0.111	0.162	BL
DMC26	D110	0.128	0.082	-0.005	BL
DMC26	D111	0.197	0.031	0.038	BL
DMC26	D112	0.161	0.019	0.178	BL
DMC26	D113	0.037	-0.001	0.101	NL
DMC26	D114	0.031	0.058	0.059	NL
DMC26	D115	0.012	0.041	0.044	NL
DMC26	D116	0.037	0.054	0.245	NL
DMC27	D127	0.135	0.069	0.245	BL
DMC27	D128	0.075	0.180	0.107	DL
DMC27	D129	0.057	0.089	0.179	DL
DMC27	D130	0.045	0.122	-0.048	DL
DMC27	D131	0.056	0.081	0.088	DL
DMC27	D132	0.049	0.130	0.190	DL
DMC27	D133	0.039	0.097	0.115	DL
DMC27	D134	0.047	0.132	0.190	DL
DMC27	D135	0.036	0.102	0.235	DL
DMC27	D136	0.036	0.097	0.208	DL
DMC27	D137	0.018	0.127	0.131	DL
DMC27	D138	0.020	0.093	0.023	DL
DMC27	D139	0.031	0.089	0.080	DL
DMC27	D140	0.047	0.096	0.207	DL
DMC27	D141	0.024	0.131	0.128	DL
DMC27	D142	0.039	0.100	0.222	DL
DMC27	D143	0.064	0.112	0.054	DL
DMC27	D144	0.034	0.116	0.087	DL
DMC27	D145	0.061	0.117	0.139	DL
DMC27	D146	0.055	0.224	0.105	DL
DMC27	D147	0.035	0.173	0.241	DL
DMC27	D148	0.060	0.101	0.258	DL
DMC27	D149	0.036	0.103	0.058	DL
DMC27	D150	0.050	0.087	0.075	DL
DMC27	D151	0.028	0.087	0.125	DL
DMC27	D152	0.211	0.067	0.042	BL
DMC27	D153	0.127	0.029	-0.025	BL
DMC27	D154	0.100	0.040	-0.062	BL
W10	D165	0.053	0.042	0.465	DL
W10	D166	0.040	0.075	0.574	DL
W10	D167	0.067	5.467	0.610	DL
W10	D168	0.060	0.130	0.514	DL
W10	D169	0.054	0.175	0.408	DL
W10	D170	0.053	0.134	0.438	DL
W10	D171	0.042	0.142	0.403	DL
W10	D172	0.053	0.156	0.360	DL
W10	D173	0.052	0.190	0.486	DL
W10	D174	0.036	0.303	1.774	DL
W10	D175	0.065	0.154	0.689	DL
W10	D176	0.038	0.173	0.582	DL
W10	D177	0.046	0.220	0.669	DL

TEST SAS A1 07/31/84 14:29

CR1	D289	0.039	0.127	0.078	DL
CR1	D290	0.036	0.092	0.059	DL
CR1	D291	0.046	0.146	0.254	DL
CR1	D292	0.040	0.149	0.351	DL
CR1	D293	0.042	0.156	0.500	DL
CR1	D294	0.043	0.161	0.494	DL
CR1	D295	0.052	0.161	0.468	DL
CR1	D296	0.067	0.149	0.439	DL
CR1	D297	0.026	0.143	0.486	DL
CR1	D298	0.030	0.183	0.373	DL
CR1	D299	0.078	0.129	0.389	DL
CR1	D300	0.051	0.182	0.430	DL
CR1	D301	0.043	0.146	0.417	DL
CR1	D302	0.039	0.158	0.304	DL
CR1	D303	0.034	0.165	0.088	DL
CR1	D304	0.034	0.274	0.350	DL
CR1	D305	0.057	0.256	0.179	DL
CR1	D306	0.046	0.259	0.104	DL
CR1	D307	0.049	0.195	0.195	DL
CR1	D308	0.058	0.211	0.488	DL
S13	D315	0.015	0.045	0.333	DL
S13	D316	0.038	0.027	0.341	DL
S13	D317	0.025	0.038	0.865	DL
S13	D318	0.052	0.153	0.153	DL
S13	D319	0.022	0.176	0.326	DL
S13	D320	0.050	0.127	0.190	DL
S13	D321	0.036	0.141	0.344	DL
S13	D322	0.023	0.211	0.383	DL
S13	D323	0.028	0.212	0.349	DL
S13	D324	0.040	0.188	0.266	DL
S13	D325	0.037	0.197	0.357	DL
S13	D326	0.044	0.209	0.497	DL
S13	D327	0.037	0.205	0.391	DL
S13	D328	0.038	0.189	0.444	DL
S13	D329	0.058	0.201	0.337	DL
S13	D330	0.036	0.215	0.347	DL
S13	D331	0.040	0.200	0.452	DL
S13	D332	0.048	0.255	0.396	DL
S13	D333	0.035	0.169	0.432	DL
S13	D334	0.015	0.096	0.166	DL
S13	D335	0.035	0.141	0.159	DL
S13	D336	0.036	0.142	0.300	DL
S13	D337	0.028	0.192	0.388	DL
S13	D338	0.059	0.190	0.414	DL
S13	D339	0.066	0.150	0.507	DL
S13	D340	0.038	0.218	0.343	DL
S13	D341	0.038	0.187	0.401	DL
S13	D342	0.046	0.150	0.365	DL
S13	D343	0.040	0.171	0.303	DL
S13	D344	0.039	0.183	0.494	DL
S13	D345	0.030	0.212	0.418	DL
S13	D346	0.046	0.195	0.430	DL
S13	D347	0.021	0.176	0.458	DL
S13	D348	0.039	0.183	0.500	DL
S13	D349	0.051	0.184	0.503	DL

TEST SAS A1 07/31/84 14:29

S4	D357	0.050	0.190	0.197	DL
S4	D358	0.042	0.149	0.242	DL
S4	D359	0.039	0.127	0.372	DL
S4	D360	0.034	0.148	0.285	DL
S4	D361	0.049	0.171	0.238	DL
S4	D362	0.051	0.156	0.287	DL
S4	D363	0.047	0.164	0.276	DL
S4	D373	0.047	0.189	0.345	DL
S4	D374	0.070	0.187	0.197	DL
S4	D375	0.059	0.198	0.372	DL
S4	D376	0.024	0.139	0.193	DL
S4	D377	0.026	0.103	0.179	DL
S4	D378	0.054	0.150	0.233	DL
S4	D379	0.050	0.106	0.172	DL
S4	D380	0.078	0.135	0.146	DL
S4	D381	0.046	0.168	0.296	DL
S4	D382	0.064	0.174	0.394	DL
S4	D383	0.061	0.180	0.330	DL
CR7	D388	0.041	0.182	0.445	DL
CR7	D389	0.013	0.129	0.340	DL
CR7	D390	0.050	0.164	0.334	DL
CR7	D391	0.040	0.162	0.359	DL
CR7	D392	0.027	0.171	0.618	DL
CR7	D393	0.018	0.138	0.303	DL
CR7	D394	0.038	0.186	0.201	DL
CR7	D395	0.027	0.165	0.462	DL
CR7	D396	0.069	0.190	0.382	DL
CR7	D397	0.051	0.215	0.467	DL
CR7	D398	0.060	0.196	0.318	DL
CR7	D399	0.044	0.151	0.394	DL
CR7	D400	0.025	0.149	0.336	DL
CR7	D401	0.032	0.155	0.264	DL
CR7	D402	0.012	0.147	0.410	DL
CR7	D403	0.038	0.136	0.199	DL
CR7	D404	0.037	0.153	0.317	DL
CR7	D405	0.074	0.163	0.321	DL
CR7	D406	0.027	0.163	0.338	DL
CR7	D407	0.034	0.183	0.402	DL
CR7	D408	0.018	0.188	0.324	DL
CR7	D409	0.024	0.156	0.352	DL
CR7	D410	0.013	0.179	0.291	DL
CR7	D411	0.045	0.130	0.340	DL
CR7	D412	0.026	0.147	0.287	DL
CR7	D413	0.039	0.165	0.420	DL
CR7	D414	0.031	0.153	0.463	DL
CR7	D415	0.014	0.140	0.273	DL
CR7	D416	0.036	0.173	0.220	DL
CR7	D417	0.022	0.132	0.177	DL
CR7	D418	0.026	0.155	0.217	DL
CR7	D419	0.031	0.148	0.431	DL
CR7	D420	0.036	0.159	0.373	DL
CR7	D421	0.039	0.177	0.523	DL
CR7	D422	0.010	0.193	0.322	DL
CR7	D423	0.015	0.107	0.379	DL
CR7	D424	0.033	0.065	0.440	DL

TEST SAS A1 07/31/84 14:29

PG1	D433	0.050	0.078	0.538	DL
PG1	D434	0.035	0.070	0.634	DL
PG1	D435	0.021	0.037	0.818	DL
PG1	D436	0.028	0.089	0.247	DL
PG1	D437	0.026	0.288	0.472	DL
PG1	D438	0.048	0.222	0.646	DL
PG1	D439	0.044	0.177	0.518	DL
PG1	D440	0.047	0.146	0.516	DL
PG1	D441	0.029	0.281	0.663	DL
PG1	D442	0.046	0.201	0.729	DL
PG1	D443	0.083	0.220	0.764	DL
PG1	D444	0.048	0.201	0.755	DL
PG1	D445	0.041	0.177	0.714	DL
PG1	D446	0.036	0.142	0.660	DL
PG1	D447	0.058	0.137	0.835	DL
PG1	D448	0.041	0.136	0.524	DL
PG1	D449	0.039	0.123	0.447	DL
PG1	D450	0.029	0.163	0.555	DL
PG1	D451	0.053	0.165	0.373	DL
PG1	D452	0.038	0.063	0.129	DL
PG1	D453	0.050	0.110	0.195	DL
PG1	D454	0.031	0.068	0.272	DL
PG1	D455	0.033	0.014	0.334	DL
PG1	D456	0.053	0.011	0.364	DL
PG1	D457	0.056	0.012	1.316	DL
RX6	D468	0.041	0.205	0.495	DL
RX6	D469	0.041	0.130	0.481	DL
RX6	D470	0.035	0.145	0.256	DL
RX6	D471	0.038	0.338	0.664	DL
RX6	D472	0.025	0.211	0.458	DL
RX6	D473	0.031	0.130	0.478	DL
RX6	D474	0.052	0.211	0.680	DL
RX6	D475	0.019	0.164	0.463	DL
RX6	D476	0.039	0.189	0.363	DL
RX6	D477	0.038	0.166	0.267	DL
RX6	D478	0.061	0.128	0.233	DL
RX6	D479	0.042	0.044	0.386	DL
RX6	D480	0.064	0.003	0.482	DL
RX6	D481	0.045	0.026	0.899	DL
RX5	D494	0.019	0.195	0.110	DL
RX5	D495	0.045	0.127	0.437	DL
RX5	D496	0.044	0.147	0.528	DL
RX5	D497	0.015	0.167	0.511	DL
RX5	D498	0.052	0.241	0.351	DL
RX5	D499	0.034	0.200	0.531	DL
RX5	D500	0.067	0.209	0.288	DL
RX5	D501	0.041	0.147	0.547	DL
RX5	D502	0.031	0.139	0.375	DL
RX5	D503	0.019	0.127	0.523	DL
RX5	D504	0.032	0.128	0.774	DL
RX5	D505	0.026	0.171	0.485	DL
RX5	D506	0.048	0.189	0.504	DL
RX5	D507	0.049	0.237	0.332	DL
RX5	D508	0.039	0.224	0.694	DL
RX5	D509	0.039	0.225	0.868	DL

TEST SAS A1 07/31/84 14:29

RX5	D510	0.061	0.148	0.265	DL
RX5	D511	0.056	0.273	0.618	DL
RX5	D512	0.049	0.235	0.477	DL
RX5	D513	0.059	0.179	0.359	DL
RX5	D514	0.059	0.154	0.247	DL
RX5	D515	0.038	0.286	0.320	DL
RX5	D516	0.043	0.330	1.318	DL
RX5	D517	0.051	0.186	0.274	DL
RX5	D518	0.069	0.237	0.516	DL
RX5	D519	0.040	0.261	0.391	DL
RX5	D520	0.036	0.275	0.522	DL
RX5	D521	0.049	0.281	0.548	DL
RX5	D522	0.039	0.275	0.641	DL
RX5	D523	0.053	0.279	0.520	DL
RX5	D524	0.022	0.261	0.450	DL
RX5	D525	0.049	0.279	0.453	DL
RX5	D526	0.047	0.356	0.237	DL
RX5	D527	0.031	0.153	0.370	DL
RX5	D528	0.045	0.115	0.193	DL
RX5	D529	0.046	0.038	0.415	DL
RX5	D530	0.030	0.197	0.343	DL
RX5	D531	0.032	0.146	0.420	DL
RX4CRI	D538	0.033	0.150	0.220	DL
RX4CRI	D539	0.033	0.094	0.164	DL
RX4CRI	D540	0.043	0.103	0.175	DL
RX4CRI	D541	0.064	0.123	0.166	DL
RX4CRI	D542	0.019	0.060	0.135	DL
RX4CRI	D543	0.038	0.100	0.217	DL
RX4CRI	D544	0.030	0.201	0.403	DL
RX4CRI	D545	0.025	0.172	0.350	DL
RX4CRI	D546	0.049	0.117	0.145	DL
RX4CRI	D547	0.035	0.061	-0.022	DL
RX4CRI	D548	0.057	0.072	-0.070	DL
RX4CRI	D549	0.048	0.119	0.107	DL
RX4CRI	D550	0.051	0.087	0.102	DL
RX4CRI	D551	0.049	0.109	0.191	DL
RX4	D561	0.056	0.057	0.385	DL
RX4	D562	0.037	0.071	0.370	DL
RX4	D563	0.038	0.097	0.129	DL
RX4	D564	0.032	0.155	0.246	DL
RX4	D565	0.049	0.118	0.346	DL
RX4	D566	0.032	0.096	0.090	DL
RX4	D567	0.034	0.124	0.152	DL
RX4	D568	0.048	0.143	0.074	DL
RX4	D569	0.041	0.139	0.116	DL
RX4	D570	0.015	0.169	0.128	DL
RX4	D571	0.062	0.114	0.206	DL
RX4	D572	0.035	0.093	0.366	DL
RX4	D573	0.052	0.140	0.416	DL
RX4	D574	0.054	0.156	0.571	DL
RX4	D575	0.021	0.243	0.283	DL
RX4	D576	0.039	0.155	0.357	DL
RX4	D577	0.028	0.194	0.460	DL
PG3 2C	D592	0.030	0.151	0.289	DL
PG3 2C	D593	0.018	0.054	0.310	DL

TEST SAS A1 07/31/84 14:29

PG3 2C	D594	0.009	0.084	0.480	DL
PG3 2C	D595	0.036	0.070	0.394	DL
PG3 2C	D596	0.036	0.055	0.535	DL
PG3 2C	D597	0.034	0.057	0.470	DL
PG3 2C	D598	0.039	0.130	0.391	DL
PG3 2C	D599	0.020	0.127	0.289	DL
PG3 2C	D600	0.052	0.065	0.234	DL
PG3 2C	D601	0.052	0.162	0.199	DL
PG3 2C	D602	0.070	0.152	0.246	DL
PG3 2C	D603	0.015	0.157	0.447	DL
PG3 2C	D604	0.077	0.170	0.233	DL
PG3 2C	D605	0.041	0.157	0.355	DL
PG3 2C	D606	0.081	0.207	0.278	DL
PG3 2C	D607	0.021	0.105	0.192	DL
PG3ARR	D620	0.052	0.005	0.303	DL
PG3ARR	D621	0.034	0.008	0.227	DL
PG3ARR	D622	0.033	0.046	0.194	DL
PG3ARR	D623	0.047	0.113	0.274	DL
PG3ARR	D624	0.030	0.160	0.319	DL
PG3ARR	D625	0.071	0.104	0.156	DL
PG3ARR	D626	0.047	0.159	0.407	DL
PG3ARR	D627	0.054	0.142	0.628	DL
PG3ARR	D628	0.046	0.102	0.454	DL
PG3ARR	D629	0.042	0.017	0.429	DL
PG3ARR	D630	0.041	0.020	0.729	DL
PG3ARR	D631	0.027	0.033	0.756	DL
PG3ARR	D632	0.028	0.022	0.718	DL
PG3ARR	D633	0.041	0.024	0.439	DL
NH8	E13	0.062	0.377	0.173	DL
NH8	E14	0.051	0.124	0.160	DL
NH8	E15	0.041	0.065	0.049	DL
NH8	E16	0.041	0.094	-0.062	DL
NH8	E17	0.029	0.051	0.126	DL
NH8	E18	0.024	0.050	0.079	DL
NH8	E19	0.043	0.055	0.090	DL
NH8	E20	0.041	0.059	0.058	DL
NH8	E21	0.054	0.051	0.015	DL
NH8	E22	0.059	0.048	0.135	DL
NH8	E23	0.041	0.111	0.235	DL
NH8	E24	0.045	0.128	0.293	DL
NH8	E25	0.076	0.180	0.273	DL
NH8	E26	0.094	0.511	1.607	DL
NH8	E27	0.095	0.209	0.241	DL
NH8	E28	0.075	0.182	0.264	DL
NH8	E29	0.081	0.177	0.273	DL
NH8	E30	0.078	0.157	0.250	DL
NH8	E31	0.092	0.197	0.310	DL
NH8	E32	0.107	0.238	0.323	DL
NH8	E33	0.088	0.355	0.384	DL
NH8	E34	0.105	1.058	0.547	DL
NH8	E35	0.083	0.211	0.367	DL
NH8	E36	0.092	0.284	0.859	DL
NH8	E37	0.131	0.628	0.909	DL
T/15DU	E79	0.050	0.304	0.133	DL
T/15DU	E80	0.049	0.083	0.133	DL

TEST SAS A1 07/31/84 14:29

T/15DU	E81	0.075	0.090	0.024	DL
T/15DU	E82	0.065	0.297	0.081	DL
T/15DU	E83	0.161	0.083	0.264	BL
T/15DU	E84	0.087	0.116	0.182	DL
T/15DU	E85	0.037	0.140	0.201	DL
T/15DU	E86	0.047	0.170	0.150	DL
T/15DU	E87	0.043	0.152	0.139	DL
T/15DU	E88	0.033	0.149	0.155	DL
T/15DU	E89	0.047	0.144	0.239	DL
T/15DU	E90	0.060	0.158	0.077	DL
T/15DU	E91	0.057	0.153	0.153	DL
T/15DU	E95	0.070	0.085	0.149	DL
T/15DU	E96	0.064	0.101	0.082	DL
T/15DU	E97	0.061	0.089	0.112	DL
T/15DU	E98	0.038	0.055	0.078	DL
T/15DU	E99	0.032	0.025	0.013	DL
T/15DU	E100	0.064	0.057	0.094	DL
T/15DU	E101	0.084	0.032	0.098	DL
MS4	E102	0.027	0.033	0.216	NL
MS4	E103	0.035	0.037	0.195	NL
MS4	E104	0.025	0.008	0.309	NL
MS4	E105	0.027	0.064	0.267	NL
MS4	E106	0.000	0.054	0.273	NL
MS4	E107	0.030	0.030	0.250	NL
MS4	E108	0.029	0.031	0.123	NL
MS4	E109	0.017	0.024	0.091	NL
MS4	E110	0.032	0.043	0.314	NL
MS4	E111	0.030	0.019	0.258	NL
MS4	E112	0.024	0.009	0.035	NL
MS4	E114	0.103	0.039	0.144	BL
MS4	E115	0.042	0.002	0.019	SL
MS4	E116	0.054	0.038	-0.026	SL
MS4	E117	0.374	0.011	0.031	BL
MS4	E118	0.267	0.141	0.069	BL
MS4	E119	0.034	0.116	0.046	DL
MS4	E120	0.041	0.023	0.059	DL
MS4	E121	0.017	0.033	0.110	DL
MS4	E122	0.041	0.080	-0.010	DL
MS4	E123	0.042	0.122	0.067	DL
MS4	E124	0.086	0.100	0.131	DL
MS4	E125	0.081	0.150	0.067	DL
MS4	E126	0.047	0.148	0.200	DL
MS4	E127	0.057	0.114	0.076	DL
MS4	E128	0.058	0.170	0.102	DL
MS4	E129	0.047	0.120	-0.012	DL
MS4	E130	0.031	0.164	0.231	DL
MS4	E131	0.037	0.170	0.136	DL
MS4	E132	0.034	0.159	0.178	DL
MS4	E133	0.057	0.179	0.197	DL
MS4	E134	0.038	0.222	0.164	DL
MS4	E135	0.042	0.150	0.193	DL
MS4	E136	0.222	0.142	0.094	BL
MS4	E137	0.440	0.147	0.005	BL
MS4	E138	0.427	0.115	0.018	BL
MS4	E139	0.038	0.014	0.034	NL

```
TEST      SAS       A1   07/31/84 14:29

MS4       E140   0.033     0.020     -0.010    NL
MS4       E141   0.037     0.018      0.010    NL
MS4       E142   0.017     0.018     -0.063    NL
MS4       E143   0.023     0.042      0.227    NL
MS4       E144   0.030     0.001      0.218    NL
MS4       E145   0.041     0.041      0.184    NL
MS4       E146   0.052     0.090      0.269    NL
MS3       E147   0.002     0.122      0.186    DL
MS3       E148   0.034     0.203      0.171    DL
MS3       E149   0.020     0.073      0.265    DL
MS3       E150   0.074     0.214      0.250    DL
MS3       E151   0.076     0.199      0.154    DL
MS3       E152   0.015     0.209      0.033    DL
MS3       E153   0.064     0.266     -0.003    DL
MS3       E154   0.048     0.238      0.086    DL
MS3       E155   0.031     0.196     -0.034    DL
MS3       E156   0.025     0.179      0.021    DL
MS3       E157   0.048     0.157      0.089    DL
MS3       E158   0.052     0.187      0.106    DL
MS3       E159   0.042     0.155      0.113    DL
MS3       E160   0.039     0.154      0.050    DL
MS3       E161   0.033     0.118      0.113    DL
MS3       E162   0.055     0.074      0.183    DL
MS3       E163   0.037     0.061      0.053    DL
MS3       E164   0.017     0.060      0.143    DL
MS3       E165   0.035     0.040      0.001    DL
MS3       E166   0.020     0.023      0.022    DL
MS3       E167   0.029     0.076      0.149    DL
MS3       E168   0.015     0.044      0.090    DL
MS3       E169   0.041     0.064     -0.034    DL
MS3       E170   0.056     0.094      0.102    DL
MS3       E171   0.102     0.112      0.035    DL
MS3       E172   0.054     0.071      0.074    DL
MS3       E173   0.079     0.084      0.031    DL
MS3       E174   0.069     0.101      0.049    DL
MS3       E175   0.058     0.061      0.067    DL
MS3       E176   0.067     0.091      0.156    DL
MS3       E177   0.060     0.044      0.118    DL
MS3       E178   0.069     0.070      0.118    DL
MS3       E179   0.068     0.109      0.121    DL
MS3       E180   0.035     0.109      0.241    DL
MS3       E181   0.032     0.090      0.212    DL
MS3       E182   0.062     0.113      0.246    DL
MS3       E183   0.095     0.242      0.410    DL
PROC PRINT;
```

Appendix B

STABLE ISOTOPIC COMPOSITIONS OF CEMENT COMPONENTS AND SKELETAL GRAINS

Listing of DOROBEK at 14:10:48 on MAY 18, 1984

CODING

COMPONENT CODE

1100 = EQUANT CALCITE CEMENT, LUMINESCENCE NOT KNOWN
1101 = " " " , NONLUMINESCENT AND BRIGHT ZONES
1102 = " " " , "ZONED DULL" ZONES
1103 = " " " , DULLY LUMINESCENT CALCITE
1106 = " " " , FRACTURE FILLING, DULLY LUMINESCENT
1806 = FRACTURE FILLING BAROQUE (OR SADDLE) DOLOMITE
1816 = VOID FILLING (INTERGRANULAR) BAROQUE DOLOMITE
2702 = ASSORTED CRINOID FRAGMENTS

STRATIGRAPHIC INTERVAL

NUMBER OF FEET ABOVE BASE OF MEASURED STRATIGRAPHIC SECTION
186.5 = 186.5 FEET ABOVE BASE

LOCALITY	SAMPLE NUMBER	COMPONENT	STRAT'C INTERVAL	DATA			LAB VALUES $\delta^{18}O$	LAB VALUES $\delta^{13}C$	PDB STANDARD $\delta^{18}O$	PDB STANDARD $\delta^{13}C$
1250	1024.01	1101	108.0	0 10	12384AMO		-4.79	-0.79	-6.10	3.20
1250	2012.01	1101	32.0	0 10	20684AMO		-5.07	-6.47	-6.44	-2.87
1250	1026.01	1101	120.5	0 10	30584AMO		-5.14	-0.80	-6.45	3.20
1250	1027.01	1101	35.0	0 10	30184DLD		-3.52	-0.70	-4.83	3.26
1250	1035.01	1102	245.5	0 10	31984AMO		-3.36	-1.76	-4.68	2.12
1250	1034.01	1102	228.0	0 10	31984AMO		-5.26	0.55	-6.56	4.65
1250	1011.01	1103	30.0	0 10	11384AMO		-9.87	-4.19	-11.21	-0.27
1250	1024.02	1103	108.0	0 10	12384AMO		-7.08	-1.02	-8.40	3.03
1250	2012.02	1103	32.0	0 10	20684AMO		-7.93	-4.07	-9.27	-0.20
1250	1026.02	1103	120.5	0 10	30584AMO		-8.73	-1.43	-10.05	2.65
1250	1035.02	1103	245.5	0 10	31984AMO		-3.94	0.79	-5.24	4.87
1250	1034.02	1103	228.0	0 10	31984AMO		-3.95	-0.62	-5.26	3.36
1250	1027.02	1103	35.0	0 10	30184DLD		-6.52	-0.72	-7.83	3.34
1250	1026.02	1106	120.0	0 10	42384AMO		-5.53	-1.15	-6.85	2.84
1250	1026.01	1106	120.0	0 10	42384AMO		-6.15	-1.19	-7.47	2.82
1250	1023.02	1106	107.0	0 10	42384AMO		-6.73	-1.11	-8.05	2.93
1250	1023.01	1106	107.0	0 10	42384AMO		-6.79	-1.30	-8.11	2.72
1250	1021.02	1106	101.0	0 10	42384AMO		-4.93	-0.44	-6.24	3.58
1250	1021.01	1106	101.0	0 10	42384AMO		-5.10	-0.53	-6.41	3.49
1250	1002.02	1106	4.0	0 10	42384AMO		-8.91	-4.34	-10.26	-0.46
1250	1002.01	1106	4.0	0 10	42384AMO		-8.72	-4.37	-10.07	-0.50
1250	1034.02	1106	228.0	0 10	43084AMO		-7.59	-2.14	-8.92	1.85
1250	1037.01	1816	0.0	0 30	51584DLD		-7.34	-6.18	-8.70	-2.48
1250	1024.01	1816	0.0	0 30	51584DLD		-6.56	-4.01	-7.90	-0.19
1250	1024.03	2702	108.0	0 10	12384AMO		-4.69	-0.63	-6.00	3.37
1250	2012.03	2702	32.0	0 10	20684AMO		-6.01	-3.44	-7.35	0.41
1250	1026.03	2702	120.5	0 10	30584AMO		-3.87	-0.61	-5.18	3.36
1250	1035.03	2702	245.5	0 10	31984AMO		-7.42	0.34	-8.72	4.50
1250	1034.03	2702	228.0	0 10	31984AMO		-6.79	-0.53	-8.10	3.55
1250	1027.03	2702	35.0	0 10	30184DLD		-3.46	-0.24	-4.77	3.75
1251	1006.01	1103	36.0	0 10	11384AMO		-6.56	-4.70	-7.91	-0.93
1251	1006.05	1103	36.0	0 10	11684AMO		-6.56	-4.82	-7.91	-1.05

Listing of DOROBEK at 14:10:48 on MAY 18, 1984

59		1251	1006.04	1103	36.0	0	10	11684AMO	-6.40	-4.71	-7.75	-0.94
60		1251	1006.03	1103	36.0	0	10	11684AMO	-6.34	-4.50	-7.69	-0.72
61		1251	1006.02	1103	36.0	0	10	11684AMO	-6.48	-4.69	-7.83	-0.92
62		1251	1099.03	1106	0.0	0	10	42384AMO	-6.21	-1.00	-7.53	3.03
63		1251	1099.01	1106	0.0	0	10	42384AMO	-5.63	-1.51	-6.95	2.46
64												
65		1252	1027.01	1100	204.0	0	10	13084AMO	-5.25	-0.04	-6.56	4.02
66		1252	1002.01	1101	105.0	0	10	30584AMO	-4.69	-0.47	-6.00	3.54
67		1252	1001.01	1101	65.0	0	10	31284AMO	-4.70	-2.86	-6.03	0.98
68		1252	2001.01	1102	65.0	0	10	50484AMO	-4.34	-3.24	-5.68	0.56
69		1252	2001.02	1103	65.0	0	10	50484AMO	-6.56	-3.07	-7.89	0.82
70		1252	1019.02	1103	143.0	0	10	40584AMO	-7.72	0.52	-9.02	4.71
71		1252	1006.01	1103	195.0	0	10	12684AMO	-5.71	0.78	-7.01	4.92
72		1252	1006.02	1103	195.0	0	10	12684AMO	-10.04	0.42	-11.34	4.68
73		1252	1027.02	1103	204.0	0	10	13084AMO	-9.39	0.08	-10.69	4.29
74		1252	1001.02	1103	65.0	0	10	31284AMO	-6.20	-3.07	-7.53	0.81
75	*	1252	1002.02	1103	105.0	0	10	41784AMO	-8.79	-0.99	-10.10	3.12
76		1252	1003.01	1106	106.0	0	10	43084AMO	-5.81	-0.60	-7.12	3.44
77		1252	1003.02	1106	106.0	0	10	43084AMO	-5.81	-0.55	-7.12	3.49
78		1252	1003.03	1106	106.0	0	10	43084AMO	-5.96	-0.62	-7.27	3.42
79		1252	1006.03	2702	195.0	0	10	12684AMO	-4.62	0.88	-5.92	4.99
80		1252	1027.03	2702	204.0	0	10	13084AMO	-4.22	0.24	-5.52	4.29
81		1252	1001.03	2702	65.0	0	10	31284AMO	-4.98	-2.64	-6.31	1.23
82		1252	1019.03	2702	143.0	0	10	40584AMO	-3.81	0.80	-5.11	4.87
83		1252	1002.03	2702	105.0	0	10	40584AMO	-4.96	-0.32	-6.27	3.71
84												
85		1253	1009.01	1106	112.0	0	10	43084AMO	-5.86	-2.16	-7.19	1.77
86		1253	1009.02	1106	112.0	0	10	43084AMO	-5.91	-2.07	-7.24	1.87
87		1253	1009.03	1106	112.0	0	10	43084AMO	-5.89	-2.15	-7.22	1.78
88		1253	1009.01	1806	0.0	0	30	51584DLD	-4.93	-6.34	-6.30	-2.74
89												
90		1254	1010.01	1101	45.0	0	10	11284AMO	-5.03	-1.77	-6.35	2.16
91		1254	1027.01	1101	171.0	0	10	11284AMO	-3.56	-0.69	-4.87	3.27
92		1254	1014.01	1101	72.0	0	10	11384DLD	-4.86	-0.22	-6.17	3.82
93		1254	1013.01	1101	70.0	0	10	13084AMO	-4.48	0.11	-5.78	4.16
94		1254	1009.01	1101	35.0	0	10	20684AMO	-5.15	-2.00	-6.47	1.92
95		1254	1024.01	1102	138.0	0	10	30584AMO	-4.52	0.30	-5.82	4.36
96		1254	1010.02	1103	45.0	0	10	11284AMO	-6.58	-2.08	-7.91	1.88
97		1254	1027.02	1103	171.0	0	10	11284AMO	-6.18	-1.08	-7.50	2.94
98		1254	1023.02	1103	126.0	0	10	11284AMO	-9.66	0.25	-10.96	4.48
99		1254	1023.03	1103	126.0	0	10	11284AMO	-9.94	0.22	-11.24	4.46
100		1254	1023.01	1103	126.0	0	10	11684AMO	-9.83	0.34	-11.13	4.58
101		1254	1023.05	1103	126.0	0	10	11684AMO	-10.73	0.52	-12.03	4.81
102		1254	1023.04	1103	126.0	0	10	11684AMO	-10.66	0.56	-11.96	4.85
103		1254	1023.01	1103	126.0	0	10	12384AMO	-10.17	0.58	-11.47	4.85
104		1254	1013.02	1103	70.0	0	10	13084AMO	-7.69	-0.05	-9.00	4.09
105		1254	1009.02	1103	35.0	0	10	20284AMO	-7.54	-2.37	-8.87	1.60
106		1254	1024.02	1103	138.0	0	10	30584AMO	-5.12	0.51	-6.42	4.61
107		1254	1023.02	1103	126.0	0	10	11284AMO	-9.66	0.25	-10.96	4.48
108		1254	1023.03	1103	126.0	0	10	11284AMO	-9.94	0.22	-11.24	4.46
109		1254	1001.02	1106	1.0	0	10	43084AMO	-7.33	-3.99	-8.67	-0.14
110		1254	1001.03	1106	1.0	0	10	43084AMO	-7.20	-4.09	-8.54	-0.25
111		1254	1007.01	1816	29.0	0	30	51584DLD	-5.25	-8.87	-6.64	-5.44
112		1254	1006.01	1816	29.0	0	30	51584DLD	-6.23	-3.74	-7.57	0.09
113		1254	1010.01	1816	45.0	0	30	51584DLD	-7.46	-1.59	-8.78	2.44
114		1254	1009.01	1816	35.0	0	30	51584DLD	-8.22	-1.77	-9.54	2.27
115		1254	1027.03	2702	171.0	0	10	11284AMO	-4.43	-0.90	-5.74	3.07
116		1254	1023.02	2702	126.0	0	10	12384AMO	-4.26	0.62	-5.56	4.70

Listing of DOROBEK at 14:10:48 on MAY 18, 1984

117		1254	1013.03	2702	70.0	0	10	13084AMO	-4.90	0.12	-6.20	4.18
118		1254	1009.03	2702	35.0	0	10	20684AMO	-6.26	-2.15	-7.59	1.80
119		1254	1024.03	2702	138.0	0	10	30584AMO	-3.44	0.62	-4.74	4.67
120												
121		1255	1006.01	1106	29.0	0	10	50484AMO	-6.24	-0.83	-7.55	3.21
122		1255	1006.02	1106	29.0	0	10	50484AMO	-6.25	-0.96	-7.56	3.07
123		1255	1005.01	1106	27.0	0	10	50484AMO	-6.27	-0.64	-7.58	3.41
124		1255	1005.02	1106	27.0	0	10	50484AMO	-6.06	-0.68	-7.37	3.36
125		1255	1027.01	1106	175.0	0	10	50484AMO	-5.74	-1.24	-7.06	2.75
126		1255	1027.02	1106	175.0	0	10	50484AMO	-5.84	-1.09	-7.16	2.92
127												
128		1256	1001.02	1102	0.0	0	10	31984AMO	-8.06	-0.13	-9.37	4.02
129		1256	1012.01	1103	77.0	0	10	12384AMO	-7.92	-0.72	-9.23	3.38
130		1256	1010.01	1103	74.5	0	10	12684AMO	-7.07	-0.72	-8.38	3.35
131		1256	1010.02	1103	74.5	0	10	12684AMO	-6.61	-0.60	-7.92	3.47
132		1256	1004.01	1103	36.0	0	10	12684AMO	-5.74	0.86	-7.04	5.00
133		1256	1004.02	1103	36.0	0	10	12684AMO	-8.26	0.56	-9.56	4.77
134		1256	1007.01	1106	55.0	0	10	22084AMO	-3.88	0.78	-5.18	4.85
135		1256	1007.02	1106	55.0	0	10	22084AMO	-5.83	-0.25	-7.14	3.82
136		1256	1007.03	1106	55.0	0	10	22084AMO	-5.64	-0.24	-6.95	3.82
137		1256	1012.02	2702	77.0	0	10	12384AMO	-4.25	-1.16	-5.57	2.79
138		1256	1004.03	2702	36.0	0	10	12684AMO	-5.24	0.80	-6.54	4.92
139		1256	1001.03	2702	0.0	0	10	32684AMO	-7.18	-2.49	-8.51	1.46
140												
141		1257	1006.02	1103	16.0	0	10	11384DLD	-6.75	-0.22	-8.06	3.88
142		1257	1016.01	1106	64.0	0	10	22084AMO	-5.45	-1.54	-6.77	2.42
143		1257	1016.02	1106	64.0	0	10	22084AMO	-5.57	-1.40	-6.89	2.58
144		1257	1012.01	1106	64.0	0	10	22084AMO	-5.45	-1.85	-6.77	2.09
145		1257	1012.02	1106	64.0	0	10	22084AMO	-5.51	-1.75	-6.83	2.20
146		1257	1006.03	2702	16.0	0	10	11384DLD	-4.09	-0.10	-5.40	3.92
147												
148		1258	1008.01	1103	94.0	0	10	11184RKG	-7.93	-2.84	-9.26	1.11
149		1258	1022.01	1108	181.0	0	10	22084AMO	-8.58	0.38	-9.88	4.58
150		1258	1022.01	1108	181.0	0	10	22084AMO	-9.22	-0.20	-10.53	3.98
151		1258	1022.01	1108	181.0	0	10	22084AMO	-6.79	0.70	-8.09	4.87
152		1258	1022.01	1816	181.0	0	30	32984AMO	-6.99	0.29	-8.29	4.43
153	*	1258	1016.01	1816	150.0	0	30	51584DLD	-13.13	-2.85	-14.46	1.28
154		1258	1008.02	2702	94.0	0	10	11184RKG	-5.81	-2.19	-7.14	1.74
155												
156		1259	1009.01	1100	25.0	0	10	31284AMO	-6.86	-2.36	-8.19	1.59
157		1259	2005.01	1101	7.0	0	10	40584AMO	-6.28	-2.74	-7.61	1.16
158		1259	1009.02	1103	25.0	0	10	40584AMO	-9.38	-2.59	-10.71	1.43
159		1259	1009.01	1816	0.0	0	30	51584DLD	-6.72	-1.89	-8.04	2.09
160		1259	1009.02	1816	0.0	0	30	51584DLD	-5.29	-3.11	-6.63	0.73
161		1259	1009.03	2702	25.0	0	10	40584AMO	-5.62	-2.09	-6.95	1.84
162												
163		1260	1011.02	1100	214.0	0	10	20684AMO	-7.63	-1.88	-8.95	2.13
164		1260	1011.03	1100	214.0	0	10	20684AMO	-5.64	-2.34	-6.97	1.57
165		1260	1011.04	1100	214.0	0	10	20684AMO	-6.54	-2.01	-7.86	1.96
166		1260	1011.05	1100	214.0	0	10	20684AMO	-6.69	-1.90	-8.01	2.08
167		1260	1012.04	1100	215.0	0	10	31284AMO	-6.25	-1.44	-7.57	2.56
168		1260	1012.03	1100	215.0	0	10	31284AMO	-3.38	-1.09	-4.70	2.83
169		1260	1011.01	1100	214.0	0	10	30184DLD	-6.16	-1.15	-7.48	2.86
170		1260	1012.01	1100	215.0	0	10	40584AMO	-7.01	-1.71	-8.33	2.29
171		1260	1012.02	1100	215.0	0	10	40584AMO	-4.80	-1.15	-6.12	2.82
172		1260	1010.01	1102	194.0	0	10	40584AMO	-3.98	-1.68	-5.30	2.22
173												
174		1261	1003.01	1101	23.0	0	10	12384AMO	-4.04	-1.45	-5.36	2.47

Listing of DOROBEK at 14:10:48 on MAY 18, 1984

175	1261	1004.01	1101	24.0	0	10	30584AMO	-3.91	-0.77	-5.22	3.19
176	1261	2002.01	1101	10.0	0	10	50484AMO	-3.81	-0.29	-5.12	3.71
177	1261	2002.02	1103	10.0	0	10	50484AMO	-6.16	-0.55	-7.47	3.51
178	1261	1005.01	1103	33.0	0	10	12384AMO	-9.30	-1.12	-10.62	3.00
179	1261	1004.02	1103	24.0	0	10	30584AMO	-5.38	-0.86	-6.69	3.15
180	1261	1003.01	1816	0.0	0	30	51584DLD	-5.32	-3.12	-6.66	0.73
181	1261	2002.03	2702	10.0	0	10	50484AMO	-4.74	-0.28	-6.05	3.75
182	1261	1003.03	2702	23.0	0	10	12384AMO	-3.79	-1.14	-5.11	2.79
183	1261	1004.03	2702	24.0	0	10	30584AMO	-3.10	-0.56	-4.41	3.39
184											
185	1262	1020.01	1100	57.5	0	10	11184RKG	-4.99	-2.88	-6.32	0.97
186	1262	1021.01	1102	71.0	0	10	13084AMO	-5.50	-0.51	-6.81	3.53
187	1262	1012.01	1102	35.0	0	10	11184RKG	-5.14	-2.93	-6.47	0.92
188	1262	1020.02	1103	57.5	0	10	11184RKG	-7.06	-3.10	-8.40	0.81
189	1262	1012.02	1103	35.0	0	10	11184RKG	-6.11	-3.16	-7.45	0.71
190	1262	1021.02	1103	71.0	0	10	30184DLD	-6.15	-0.91	-7.46	3.12
191	1262	2007.01	1103	14.5	0	10	40584AMO	-8.33	-3.15	-9.67	0.79
192	1262	1020.03	2702	57.5	0	10	11184RKG	-4.88	-2.83	-6.21	1.02
193	1262	1012.03	2702	35.0	0	10	11184RKG	-5.51	-2.77	-6.84	1.11
194	1262	1021.03	2702	71.0	0	10	30184DLD	-4.68	-0.56	-5.99	3.45
195											
196	1263	1007.01	1100	86.0	0	10	11684AMO	-3.38	-1.27	-4.70	2.64
197	1263	1002.01	1102	24.0	0	10	11184RKG	-5.66	0.57	-6.96	4.69
198	1263	1006.01	1103	86.0	0	10	11684AMO	-3.41	-0.57	-4.72	3.39
199	1263	1007.04	1103	86.0	0	10	11684AMO	-9.21	-0.95	-10.52	3.18
200	1263	1007.03	1103	86.0	0	10	11684AMO	-8.68	-0.93	-9.99	3.18
201	1263	1007.02	1103	86.0	0	10	11684AMO	-9.22	-0.86	-10.53	3.28
202	1263	1002.02	1103	24.0	0	10	11184RKG	-8.05	0.50	-9.35	4.69
203	1263	1002.03	2702	24.0	0	10	11184RKG	-3.70	0.64	-5.00	4.70
204											
205	1264	1016.01	1101	0.0	0	10	12684AMO	-5.32	1.25	-6.61	5.41
206	1264	1016.02	1103	0.0	0	10	12684AMO	-8.72	1.46	-10.01	5.75
207	1264	1024.01	1806	160.5	0	30	32984AMO	-4.72	-5.70	-6.08	-2.06
208	1264	1016.03	2702	0.0	0	10	12684AMO	-4.96	1.71	-6.25	5.89
209											
210	1265	1003.01	1101	0.0	0	10	13084AMO	-3.38	-0.93	-4.70	3.01
211	1265	1003.02	1103	0.0	0	10	13084AMO	-8.43	-1.32	-9.75	2.76
212	1265	1003.03	2702	0.0	0	10	13084AMO	-4.11	-0.83	-5.42	3.14
213											
214	1266	1013.01	1102	50.0	0	10	32684AMO	-3.80	-0.76	-5.11	3.20
215	1266	1013.02	1103	50.0	0	10	32684AMO	-6.04	-0.46	-7.35	3.60
216	1266	1019.01	1103	126.0	0	10	11384DLD	-3.85	-1.17	-5.17	2.76
217	1266	1019.02	1103	126.0	0	10	11384AMO	-8.10	-1.69	-9.42	2.35
218	1266	1019.03	2702	126.0	0	10	11384AMO	-5.39	-2.00	-6.71	1.93
219	1266	1013.03	2702	50.0	0	10	32684AMO	-3.76	-1.08	-5.08	2.86
220											
221	1267	1017.01	1103	141.0	0	10	11384DLD	-3.90	0.40	-5.20	4.45
222	1267	1017.02	1103	141.0	0	10	11384DLD	-8.44	0.22	-9.74	4.41
223	1267	1017.03	2702	141.0	0	10	11384DLD	-3.84	0.11	-5.14	4.14
224	1268	2001.01	1816	0.0	0	30	51584DLD	-5.49	-5.53	-6.85	-1.85
225											
226											

Appendix C

FLUID INCLUSION DATA

T_e = eutectic temperature; appearance of first melt

$T_{m\text{-}ice}$ = temperature

wt % NaCl = equivalent weight percent NaCl

Th = homogenization temperature; disappearance of vapor bubble into liquid phase

$T_{HP\text{-}C}$ = hydrostatic pressure-corrected trapping temperature, 400 bars pressure

$T_{LP\text{-}C}$ = lithostatic pressure-corrected trapping temperature, 880 bars pressure

D = dull calcite cement
Q = quartz cement
L = leaked inclusion
* = no data

wt % NaCl determined using the equation (Potter et al., 1978):

$$w_s = 1.76958\theta - 4.2384 \times 10^{-2}\theta^2$$
$$5.2778 \times 10^{-4}\theta^3 \pm 0.028$$

where: w_s = wt % NaCl in solution
θ = freezing point depression in °C

Pressure-corrections after Potter (1977).

PRIMARY TWO-PHASE FLUID INCLUSIONS

Sample	T_e	$T_{m\text{-}ice}$	wt % NaCl	Th	$T_{HP\text{-}C}$	$T_{LP\text{-}C}$	Cement
W11	-24.0	-18.8	21.8	126.9	181.9	217.9	D
	*	-19.5	22.3	46.2	94.2	131.2	D
	*	-20.0	22.7	48.8	96.8	133.8	D
FC6	-36.6	-11.9	15.9	141.3	195.3	231.3	D
	-31.6	-9.8	13.8	99.1	154.1	191.1	D
DB16	-31.9	-18.5	21.6	L	*	*	D
	-36.1	-25.0	26.0	140.5	192.5	230.5	D
	*	-19.8	22.5	L	*	*	D
	*	-22.1	24.1	160.3	201.3	244.3	D
	*	-28.8	28.4	158.7	198.7	242.7	D
DB22	-43.1	-20.8	23.2	L	*	*	D
	-45.2	-24.0	25.4	120.5	158.5	200.5	D
	-44.0	-24.2	25.5	119.3	157.3	199.3	D
FK2	*	-22.8	24.6	105.5	143.5	185.5	D
	*	-20.8	23.2	L	*	*	D
	*	-22.0	24.0	110.3	148.3	190.3	D
	*	-20.2	22.8	91.1	128.1	169.1	D
S8	-20.1	-1.7	2.9	102.8	147.8	184.8	D
PG6	-35.8	-16.3	19.3	88.1	140.1	176.1	D
	-36.0	-16.5	20.0	140.3	192.3	230.3	D
B4	*	*	*	45.7	*	*	D
PG6	-25.5	-1.4	2.4	139.6	181.6	218.6	Q
	*	-1.4	2.4	L	*	*	Q
HR9	-24.1	-5.0	7.9	175.0	220.0	259.0	Q
	-23.9	-3.5	5.7	174.7	214.7	249.7	Q

SECONDARY TWO-PHASE FLUID INCLUSIONS

Sample	T_e	$T_{m\text{-}ice}$	wt % NaCl	Th	$T_{HP\text{-}C}$	$T_{LP\text{-}C}$
FC6	-39.0	-18.9	21.9	188.3	239.3	281.3
	-38.8	-18.9	21.9	191.5	242.5	284.5
	-38.6	-18.9	21.9	*	*	*
	-24.0	*	*	235.3	*	*
	*	*	*	197.1	*	*
	*	*	*	192.5	*	*
HR9	*	-20.6	23.1	184.5	230.5	275.5
	*	-20.6	23.1	185.9	231.5	276.9
	*	-18.0	21.2	226.5	274.5	319.5
	*	-22.1	24.1	L	*	*
	*	-22.1	24.1	229.1	267.1	315.1
	*	-22.6	24.4	L	*	*
	-51.5	-17.9	21.1	175.9	228.9	265.9
	-50.1	-19.1	22.0	L	*	*
	*	*	*	229.7	*	*
	*	*	*	235.2	*	*
DB1	-41.0	-23.2	24.8	L	*	*
	-37.6	-20.2	22.8	L	*	*
	-40.8	-25.1	26.1	218.5	258.5	303.5
	-35.1	-24.6	25.7	156.6	196.6	241.6
	*	*	*	210.5	*	*
W11	-35.0	-16.6	20.1	L	*	*
	-36.0	-16.5	20.0	207.9	257.9	300.9
	-52.0	-15.1	18.9	136.9	186.9	226.9
	*	*	*	158.8	*	*
	*	*	*	124.3	*	*
PG8	-40.2	-22.1	24.1	L	*	*

Sample	T_e	$T_{m\text{-}ice}$	wt % NaCl	Th	$T_{HP\text{-}C}$	$T_{LP\text{-}C}$
PG6	*	*	*	195.7	*	*
	-50.8	-14.9	18.7	195.1	246.1	288.1
	-47.8	-15.0	18.8	196.7	247.7	289.7
	-51.2	-17.2	20.6	223.5	270.5	316.5
	*	*	*	250+	*	*
	-48.4	-19.2	22.1	190.7	242.7	282.7
	*	-17.5		*	*	*
	*	-19.1	22.0	252.0	294.0	342.0
	*	-19.8		*	*	*
	*	-19.9		*	*	*
	*	-19.2	22.1	232.0	270.0	317.0
	*	*	*	267.0	*	*
	*	*	*	208.2	*	*
	*	*	*	212.1	*	*
PG2	-45.1	-21.1	23.4	L	*	*
	-41.0	-22.0	24.0	186.3	232.3	277.3
	-40.8	-23.0	24.7	L	*	*
S8	-45.8	-22.6	24.4	156.7	196.7	241.7

Appendix D

MEASURED SECTION LOCALITIES

Sixty-one (61) geologic sections were used in interpreting the stratigraphy, sedimentology, and basin evolution for the Helderberg Group in Virginia-West Virginia-Maryland. Of the 61 sections, 35 sections were measured, logged, and sampled by the author. The other 36 sections were obtained from the literature and thickness data were used in some of the stratigraphic cross-sections. Sections taken from the literature are appropriately cited after the locality description.

Virginia

Alleghany County: Lowmoor Section. Covington 7.5' Quadrangle. On southeast flank of Fore Mountain where it is cut by the Jackson River. Located about 4 miles west of Route 696-Lawmoor exit off U.S. Interstate 64 along Alleghany C.R. 1104 (Sartain, 1981).

Alleghany County: Callaghan Section. Callaghan 7.5' Quadrangle. Along S.R. 600 at Dunlap Beach about 2 miles southeast of Callaghan, VA (Edmundson, 1958).

Alleghany County: Island Ford Section. Covington 7.5' Quadrangle. About 6 miles southeast of Clifton Forge, VA, along U.S. Interstate 64 where it crosses the Jackson River.

Alleghany County: ' Clifton Forge Section. Clifton Forge 7.5' Quadrangle. Along north side of Chesapeake and Ohio Railway, east of U.S. 220 bridge in Clifton Forge, VA (Edmundson, 1958).

Alleghany County: Iron Gate Section. Clifton Forge 7.5' Quadrangle. Along James River where U.S. 220 crosses the river, about 1 mile south of Iron Gate, VA.

Alleghany County: Gathright Dam Section. Falling Spring 7.5' Quadrangle. Turn left off U.S. 220 onto C.R. 640 to Falling Spring, VA, about 8 miles north of Covington, VA. Continue to intersection with C.R. 687, turn right. Continue to intersection with C.R. 605, make sharp left turn to Gathright Dam. Section in front of dam.

Augusta County: Deerfield Section. Deerfield 7.5' Quadrangle. Along Clayton Mill Creek near Marble Valley about 4.5 miles southwest of Deerfield, VA (Edmundson, 1958).

Augusta County: Fordwick Section. Craigsville/Augusta Springs 7.5' Quadrangles. At Craigsville, VA, turn off S.R. 42 onto C.R. 687 (Fordwick Road), go 0.35 miles, turn left onto "Fordwick Road," cross bridge over creek, continue to railroad tressel; section is along railroad.

Bath County: Bolar Section. Burnsville 7.5' Quadrangle. About 3.5 miles south of Bolar, VA, west of Jack's Mountain, just east of bridge over Jackson River along U.S. 220 (Swartz, 1929).

Botetourt County: Price's Bluff Section. Eagle Rock 7.5' Quadrangle. 1 mile northwest of Gala, VA, turn onto C.R. 622 off U.S. 220; section along railroad tracks between James River and C.R. 622.

Craig County: New Castle Section. New Castle 7.5' Quadrangle. Along S.R. 311; 3.7 miles south of New Castle, VA, and VEPCO Station. Section along creek and continues in abandoned quarry along road.

Craig County: Barbour's Creek Section. New Castle 7.5' Quadrangle. 1.9 miles east along C.R. 611 from its intersection with C.R. 609 near New Castle, VA.

Craig County: Paint Bank Section. Paint Bank 7.5' Quadrangle. Along S.R. 311, about 0.5 miles south of Paint Bank, VA.

Craig County: Johns Creek Section. Potts Creek 7.5' Quadrangle. On southeast flank of Nutters Mountain, 2.5 miles along a jeep trail from C.R. 678 on the property of Mrs. Anne Willis Taylor of Roanoke, VA. The Taylor property is located at the end of C.R. 678, northwest of New Castle, VA (Sartain, 1981).

Craig County: Catawba Mountain Section. Quadrangle. Section along S.R. 311 from Catawba Creek southeastward across Catawba Mountain to Masons Creek (Tillman, 1963).

Frederick County: Baldwin Gap Section. Baldwin Gap through Little North Mountain about 1 mile east of Marlboro.

Highland County: McDowell Section. McDowell 7.5' Quadrangle. Along U.S. 250 on east slope of Bullpasture Mountain, about 4 miles east of McDowell, VA.

Highland County: Monterey Section. Monterey 7.5' Quadrangle.' 0.5 mile east of Monterey, just north of U.S. 250 to Staunton.

Highland County: Strait Creek Section. Monterey 7.5' Quadrangle. About 4 miles north along C.R. 629 off U.S. 250 near Monterey, VA.

Highland County: Mustoe Section. Mustoe 7.5' Quadrangle. About 0.25 miles east along C.R. 607 after turning off U.S. 220 (Smosna and Warshauer, 1979).

Montgomery County: Fagg Section. Ironto 7.5' Quadrangle. Section is along North Fork Roanoke River at Fagg, VA, on C.R. 603 (Tillman, 1963).

Rockbridge County: Bells Valley Section. Craigsville 7.5' Quadrangle. Along S.R. 614, near an inactive quarry 0.25 mile southeast of Bells Valley, VA.

Rockingham County: Fulks Run Section. Fulks Run 7.5' Quadrangle. Along S.R. 259, about 7 miles west of Broadway, VA.

Shenandoah County: Passage Creek Section. Strasburg 7.5' Quadrangle. Section is south of S.R. 678 along Passage Creek, 1.3 miles south of Blue Hole.

Maryland

Alleghany County: Flintstone Creek Section. Flintstone 7.5' Quadrangle. Along U.S. 40 and in Flintstone Creek about 0.2 miles west of Flintstone, MD, behind the new Flintstone School.

Alleghany County: Devil's Backbone Section. Cumberland 7.5' Quadrangle. At Corriganville, MD, go left on Cash Valley Road, go 1.5 miles to railroad crossing, take railroad service road (left) for 1.3 miles to section along Western Maryland RR.

Alleghany County: Corriganville Section. Cumberland 7.5' Quadrangle. In Corriganville Quarry on north side of Wills Creek about 0.5 mile ENE of Corriganville, MD.

Washington County: Hancock Section. Hancock 7.5' Quadrangle. In abandoned quarry and in road cuts of Route 40 through Tonoloway Ridge at Sandyville Road intersection.

Washington County: Woodmont Section. Great Cacapon 7.5' Quadrangle. Turn off U.S. 40 outside of Hancock, MD, onto Woodmont Road; go 6.4 miles, turn left onto Pearre-Deneen Road (dirt road) for 1.4 miles to small parking area. Section along railroad tracks.

West Virginia

Berkeley County: Johnstontown Section. Big Pool 7.5' Quadrangle. In abandoned quarry and along Tillhance Creek, at north end of Ferrel Ridge, about 0.2 miles west of Johnsontown (Head, 1969).

Berkeley County: Tomahawk Section. Big Pool 7.5' Quadrangle. Go about 1 mile west of Hedgesville, WV, on Route 9 to Back Creek-Tomahawk Road (Route 7), turn left right onto "Route 2" (unmarked road between two large white frame houses), continue for 0.25 miles to

old C.C.C. lime kiln (visible from road). Section is in abandoned quarry behind kiln and along road.

Berkeley County: Wilson Ridge Section. Gerrardstown 15' Quadrangle. In small stream cut in west flank of Wilson Ridge, about 1.2 miles SSE of Jones Springs and about 2.5 miles NNE of Shanghai, WV (Woodward, 1943).

Greenbrier County: Alvon Section. Section along country road following Anthony Creek through Browns Mountain Anticline, 0.5 mile west of Alvon, WV (Woodward, 1943).

Hampshire County: Hanging Rock Section. Just east of Pleasantdale, WV, along U.S. 50. Section starts along road before sharp bend.

Hampshire County: "Rocks" Section. Go 0.3 miles down unmarked road off S.R. 28, about 4 miles north of Romney, WV. Turnoff is at farm of Carmen P. Buckbee, Rocks, WV. Section can be seen from Route 28, going north.

Hampshire County: Sector Section. Turn off U.S. 220, 1 mile north of Purgitsville, WV, onto paved Stringtown Road, continue for 0.5 miles to Y-intersection, go left down dirt road. Continue for 3.7 miles to Sector Section. Section is along road and creek alongside road.

Hardy County: Mill Gap Run Section. Lost City, WV-VA 7.5' Quadrangle. Section on hillside and along Mill Gap Run. Turn off S.R. 259 at Lost River Village, WV, onto Mill Gap Run Road, continue about 0.5 miles to section. Section starts on property of Captain Charlie Breeding (house to east with steel roof).

Hardy County: Thrasher Spring School Section. Turn off U.S. 220 at Old Fields, WV (north of Moorefield, WV) onto Old Fields Road. Continue west to section exposed along road.

Hardy County: Petersburg Gap Section. Section is about 1.5 miles east of Petersburg, WV, along U.S. 220.

Hardy County: Elkhorn Mountain Section. Section near Baker Rocks (off U.S. 220), 2 miles southeast of Durgon, WV. Section exposed along private road leading up mountain from U.S. 220 (Woodward, 1943).

Hardy County: Trout Run Section. Section along Trout Run, about 4 miles southwest of Wardensville, WV (Woodward, 1943).

Mercer County: Bluefield Section. Bluefield, VA-WV 7.5' Quadrangle.

Mineral County: New Creek I Section. Elk Garden 15' Quadrangle. Section in quarry at Y-junction of U.S. 220 and U.S. 50, near where they cross over New Creek.

Mineral County: New Creek II Section. Westernport 7.5' Quadrangle. In abandoned quarry and along road through gap in New Creek Mountain leading from U.S. 220 to U.S. 50, about 0.3 miles northwest of Duling Church (Head, 1969).

Mineral County: Keyser Quarry Section. Section exposed in abandoned quarry now being used as a dump (Fulk Brothers Dump), just east of Keyser, WV, city limits, off Route 46.

Morgan County: Cherry run Section. Cherry Run 7.5' Quadrangle Turn off Route 9, east of Berkeley Springs, WV, onto Cherry Run Road, continue for about 3 miles to Y-intersection, turn right to B&O Railroad tracks. Section is along railroad tracks.

Morgan County: Berkeley Springs Section. Section along Route 9, at crest of Warm Spring Mountain, 0.5 mile west of Berkeley Springs, WV (Woodward, 1943).

Pendleton County: Smoke Hole Section. About 1.5 miles north of Upper Tract, WV, turn off U.S. 220 onto country road leading to Smoke Hole Recreation Area (just before bridge over Potomac River). Continue about 1.5 miles to section along road.

Pendleton County: Ruddle Section. Composite section from limestone quarry 0.75 mile west of Ruddle, WV, and along U.S. 220, 0.5 mile east of Ruddle (Woodward, 1943).

Pendleton County: Oak Flat Section. Section along U.S. 33 about 7.1 miles east of Franklin, WV, in old roadside quarry near a Roadside Rest area.

Pendleton County: Friends Run Section. Section along U.S. 33, about 4 miles west of Franklin, WV (Woodward, 1943).

Pendleton County: Moyers Gap Road Section. Turn right off U.S.250 onto C.R. 614, about 4 miles west of McDowell, VA. Continue for 15 miles to Sugar Grove, WV, turn left onto Moyers Gap Road. Section is about 1 mile, along the road.

Pocahontas County: Dunmore Section. Take Sheets Road off S.R. 92, continue about 0.3 miles to sharp bend in road. Quarry in Tonoloway Limestone is visible from road. Section is along Sitlington Creek. Ask permission at farmhouse at sharp bend in road.

Pocahontas County: Frost Section I. About 6.8 miles north of junction with route 39, along Route 28/92. Section exposed in creek bed.

Pocahontas County: Frost Section II. About 1.6 miles south of Frost, WV, along S.R. 92. Section is in pasture on hillside.

The vita has been removed from the scanned document

STRATIGRAPHY, SEDIMENTOLOGY, AND DIAGENETIC HISTORY OF THE SILURO-DEVONIAN HELDERBERG GROUP, CENTRAL APPALACHIANS

by

Steven L. Dorobek

(Abstract)

The Late Silurian-Early Devonian Helderberg Group, Central Appalachians, is a sequence of mixed siliciclastic-carbonate sediments that was deposited during relative tectonic quiescence on a ramp that built out from low-relief tectonic highlands bordering the eastern side of the Appalachian Basin. Three transgressive-regressive sequences are recognized. Each sequence was deposited over 2-3 m.y.; subsidence rates during deposition were 1 to 2 cm/1000 years. Skeletal grainstone/rudstone formed fringing skeletal banks that formed during regression and prograded away from the eastern side of the basin. Thick Middle Devonian siliciclastic sediments buried the Helderberg Group and updip subaerial exposures accompanying the onset of the Acadian Orogeny.

Cementation of the Helderberg Group began on the sea floor, but most cements formed under shallow (<300 m depth) to deep burial (300 m to 4 km) conditions. Regional cathodoluminescent zonation patterns in early, clear calcite cements indicate meteoric groundwaters, that become progressively more reducing away from recharge areas, were involved in shallow burial cementation. Progressive downdip reduction of meteoric groundwaters resulted in updip nonluminescent calcite cements that pass downdip into time-correlative "subzoned" dull cement and finally, nonzoned dull cements. Calculated stable isotopic compositions of Helderberg shallow burial pore fluids are similar to values in modern coastal meteoric groundwaters. Extensive meteoric groundwater systems developed over a 3-4 m.y. period when the Helderberg Group was subaerially exposed along the eastern basin margin and when Helderberg aquifers were confined by fine-grained sediments at <300 m burial depth. Meteoric groundwaters had recharge areas in eastern tectonic highlands which supplied sufficient hydraulic heads to expel connate marine pore fluids and discharge at least 150 km offshore onto the floor of the Appalachian Basin.

Void-filling dull calcite cement formed from deep burial (300 m to 4 km) pore fluids with calculated chemical compositions similar to modern oil field brines. Migration of hydrocarbons and high-temperature, high-pressure brines occurred during Late Paleozoic deformation after Helderberg

sediments were totally cemented. Brines probably came from eastern overthrusted terranes and migrated through fractures without altering conodont CAI values. Late hydrocarbons probably had several source rocks.